THE TAPHONOMY AND PHYLOGENETIC RELATIONSHIPS OF THE TALKEETNA

MOUNTAINS HADROSAUR

By

Kevin P. Stack

RECOMMENDED: _____

_____

_____
Advisory Committee Chair

_____
Chair, Department of Geology & Geophysics

APPROVED: _____
Dean, College of Natural Science and Mathematics

_____
Dean of the Graduate School

April 12, 2012
_____
Date

THE TAPHONOMY AND PHYLOGENETIC RELATIONSHIPS OF THE TALKEETNA

MOUNTAINS HADROSAUR

A

THESIS

Presented to the Faculty

of the University of Alaska Fairbanks

in Partial Fulfillment of the Requirements

for the Degree of

MASTER OF SCIENCE

By

Kevin P. Stack, B.S.

Fairbanks, Alaska

May 2012

Abstract

The fossil record of hadrosauroids (Ornithopoda, Hadrosauroidea) from the Albian to Santonian is very sparse, with few described North American and Asian taxa compared to the diverse record of Campanian to Maastrichtian hadrosaurids. In 1994, the partial postcranial remains of a hadrosauriform dinosaur were found in the Matanuska Formation of southern Alaska. The Matanuska Formation is a thick succession of Albian- to Maastrichtian-aged, dominantly marine, sediments deposited in a forearc basin along the actively accreting western North American margin. The Alaskan specimen is assigned a Turonian age based on molluscan biostratigraphy. The skeleton consists of postcranial elements including cervical, dorsal and caudal vertebrae, a partial pectoral girdle, proximal elements of the forelimbs, a partial pelvic girdle, and representative portions of the hindlimbs. This fossil represents the most complete, single skeleton of a dinosaur known from Alaska, and one of the few skeletal remains recovered outside of the North Slope. It is only the second North American Turonian hadrosauroid described, the other being *Jeyawati rugoculus* from New Mexico. This specimen also represents a new taxon of basal hadrosauroid that can be diagnosed by its unique combination of humeral, ilial, and femoral characters. A phylogenetic analysis recovers the new taxon nested within a paraphyletic assemblage of non-hadrosaurid hadrosauroids, being more derived than the North American Cenomanian taxa *Eolambia* and *Protohadros* but more basal than stratigraphically younger hadrosauroids from Asia, including *Tanius*, *Bactrosaurus*, and *Gilmoreosaurus*. The temporal and geographic occurrence of the Alaskan taxon provides an important new data point for hypotheses of hadrosauroid biogeography in the Late Cretaceous.

Table of Contents

List of Figures

Chapter 1 – Introduction to the Talkeetna Mountains Hadrosaur (UAMES 12275)

Chapter 2 – The Geology and Taphonomy of UAMES 12275

Chapter 3 – Description

List of Tables

Chapter 1: Introduction to the Talkeetna Mountains Hadrosaur (UAMES 12275), its Geologic Setting, and Potential Significance

1. Geography

The Talkeetna Mountains Hadrosaur (UAMES 12275) was discovered by accident during excavation of a quarry in the Matanuska Valley, approximately two hours northeast of Anchorage, along the Glenn Highway/Alaska Route 1 in 1994 (Fig. 1.1). The initial discovery was made by Elisabeth May, daughter of one of the principal authors on the first two papers published on this fossil.

The fossil was recovered from the Matanuska Formation (Albian-Maastrichtian) over the course of two field seasons (1994 and 1996) as a mix of loose bone in shale and loose to partially articulated elements embedded in well-indurated carbonate concretions. Kevin May prepared material from the shale matrix and collaborated with Dr. Ann Pasch from the University of Alaska Anchorage on two papers discussing the taphonomy and biostratigraphy of the fossil (Pasch and May, 1997; 2001). Difficulties stemming from the well-indurated nature of the carbonate concretion led to the preparation process being abandoned. UAMES 12275 languished in the University of Alaska Museum's Earth Science Collection until 2008, when the remaining material was prepared mechanically and chemically.

2. Hadrosauriformes, Hadrosauroidea, and Hadrosauridae

The Hadrosauriformes (known colloquially as 'duck-bills') were a diverse and successful clade of non-avian ornithischian ornithopod dinosaurs whose earliest members evolved in the middle Early Cretaceous (Barremian, ~130-125 Ma; Horner, Weishampel, and Forster, 2004; McDonald et al., 2010). The diversity of the group increased through the Cretaceous and peaked during the Campanian-Maastrichtian with the radiation of its most derived members (the Hadrosauridae) prior to the

Figure 1.1: Map Alaskan hadrosauriform body fossil sites in relation to each other and major cities. Dark gray areas on land represent national parks. Image modified from Google Maps, ©2011 Europa Technologies, Geocentre Consulting, Google.

eradication of all non-avian dinosaurs in the end-Cretaceous mass extinction (Horner, Weishampel, and Forster, 2004; Lund and Gates, 2006).

The nomenclature of this group of dinosaurs is complicated by the similarity of the informally used group name ('hadrosaurs' *sensu lato*) to the less-inclusive sub-groups that compose it. Hadrosauriformes (hadrosauriforms) is the most inclusive level, encompassing every dinosaur more closely related to *Iguanodon* and its descendants than the polytomous assemblage of *Cedrorestes* + *Dakotadon* + *Iguanacolossus* + *Lanzhousaurus* (McDonald et al., 2010). The Hadrosauroidea (hadrosauroids) is composed of *Hadrosaurus foulkii* Leidy, 1858 and all taxa more closely related to it than to *Iguanodon* (Prieto-Marquez, 2010a). Finally, the Hadrosauridae (hadrosaurids,

or hadrosaurs *sensu stricto*) is the most exclusive group and is comprised of the most recent common ancestor of *Hadrosaurus foulkii* Leidy, 1858, *Edmontosaurus regalis* Lambe, 1917b, *Saurolophus osborni* Brown, 1913, and *Lambeosaurus lambei* Parks, 1923, and all its descendants (Prieto-Marquez, 2010a). In the same way that all squares are rectangles but not all rectangles are squares, all hadrosaurids are hadrosauroids, but not all hadrosauroids are hadrosaurids. Figures 1.2, 1.3, and 1.4 are simplified phylogenies showing the position of Hadrosauriformes within Dinosauria and its subdivisions into Hadrosauroidea and Hadrosauridae.

Of the three broad taxonomic groups comprising the Hadrosauriformes, the best known and understood is the Hadrosauridae, the most derived group of animals to evolve before the lineage's extinction at the end of the Cretaceous Period. It is currently believed that the Hadrosauridae arose in North America during the Santonian (~86-83.5 Ma) before diversifying and migrating to South America, Europe, and Asia throughout the Campanian-Maastrichtian (~83.5-66 Ma) (Prieto-Marquez, 2010b).

The basal hadrosauroids, a paraphyletic assemblage of forms from whom the common ancestor of the Hadrosauridae would arise, however, are significantly less well-known. Depending upon various authors, the number of known basal hadrosauroids falls somewhere between half a dozen (Godefroit et al., 2005) and thirteen (Prieto-Marquez and Norell, 2010; You and Li, 2009) species, compared to the dozens of species of hadrosaurids known. This lack of knowledge of the early evolution of Hadrosauroidea is particularly acute when one considers the late Cenomanian to early Santonian (~95-87 Ma), the period immediately prior to the hadrosaurid explosion recorded in Campanian-Maastrichtian strata: only two hadrosauroids (*Jeyawati rugoculous* of New Mexico and *Levnesovia transoxiana* of Uzbekistan) are known from this entire 8-million year timeframe.
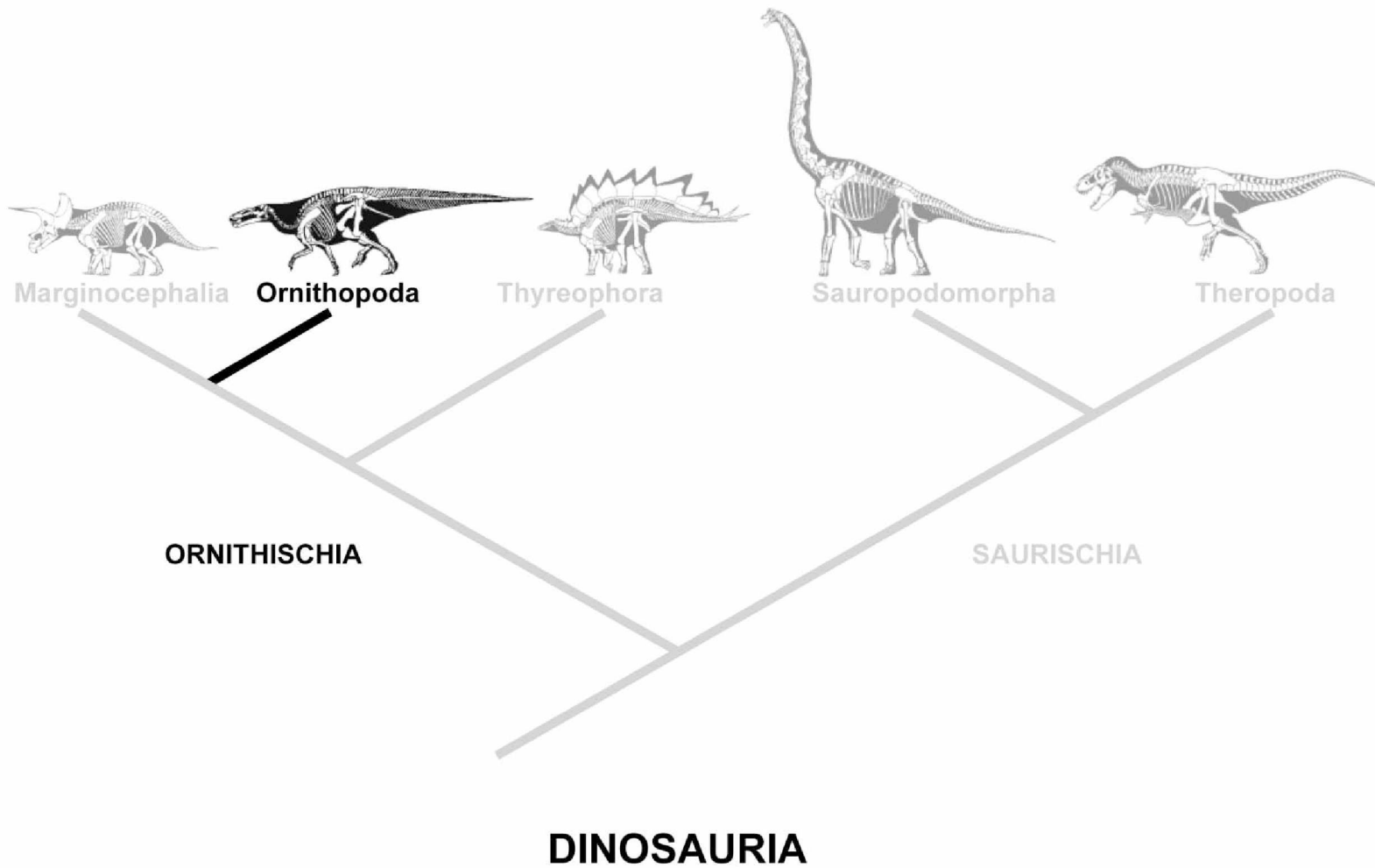
Figure 1.2: Simplified phylogeny of the Dinosauria showing the position of the Ornithopoda within Ornithischia. Hadrosauriformes is nested within Ornithopoda. Modified from: http://www.geol.umd.edu/~tholtz/G104/handouts/104Dinosauria.pdf
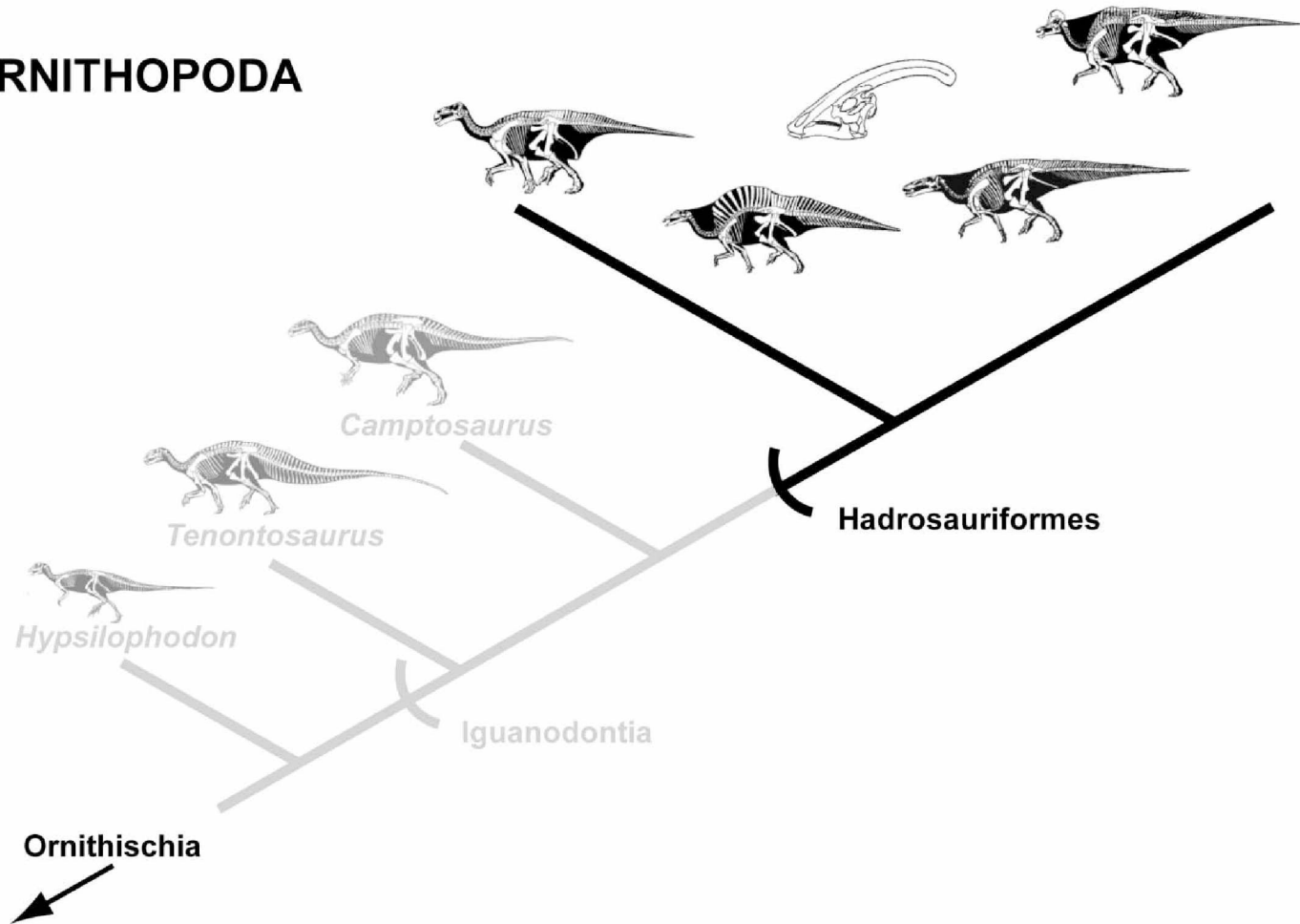
Figure 1.3: Simplified phylogeny of the Ornithopoda showing the position of the Hadrosauriformes relative to more primitive clades.
Modified from: http://www.geol.umd.edu/~tholtz/G104/handouts/104Styracosterna.pdf

HADROSAURIFORMES

basal hadrosauroids =
non-hadrosaurid hadrosauroids

Gilmoreosaurus

Bactrosaurus

Eolambia

Hadrosauridae

Mantellisaurus

Hadrosauroidea

Iguanodon

Iguanodontia
+
Ornithischia
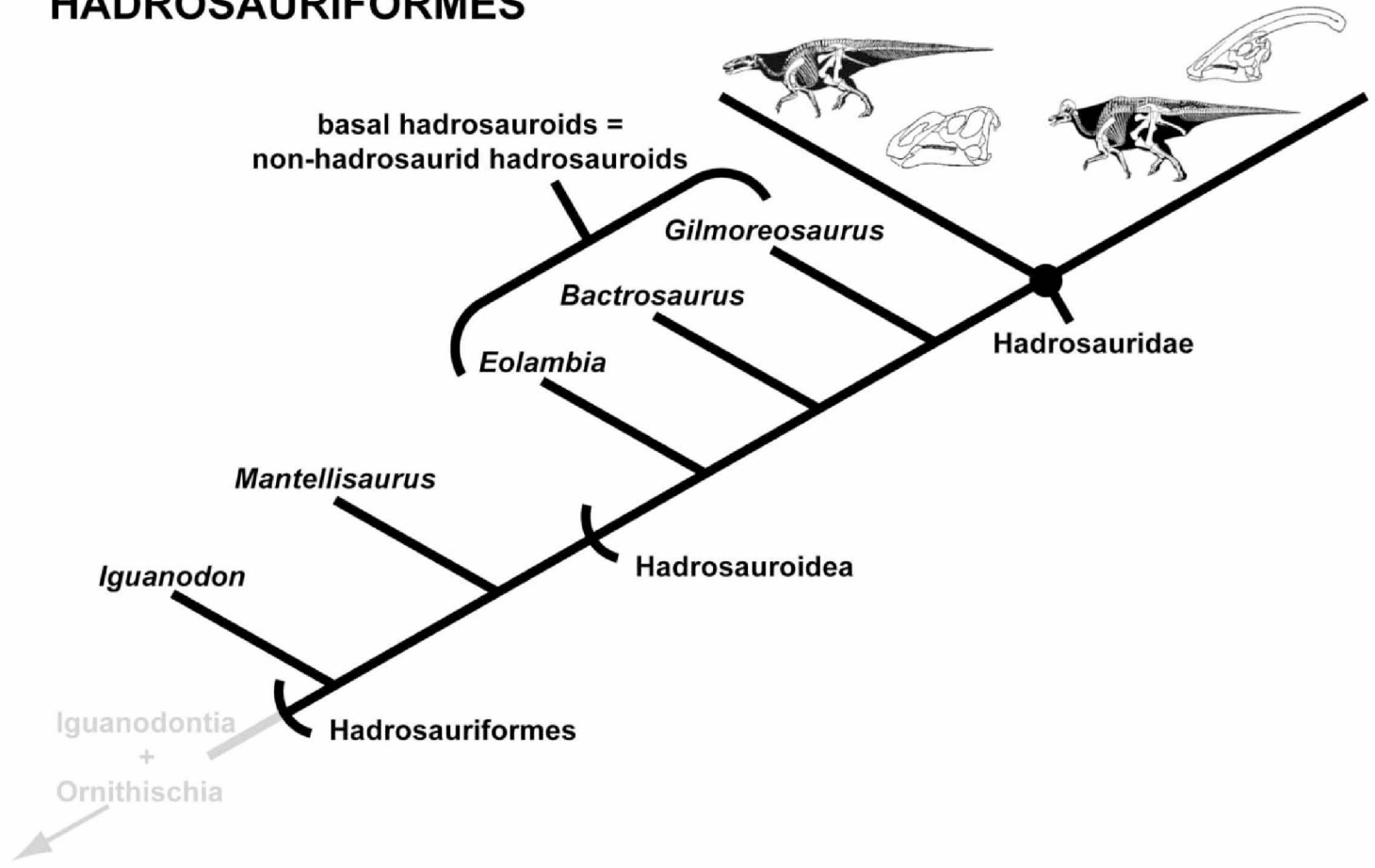
Hadrosauriformes

Figure 1.4: Phylogeny of the Hadrosauriformes, showing its subdivisions into the Hadrosauroidea and the Hadrosauridae. The terms "basal hadrosauroids" and "non-hadrosaurid hadrosauroids" will be used interchangeably throughout this thesis. Modified from: http://www.geol.umd.edu/~tholtz/G104/handouts/104Styracosterna.pdf

With the exception of UAMES 12275, the Alaskan fossil record of Hadrosauriformes is restricted to tracks in the Campanian-Maastrichtian Cantwell Formation of Denali National Park (Fiorillo, 2006), and body fossils and tracks from the Campanian-Maastrichtian Prince Creek Formation of the North Slope (Gangloff, 1998; Fiorillo 2006). Body fossils from the Liscomb bone bed are invariably scattered elements of juvenile or subadult animals that are currently attributed to *Edmontosaurus* sp.. The focus of this thesis, UAMES 12275, is the first hadrosauriform body fossil found south of the Brooks Range, as well as the most complete individual hadrosaur (*sensu lato*) known from the state of Alaska.

3. Taphonomy and Biostratigraphy

Hadrosaurs, like all dinosaurs, were strictly terrestrial animals, and the occurrence of UAMES 12275 within a marine shale interval of the Matanuska Formation means the fossil is a "bloater and floater" that was swept out to sea before eventually sinking to the bottom (Pasch and May, 1997; Pasch and May, 2001). Postmortem modification to the skeleton shows evidence of scavenging by vertebrates and probable exploitation by invertebrates and microbes (Pasch and May, 1997; Smith and Baco, 2003; Barnes and Hiller, 2010).

UAMES 12275 has been assigned a Turonian age based on invertebrate fossils recovered from the quarry (Pasch and May, 1997; 2001), placing the fossil squarely in the middle of the Cenomanian-Santonian 'gap' discussed above.

4. Regional and Global Significance

From an Alaskan perspective, UAMES 12275 represents the only collection of hadrosaur (*sensu lato*) remains in the state that can confidently be attributed to a single individual. It is also the most complete dinosaur skeleton known from anywhere in Alaska. *Alaskacephale gangloffi*, a pachycephalosaur known from a lone

left squamosal, is the only named dinosaur taxon unique to Alaska (Gangloff, Fiorillo, and Norton, 2005; Sullivan, 2006). Given the age of UAMES 12275 and our dearth of knowledge of hadrosauroid evolution from the Cenomanian to Santonian, it raises the possibility that UAMES 12275 represents a new Alaskan dinosaur taxon.

Globally, UAMES 12275 is only the third hadrosaur (*sensu lato*) known from the Turonian. Given the distribution of *Jeyawati* (New Mexico) and *Levnesovia* (Uzbekistan), this fossil will add to our knowledge of Cenomanian-Santonian evolutionary gap, as it will expand the known paleogeographic range of the Hadrosauriformes and potentially provide insights into the paleobiogeography of the group as well.

5. Thesis Scope and Goals

My efforts in this project have been focused on four main areas:

1. Constructing a more complete picture of the taphonomy of UAMES 12275, focusing in particular upon modification/utilization of the carcass by opportunistic vertebrate, invertebrate, and microbial marine organisms.

2. Assessing the current biostratigraphic age assignment of the fossil through the use of palynomorphs and foraminiferans.

3. Providing an osteological description of the specimen and comparison with known taxa to evaluate its potential as a new taxon and identify autapomorphies (if any) or unique suites of skeletal characters.

4. Conducting a phylogenetic analysis of the specimen to determine its relationships within Hadrosauriformes.

Each chapter of the thesis will be devoted to one of the goals in the above list and will provide needed background material before delving into methodologies and thought

processes. A summary chapter will tie the key ideas of the previous chapters together and discuss the implications of my conclusions.

Chapter 2: The Geology and Taphonomy of UAMES 12275

1. Regional Geology and Paleogeography

   1. Regional Geology

   Southern Alaska is composed of numerous accreted allocthonous terranes and is regarded as a classic region in which to study the processes controlling continental accretion (Trop, 2008; Coney et al., 1980; Plafker and Berg, 1994; Trop and Ridgway, 2007). The largest of these terranes extends from the Alaska Peninsula in the northwest to Vancouver Island in the southeast. In southern Alaska, it is lodged between the Alaska Range to the north and the Chugach Range to the south. The Talkeetna Mountains of the Matanuska River Valley region are a part of this massive composite terrane, which goes by many names; I prefer the term Wrangellia Composite Terrane (Plafker and Berg, 1994) and will use that exclusively in this thesis.

   Sedimentary rocks of Middle Jurassic to Oligocene age crop out in the Matanuska River Valley of southern Alaska and lie nonconformably atop Jurassic igneous rocks of the Talkeetna oceanic arc, which forms a section of the Wrangellia Composite Terrane (Trop, 2008). The timing of accretion of the Wrangellia Composite Terrane to the inboard Yukon-Tanana Terrane is equivocal: authors have proposed dates ranging from Triassic to early Late Cretaceous (Garver, 1992; Umhoefer, 2003; Wyld and Umhoefer, 2006; Hampton et al., 2007). Post-collision magmatism of Late Cretaceous-Paleocene age, attributed to the northward (present coordinates) subduction of the Pacific Plate under North America, marks the final suturing of the Wrangellia Composite Terrane with the Yukon-Tanana Terrane (Trop, 2008).

   The Matanuska Formation is a thick (>3 km) succession of shale, sandstone, turbidites, and conglomerate deposited in a forearc basin along the southern

(present coordinates) margin of the Wrangellia Composite Terrane (Grantz, 1964; Trop, 2008). The sediment accumulated over a period of time spanning the Albian to Maastrichtian (~112-66 Ma). The Matanuska Formation rests unconformably upon the Middle Jurassic Naknek Formation in the Matanuska Valley itself; to the north, in the region of Limestone Gap and the Little Nelchina River, it is underlain by the Lower Cretaceous Nelchina Limestone. Unnamed sedimentary and volcanic rocks of Paleogene age crop out above the Matanuska Formation (Trop et al., 2002). Figure 2.1 is a simplified stratigraphic column showing the Mesozoic rocks exposed in the Matanuska Valley.

2. Paleogeography

The paleolatitude of the Wrangellia Composite Terrane in the mid-Cretaceous is the subject of intense debate among members of the geological community. Fault reconstruction and sediment source models argue for < 1000 km of northward displacement (present coordinates) of the terrane since approximately 100 Ma (Wyld and Umhoefer, 2006). Paleomagnetic studies, however, argue for 1600+ km of northward displacement (present coordinates) since approximately 100 Ma (Umhoefer and Blakey, 2006). 1000 km of northward displacement or less translates into approximately 9° latitude of displacement at maximum. I favor the model requiring < 1000 km of northward displacement for three reasons:

1. Trop (2008) argues that the upper Matanuska Formation (Campanian-Maastrichtian strata) includes recycled sediment from the Yukon-Tanana Terrane and/or the Kahiltna Assemblage, a package of dominantly marine sedimentary rocks located in the suture zone between the Wrangellia Composite Terrane and the Yukon-Tanana Terrane. The Kahiltna Assemblage is located approximately 200 km to the north of the quarry site (present coordinates). This seems to suggest that the Kahiltna Assemblage and the Cretaceous sediments of the Matanuska
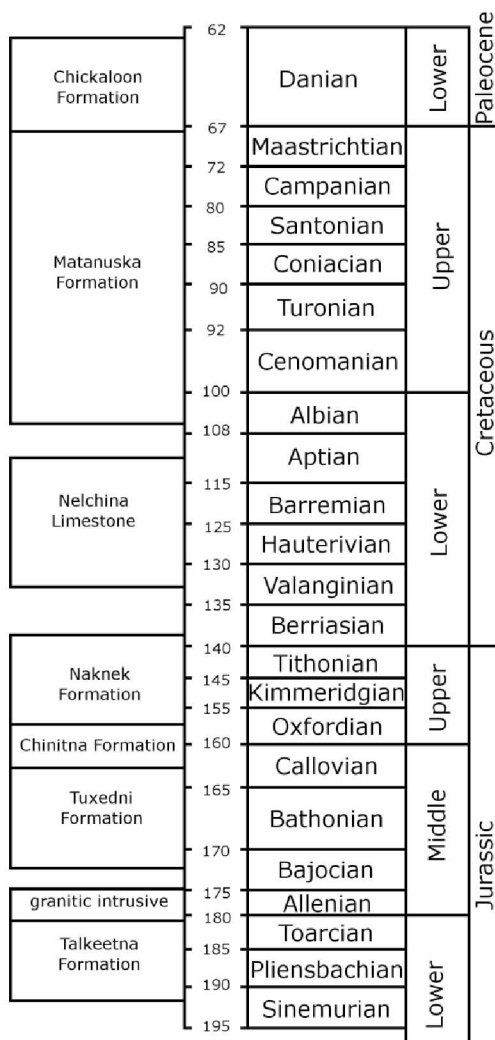
Fig. 2.1: Simplified stratigraphic column of the Talkeetna Mountains showing temporal relationships between exposed strata. Note that thickness in time does not necessarily correlate with actual unit thickness. Modified from Schaff and Gilbert (eds.), 1987.

River Valley have been in close proximity since at least the Campanian. In turn, this suggests the Wrangellia Composite Terrane was located outboard of the Yukon-Tanana Terrane by the Campanian or earlier, and that there may have been a terrestrial link between the Wrangellia Composite Terrane and North America by this time.

2. A paleomagnetic study of the Campanian (~83.5-70.5 Ma) MacColl Ridge Formation from Wrangell-St. Elias National Park to the east of the dinosaur site suggests that the formation was deposited around 80 Ma at a paleolatitude of ~53° N versus its present latitude of ~61° N. (Stamatakos et al., 2001). Unless plate motion velocities during the Late Cretaceous were significantly faster than those currently observed, it is unlikely that the Wrangellia Composite Terrane could have traversed more than approximately 4° of latitude (or roughly 450 km) between the Turonian and Campanian.

3. The Methow-Tyaughton Basin, a sedimentary basin which is developed on three small tectonostratigraphic terranes (Cadwallader, Bridge River, and Methow) sandwiched in between the Wrangellia Composite Terrane and the inboard Intermontane Superterrane, contains an Albian-aged formation with detrital zircons older than 2.5 Ga. Similarly ancient zircons are known from the Queen Charlotte and Nanaimo Basins, which were developed on southern segments of the Wrangellia Composite Terrane. The only known sources for zircons of this age in North America crop out no further south than approximately 40° N latitude, or roughly the California-Oregon border (Mahoney et al., 1999).

Most workers reconstruct the Wrangellia Composite Terrane as an approximately linear belt off the coast of North America (Johnston, 2001; Umhoefer, 2003; Umhoefer and Blakey, 2006; Wyld and Umhoefer, 2006). Following their lead and using the translation constraints suggested above places UAMES 12275 at

approximately 53° N latitude (present coordinates), or off the coast of British Columbia roughly midway between Queen Charlotte Island to the north and Vancouver Island to the south. Given the margins for error inevitable in paleolatitude estimates regardless of method and that the site of UAMES 12275 was likely further north than what would become the depositional environment of the MacColl Ridge Formation, this does not appear to be an unreasonable result.

It is probable that the Wrangellia Composite Terrane had already docked with continental North America some time before the Turonian, as hadrosauriform dinosaurs were entirely terrestrial animals and it is unlikely that they could have migrated long distances across open ocean to reach new habitat. The presence of a marine basin (the Kahiltna Assemblage) to the north of the Wrangellia Composite Terrane suggests that terrestrial links between the Wrangellia Composite Terrane and continental North America were intermittent, rather than constant, and that the spatial relationship between the terrane and North America when UAMES 12275 was alive may have been similar to what currently exists between Baja California and Mexico proper, or Queen Charlotte Island/Vancouver Island and Canada proper.

2. Objectives and Methodology

1. Additional Preparation

As discussed previously, preparation of UAMES 12275 halted after the bones encased only in shale were prepared due to the well-indurated nature of the carbonate concretions. Traditional mechanical preparation using airscribes was supplemented with acid treatment using a 20% formic acid solution. Bones were coated 3-6 times with vinac before being submerged in the acid solution to prevent accidental dissolution of bone. Unfortunately, the vinac layers did not protect the bones as well as hoped.

2. Mineralogy

Pasch and May (1997; 2001) neglected to report on the mineralogy of either the quarry shale or the carbonate concretions recovered with the fossil. As both their papers were concerned chiefly with the nature and significance of UAMES 12275, this is understandable. However, sedimentary mineralogy is an important part of piecing together the puzzle of environment and depositional setting (i.e. glauconite as an indicator of reducing marine settings).

Due to the fine-grained nature of the sediment, the mineralogy of the shale had to be analyzed utilizing a combination of x-ray diffractometry (XRD) and x-ray fluorescence (XRF) spectrometry. Pulverized smear mounts were scanned with a Rigaku MiniFlex II Desktop X-ray Diffractometer to identify major minerals present in both the shale and the concretions. I conducted major element analysis via XRF to provide semi-quantitative data on the differences in relative mineral abundances between the shale and the concretions. A total of 7 pressed pellets (2 composed of pulverized shale and 5 composed of pulverized carbonate concretion) were analyzed using the University of Alaska Advanced Instrumentation Laboratory's PanAlytical Axios 4 kW Wavelength Dispersive XRF.

Based on analyses of natural rock standards not employed in the standardization of the major elements, Si, Al, Fe, K, and Ca display a precision of 0.2% of the amount present and accuracy within 1% of the amount present (e.g., for a rock with 50% SiO_2 the error is approximately +/- 0.5%). For the elements Mg, Na, Mn, Ti, and P the precision is ~ .5% of the amount present and accuracy ~ 5% of the amount present (e.g., for 5.0% claimed, the value is most likely 5.0% +/- 1.25% of that) (Newberry, pers. comm.).

Average compositions for the major minerals identified via x-ray diffractometry were calculated from analyses in Deer et al. (1996) and converted into percent concentrations of major oxides (SiO_2, TiO_2, Al_2O_3, etc.) present in a given mineral (for example, the concentration of SiO_2 in quartz is 100%). Given these average compositions and the XRF data, the next step was to calculate the abundance of the minerals identified via XRD that best approximated the XRF results. Large differences (i.e., > +/- 10%) in TiO_2, MnO, Na_2O, K_2O, and P_2O_5 in calculated abundance versus measured abundance were deemed acceptable due to the low concentrations of these elements in both the rocks and the major minerals identified by XRD. For all other oxides, efforts were made to keep the difference between measured concentrations and calculated concentrations at or below +/- 5%.

3. Sedimentology

Pasch and May (1997; 2001) reported on the sedimentology of the quarry and provided their own interpretation of the data: UAMES 12275 sank to the bottom in relatively deep marine waters (>50m, based on the invertebrate community present; Pasch and May, 1997; 2001) and was entombed within oxygen-deficient sediments. The decomposing tissues of the carcass formed precursor material as suggested by Berner (1968) for the eventual formation of carbonate concretions.

I wished to examine the evidence for myself and test the conclusions made by Pasch and May (1997; 2001) in their papers. This necessitated examination of thin sections of both quarry shale and carbonate concretion under plane- and crossed-polarized light to search for sedimentary structures, microfossils, and trace fossils.

4. Biostratigraphy

Pasch and May (1997; 2001) assigned a Turonian age to UAMES 12275 based on foraminifera and invertebrates collected from the quarry site. The presence of the ammonite *Muramotoceras* sp. (Matsumoto, 1977) was cited as particularly strong evidence of the site's Middle Turonian age because this genus was, up until this discovery, only known from Middle Turonian sequences in Japan (Pasch and May, 2001). They reported the presence of fossil palynomorphs but did not elaborate on form genera recovered (Pasch and May, 2001). Reid and Pasch (1999) identified 85 different form genera in a study of the paleoecology of the region inhabited by UAMES 12275, but made no mention of any biostratigraphic implications.

I wished to corroborate and expand upon the age assignment for the fossil. The potential significance of UAMES 12275, combined with the knowledge that identifiable palynomorphs had been recovered in abundance from the site, suggested that palynomorph biostratigraphy could provide further age constraints.

Samples of quarry shale and carbonate concretion were pulverized and treated with hydrochloric and hydrofluoric acids to free remnant organic matter, the standard method of preparing fossil pollen for analysis (Traverse, 2008). Once the organic matter had been concentrated, glycerin jelly was added and the mixture was placed onto several slides and studied with a Nikon OptiPlot 2 transmitted light microscope.

5. Taphonomy

The occurrence of a terrestrial animal in marine sediments is not entirely uncommon. Horner (1979) listed nearly 100 occurrences of Late Cretaceous dinosaur remains in marine sediments from North America alone, and the Italian non-hadrosaurid hadrosauroid *Tethyshadros insularis* Vecchia (2009) is known

strictly from occurrences in a chalk lens within the Campanian-Maastrichtian Liburnian Formation (Vecchia 2009).

Barring a tsunami, transport of a terrestrial animal to a marine setting requires bloating of the carcass from decomposition gases to achieve buoyancy and a river or stream to move the carcass once it has become buoyant. Eventually, the gases escape, whether by sufficient decomposition of the body cavity or breaching of the body cavity by scavengers. Having lost its buoyancy, the carcass sinks to the sea floor (Pasch and May, 2001).

Based on research into modern whale falls (both natural and artificial), Smith and Baco (2003) propose that large vertebrate carcasses on the seafloor undergo three major decompositional stages, followed by a final "reef" stage:

1. Mobile-scavenger stage: sharks, hagfish, and other scavengers remove soft tissues from the carcass. Depending on the size of the carcass, this stage could last anywhere from days to years.

2. Enrichment opportunist stage: sloppy eating by the large scavengers during stage 1 would enrich sediment in the vicinity of the carcass with organic matter, which could then be exploited by opportunistic detritus feeders such as polychaetes and crustaceans. Again, depending upon the size of the carcass, this stage could last from weeks to years.

3. Sulphophilic stage: a chemosynthetic community based around the production of sulfide from the anaerobic decay of bone lipids arises. This stage is believed to last from years to decades. Unlike stages 1 and 2, which are controlled by carcass size, this stage is presumably controlled by both carcass size and the amount of lipid present in the bones of the carcass.

4. Reef stage: Now depleted of organic matter, encrusting filter-feeding organisms favoring hard ground conditions colonize the skeleton exposed above the sediment-water interface to exploit enhanced water currents around the bones.

Given the reliance of taphonomic interpretation of fossils upon the principle of uniformitarianism, it is presumed that similar processes affected large vertebrate falls in the early Late Cretaceous (Hogler, 1994). The taphonomy of UAMES 12275 will be discussed in terms relating to the stages of Smith and Baco (2003) and will then be compared to and contrasted with an elasmosaurid plesiosaur (Reptilia, Sauropterygia, Plesiosauria) fall from the Maastrichtian of New Zealand (Barnes and Hiller, 2010).

3. Results

1. Lithology and Mineralogy

UAMES 12275 was excavated from a poorly indurated, dark gray, thinly laminated shale interval of the Matanuska Formation. Pasch and May (2001) reported visible laminae and signs of bioturbation on wet fresh surfaces, but I was only able to see these in thin section. The unit is cut by two sets of joints, and a third poorly developed or wavy cleavage plane causes chips to break off with concavo-convex surfaces. Very well indurated carbonate concretions of variable morphology are present and restricted to the immediate vicinity of the fossil; some contain fossil bone, others are barren save for microscopic bone fragments. A system of quartz-calcite veins and veinlets crosscuts the largest of the carbonate concretions and postdates concretion lithification based on isolated occurrences of brecciated concretion suspended within a matrix of coarsely crystalline quartz + calcite.

Table 2.1 summarizes the major element compositions of the samples, listed as percent oxides. These data were then utilized to calculate percentages of major

minerals present, as explained in the methods section above. See Table 2.2 for calculated percentages of major minerals.

Table 2.1: Major element analysis of 7 pressed pellet samples expressed as percent oxides. Fe_2O_3* includes both FeO and Fe_2O_3.

	SiO_2	TiO_2	Fe_2O_3*	MnO	MgO	CaO	Na_2O	K_2O	P_2O_5
TMH Matanuska 3mB	66.3	0.85	7.91	0.14	2.67	1.41	1.33	2.20	0.18
TMH Matanuska 3mB1	66.3	0.83	7.89	0.14	2.64	1.43	1.32	2.18	0.18
TMH Concretion 1	51.8	0.76	6.91	1.63	2.18	19.5	1.25	1.66	0.46
TMH Concretion 2	53.6	0.74	7.17	1.48	2.25	16.9	1.29	1.75	0.33
TMH Concretion 2.2	53.5	0.74	7.22	1.48	2.26	17.0	1.29	1.76	0.33
TMH Concretion 3	46.0	0.70	6.61	2.14	2.01	26.5	1.12	1.66	0.19
TMH Concretion 3.2	45.8	0.70	6.59	2.14	2.03	26.5	1.15	1.65	0.20

Table 2.2: Major mineralogy of 7 pressed pellet samples expressed as percent abundance and based on quantification of major element data (Table X.1) and x-ray diffractometry of smear mount samples.

	Muscovite	Illite	Chlorite	Kaolinite	Glauconite	Albite	Quartz	Apatite	Calcite
TMH Matanuska 3mB	0	5	8	20	18	12	30	0	1.75
TMH Matanuska 3mB1	0	5	10	25	20	12	30	0	1.75
TMH Concretion 1	0	0	9	15	11	12	20	0.8	27
TMH Concretion 2	5	0	9	15	11	12	20	0.8	25
TMH Concretion 2.2	5	0	9	15	12	12	20	0.8	25
TMH Concretion 3	6	0	7	10	12	12	15	0.8	37
TMH Concretion 3.2	6	0	7	10	12	12	15	0.4	37

The quarry shale specimens are dominated by quartz, kaolinite, glauconite, and albite. Traces of chlorite, illite, and calcite are also present. In contrast, the quarry concretion specimens are dominated by calcite and albite. The trace mineralogy of the concretions is also different, as muscovite appeared while illite disappeared and traces of apatite are present.

2. Sedimentary Structures, Trace Fossils, Pyrite Framboids, and Microfossils

Thin sections of the quarry shale and concretions were analyzed for physical non-biogenic sedimentary structures, biogenic sedimentary structures, and microfossils.

A. *Non-biogenic sedimentary structures*: Fine laminae were the only non-biogenic sedimentary structures observed in any of the thin sections and were present in examined sections of both shale and concretion samples. (Figure 2.2)

B. *Trace fossils*: Structures suggestive of biologic activity include calcified worm tubes (Figure 2.3), peloids (Figure 2.4), and phosphatic clasts assumed to be remnant fragments of dinosaur bone (Figure 2.5). These structures occurred in thin sections of concretion material but were absent from thin sections of quarry shale. Invertebrate burrows were the rarest structure observed. Phosphatic clasts were abundant, typically ovoid or rounded, and ranged in size up to ~1 mm.
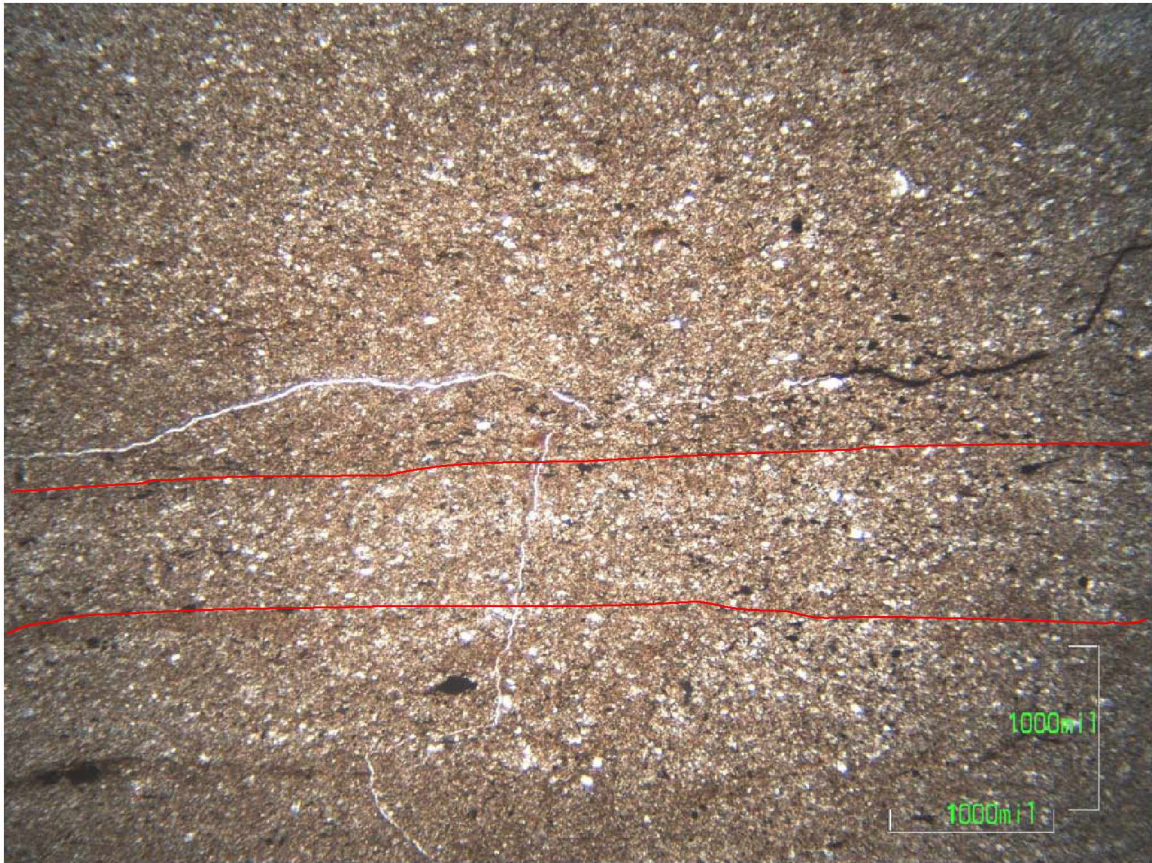
Figure 2.2: Laminated shale in an oriented thin section taken from a portion of the carbonate concretion in plane polarized light. Red lines highlight general trend of laminae. Scale bar: 1 mm
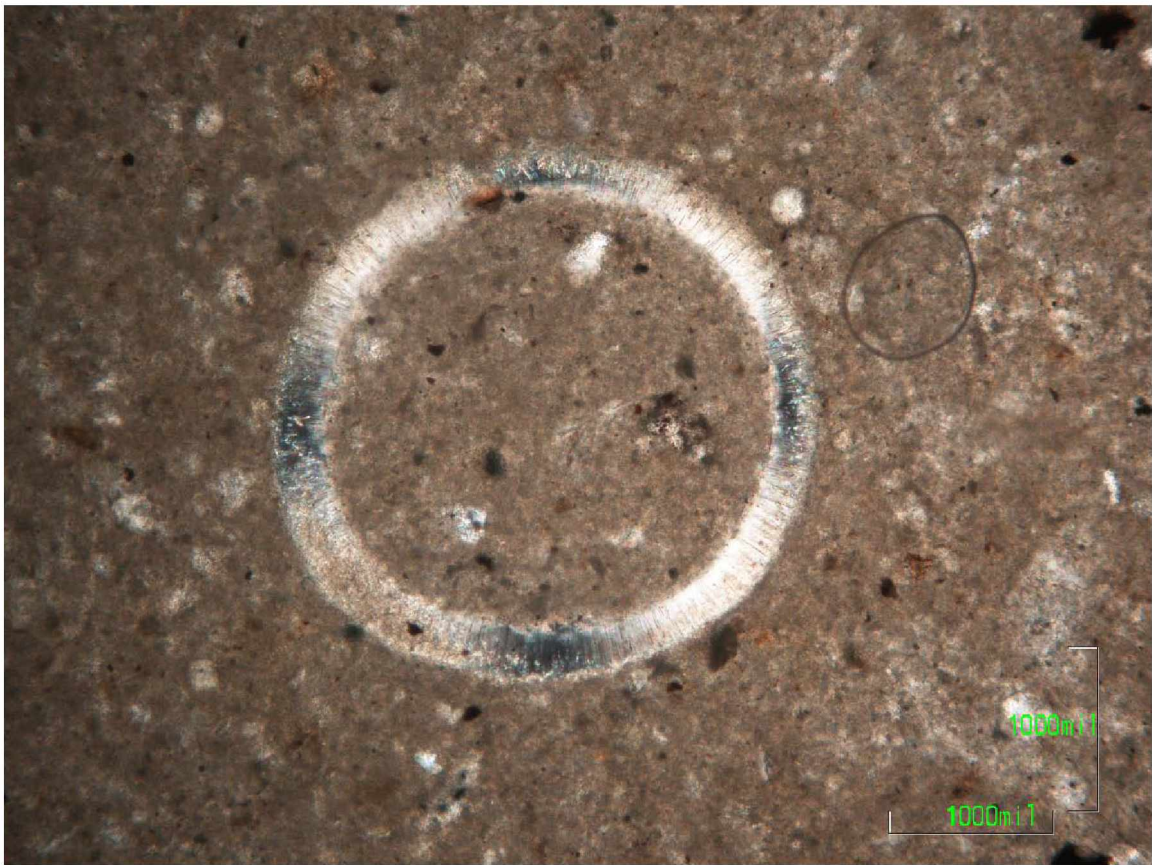
Figure 2.3: Latitudinal cross-section through a calcified worm tube(?), cross polarized light. Scale bar: 1 mm
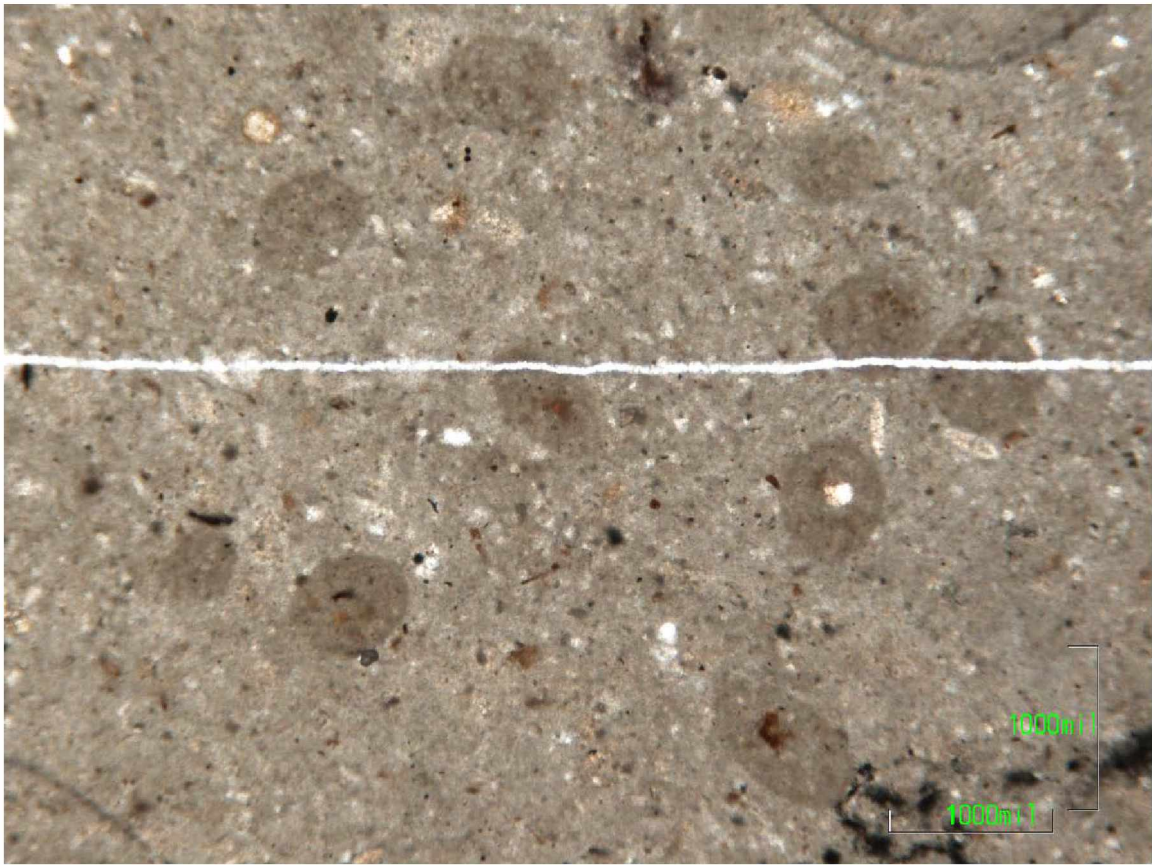
Figure 2.4: A grouping of large peloids from a thin section of the carbonate concretion, plane polarized light. Scale bar: 1 mm
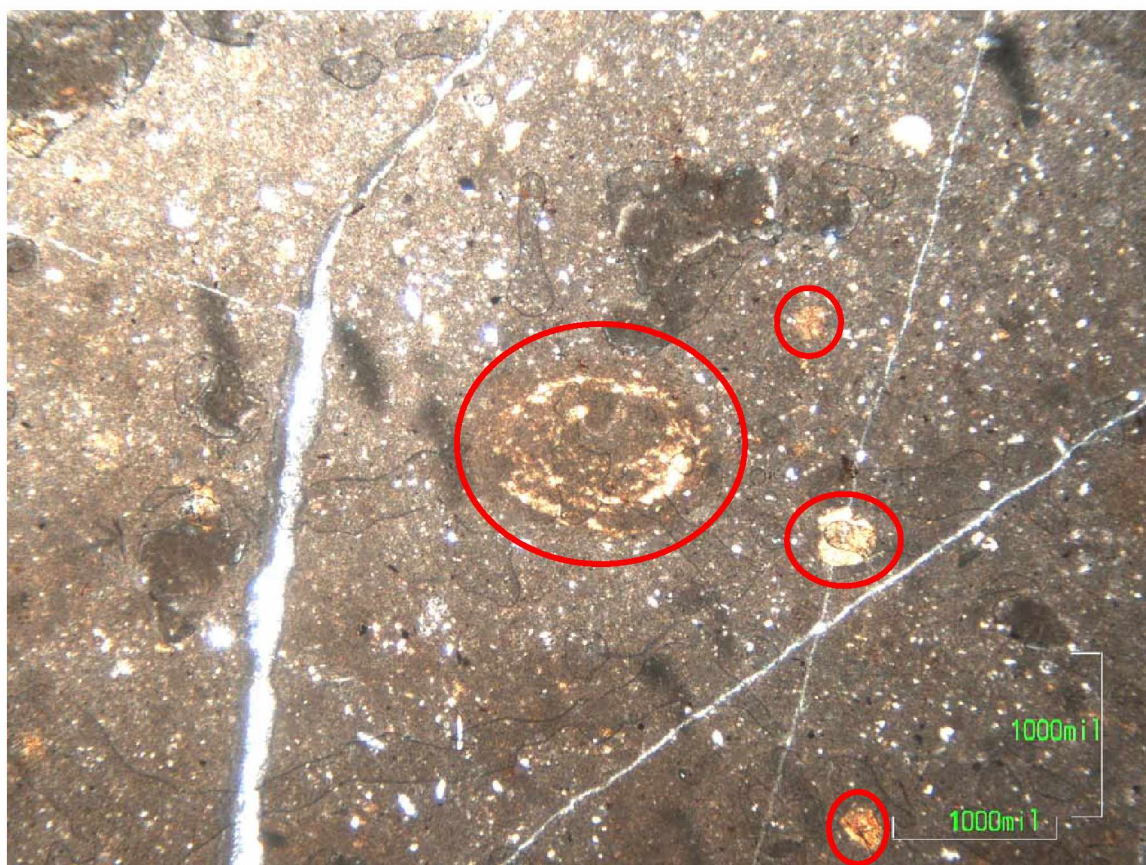
Figure 2.5: Macerated dinosaur bone fragments (outlined in red) in a thin section of the carbonate concretion, plane polarized light. Scale bar: 1 mm

C. *Pyrite Framboids*: The origins of framboidal pyrite are equivocal (Butler and Rickard, 2000; Folk et al., 1995; Mozer, 2010; Wilkin and Barnes, 1997), as framboids are known from the Bereznyakovskoe ore field in Russia (Plotinskaya et al., 2009), as well as more typical sedimentary settings, where their presence is used to infer sedimentary paleoredox conditions (Berner, 1970; Wignall and Newton, 1998; Wilkin et al., 1996).

Pyrite framboids of varying size and degree of infilling with secondary pyrite (Wilkin et al. 1996; see Figure 2.6) were noted in a number of thin sections and subsequently examined using the University of Alaska Fairbanks Advanced Instrumentation Laboratory's Cameca SX-50 electron microprobe to better characterize the scale and texture of the pyrite microcrystals in the framboids (Figure 2.7, Figure 2.8). Individual microcrystals appear to be on the order of 1-2 μm, while associations of microcrystals and euhedral pyrite cubes tend to be in the range of 5-10 μm. These size ranges are consistent with what has been observed in both natural and synthetic framboids (Ohfuji and Rickard, 2005). This seems to suggest that the different morphologies observed in the sediments associated with UAMES 12275 are the result of variable degrees of pyrite recrystallization and/or post-crystallization deposition of secondary pyrite affecting the first generation of pyrite (Wilkins et al., 1996). Unfortunately, there is no easy way to quantify the amount of secondary pyrite overprinting the original framboids, making analysis of framboid size distribution to determine paleoredox conditions impossible.
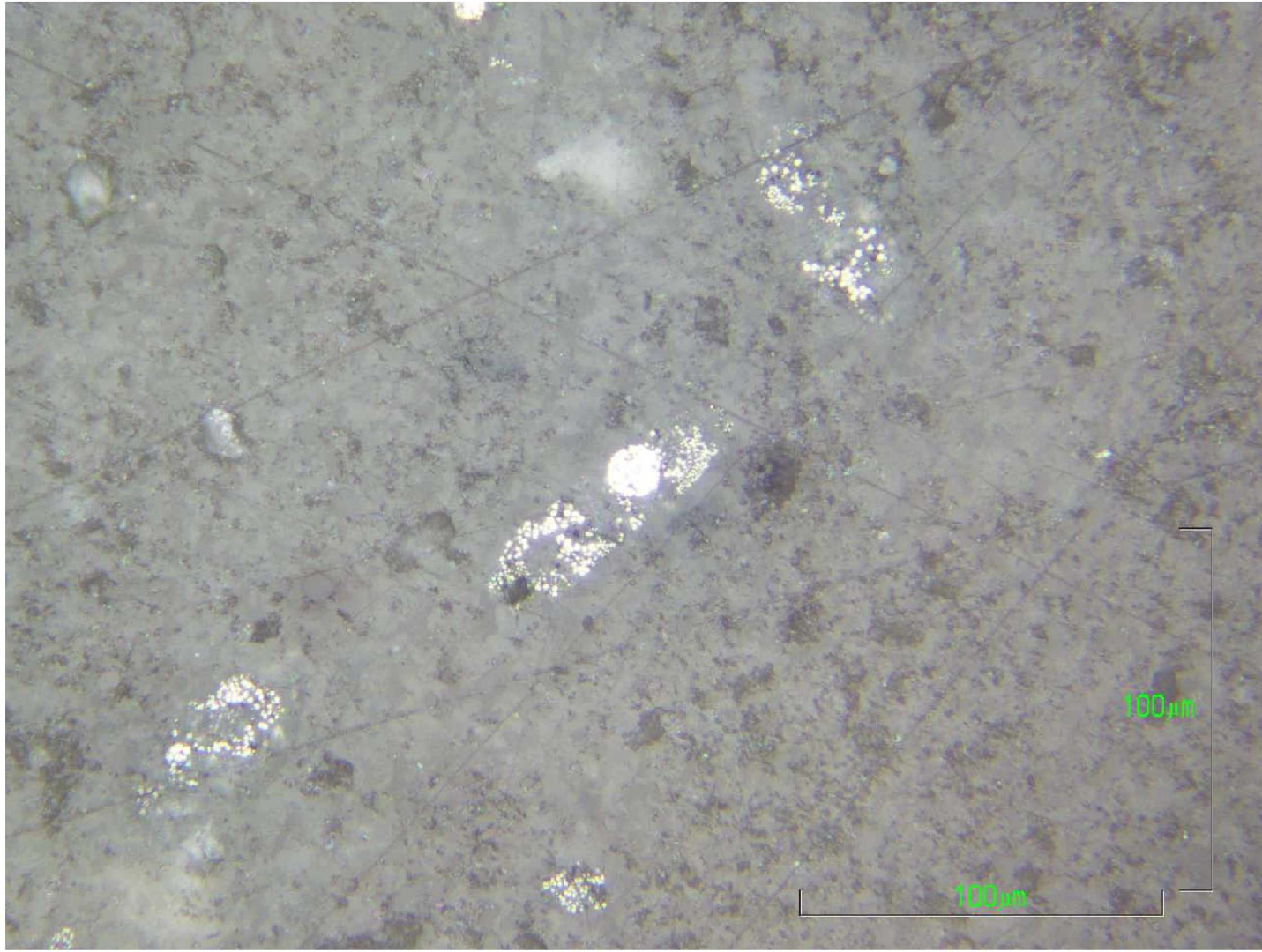
Figure 2.6: Disseminated pyrite framboids showing the variety of pyrite textures present over a small area common to the carbonate concretion, reflected plane polarized light. Scale bar: 1 mm
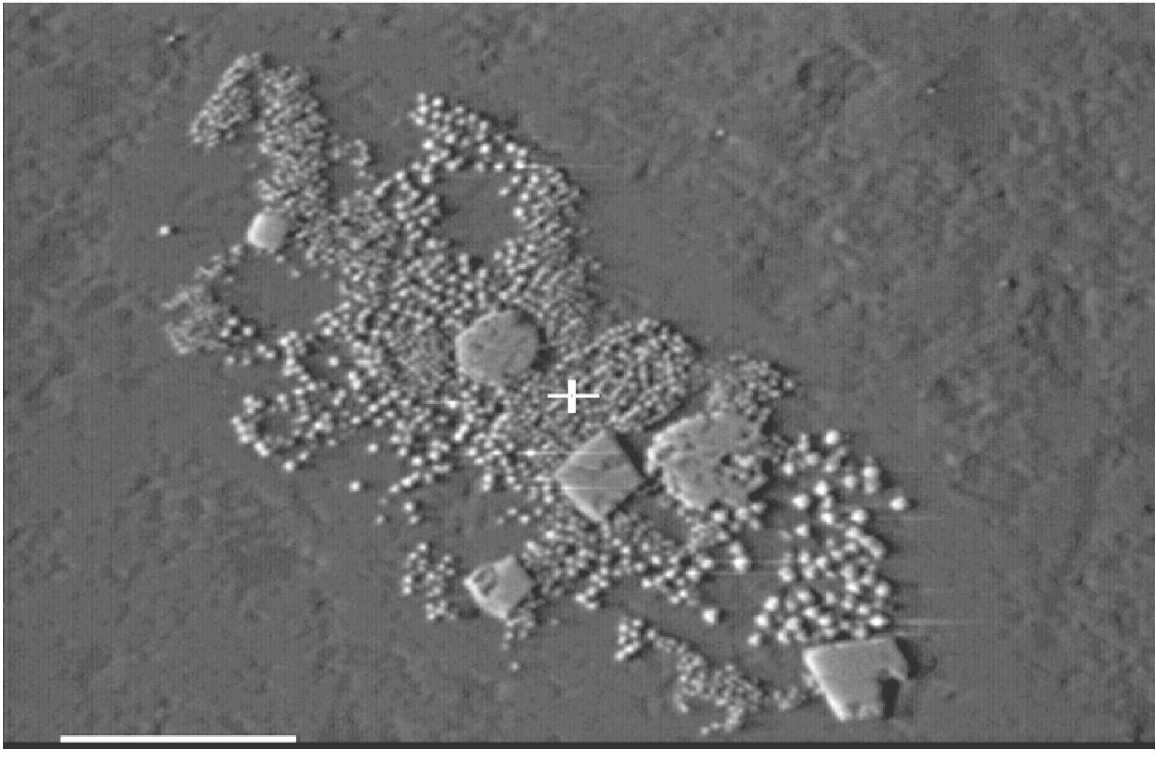
Figure 2.7: Electron backscatter image of disseminated pyrite taken with AIL's Cameca SX-50 electron microprobe, showing multiple textures in close association. Note the cubic crystal below the crosshairs and the two framboids partially filled in by secondary pyrite in close proximity to it. Scale bar: 20 μm.
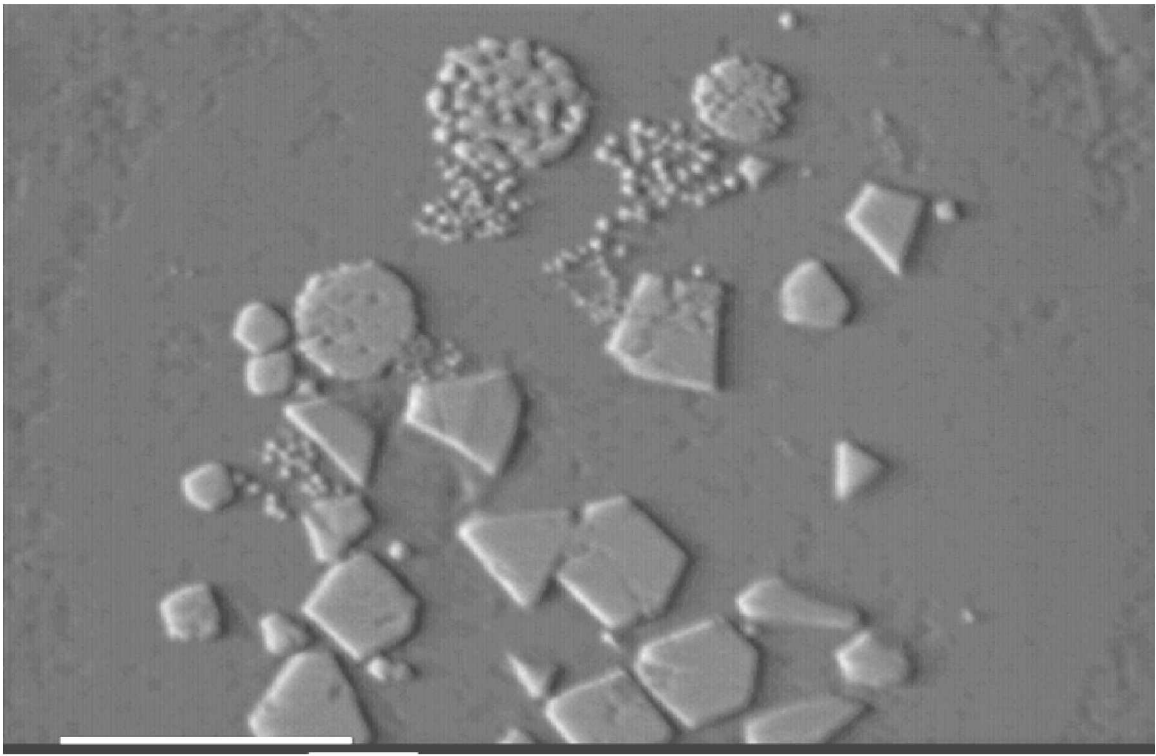
Figure 2.8: Disseminated pyrite framboids and crystals (electron backscatter image taken with AIL's Cameca SX-50 electron microprobe) showing multiple textures in close association. Note the differing degrees of secondary pyrite formation in the three framboids in the upper middle portion of the picture and their proximity to polygonal crystalline pyrite. Scale bar: 20 μm

In addition to being present in the concretion sediments, pyrite is also found on the surfaces of many of the recovered bones. The pyrite occurs in a variety of morphologies, including disseminated millimeter-scale patches, large centimeter-scale patches with obvious veins and rounded knobby protrusions, and as coatings on bone trabeculae where the exterior cortical bone is missing. These coatings are typically tarnished, and combined with the charcoal color of the bones they occur on, attempts to photograph these coatings have not been successful. The one common factor between all the occurrences of pyrite on bone surfaces is that all of the coating morphologies described above are exclusive to bones recovered from the quarry shale. In the carbonate concretions, pyrite only occurs as disseminated framboids and euhedral crystals in the matrix and never coats bones. Given the mutually exclusive nature of pyrite morphology plus pyrite location, it seems reasonable to suggest that the different morphologies are the result of different processes of formation. No further conclusions can be drawn beyond this broad generalization without sulfur isotope analysis to determine which (if any) pyrite morphology is systematically enriched in the light isotope favored by living organisms.

D. *Microfossils*: The only definitive microfossils found in the thin sections were tests of planktonic foraminifera (Figure 2.9; *Hedbergella* sp.?, *Whiteinella* sp.?). Figure 2.10 is a photograph of an unusual and unidentified specimen. It appears to be a silicified trilete spore, but I was unable to find any literature that dealt with the possibility of replacing sporopollenin.
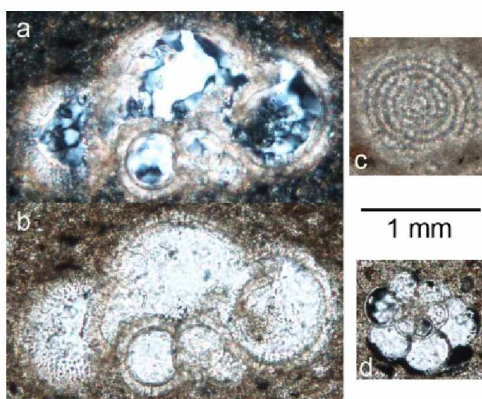
Figure 2.9: Light microscope images of 3 foraminifera from thin sections of carbonate concretion.
a: Longitudinal cross-section of a silica-filled planktonic foraminiferan in cross polarized light. *Hedbergella* sp. or *Whiteinella* sp.?
b: Longitudinal cross-section of the planktonic foraminiferan in photo a in plane polarized light.
c: Latitudinal cross-section of a benthic foraminiferan(?) in plane polarized light.
d: Latitudinal cross-section of a silica-filled planktonic foraminferan in cross polarized light. *Hedbergella* sp. or *Whiteinella* sp.?
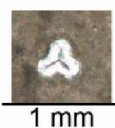
Figure 2.10: A silicified(?) trilete spore(?) found in a thin section of the carbonate concretion.

Palynological processing of samples of the shale and concretion were not as productive as initially hoped. Bisaccate gymnosperm pollen grains (*Parvasaccites* sp.) were found (Figure 2.11), as well as an abundance of trilete spores (*Appendicisporites* sp. in Figure 2.12, *Cicatricosisporites* sp. in Figure 2.13), but unfortunately all appear to belong to form genera that first arose in the Late Paleozoic or Early Mesozoic and endured into the Cenozoic. Organic remains that may be .

Figure 2.11: *Parvasaccites* sp., distal polar view. *Parvasaccites* is a bisaccate gymnosperm form genus ranging from the Upper Jurassic to the Lower Cretaceous (Traverse, 2008). Scale bar: 20 μm

Figure 2.12: *Appendicisporites* sp., distal view. *Appendicisporites* is a form genus of trilete spore whose first members appeared in the late Paleozoic. Genus diversity increased into the Mesozoic, leading to several distinctive Jura-Cretaceous species (Traverse, 2008). Scale bar: 20 μm

Figure 2.13: *Cicatricosisporites* sp., lateral view. *Cicatricosisporites* is a form genus of trilete spore whose first members appeared in the Triassic (Traverse, 2008). Scale bar: 20 μm

4. Associated Vertebrate and Invertebrate Fossils

A. *Other Vertebrate Remains*: Direct evidence for the presence of other vertebrates includes the teeth and scales of teleost fish and "mako-type" shark teeth (Pasch and May, 2001). However, with the exception of one teleost tooth found among the bones, the other vertebrate remains were recovered from horizons above the dinosaur and approximately 120 m to the south.

B. *Invertebrates*: Pasch and May (1997; 2001) report an assemblage of invertebrate fossils including 7 genera and species of cephalopods, 6 species of bivalves, 2 genera of gastropods, 1 scaphopod genus, and 1 hexacoral genus. The majority of the fossils were recovered from sites approximately 30 m south of the dinosaur and in horizons topographically closer to the dinosaur than the majority of the non-dinosaurian vertebrate remains mentioned above. Many of the cephalopods had Tethyan affinities, and in fact two of the identified species represented the first occurrence of that species in North America (Pasch and May 1997; 2001).

Acid preparation of bone-bearing calcareous concretions revealed several additional cephalopods. However, efforts to save these specimens for collection proved unsuccessful. The vinac used to protect the bones from the formic acid solution did not protect the fragile calcite ammonite shells, while efforts to air scribe the cephalopods ultimately proved destructive. A peel was made of a large (approximately 3 cm x 6 cm) impression on the surface of the largest bone-bearing concretion that is presumed to represent part of a mollusc (cephalopod?) shell, but further identification of this impression was not possible because of its incompleteness.

I made short trips to the quarry in the summers of 2009 and 2010 to look for additional invertebrate fossils but recovered few useful specimens. Most were only identifiable to the family level due to severe compaction or other damage.

4. Interpretation

1. Lithology and Mineralogy

The presence of glauconite, combined with a low-diversity invertebrate assemblage, and the abundance of pyrite on and around the dinosaur remains, suggests that the sediments were deposited in an oxygen-deficient environment. The restriction of apatite to the concretion samples seems to lend support to the hypothesis of Pasch and May (1997; 2001) that the concretions represent pieces of the dinosaur carcass that were dispersed by scavengers prior to decomposition.

The presence of obvious laminae in concretion sediments suggests that concretion formation post-dates complete decay of the dinosaur's soft tissues. It does not seem likely that formation of the concretion could have occurred while soft tissue was still present and allow sediment laminae to form. The lack of other concretions within the quarry does appear to suggest that the sediments around the carcass were enriched in carbonate precursor material(s) (calcium-rich organic molecules such as calcium palmitate) as suggested by Berner (1969). The presence of fine laminae, relative lack of bioturbation (ichnofabric index 2 of Droser and Bottjer, 1986), and presence of millimeter-scale (medium to coarse sand-sized) fragments of bone in matrix suggest a low-energy, low-oxygen environment of deposition.

2. Taphonomy

Pasch and May (1997; 2001) attributed the absence of a skull to the weak connection between the skull and the rest of the vertebral column. Intensive screening of quarry sediments during excavation failed to turn up even a single

hadrosaur tooth fragment, which supports the idea that the skull was lost prior to deposition. This is consistent with the interpretation that the carcass floated for some time prior to sinking.

Trace evidence for the presence of large mobile scavengers exists in the way the bones of the skeleton were jumbled and disarticulated. Furthermore, Pasch and May (2001) argue that conical depressed fractures found in some of the bones represent tooth marks, presumably from mosasaur scavengers (Stage I of Smith and Baco, 2003). However, these depressed fractures can be of highly variable size and morphology and are typically restricted to only one surface of a given bone (see Figures 2.14-2.15). In addition, they generally lack any sort of pattern one would attribute to teeth (i.e., linear or arcuate alignment of depressions). Given those factors, it seems more likely that these depressed fractures represent the activity of invertebrate scavengers (Stage II or III of Smith and Baco, 2003) akin to the Recent bone-mining polychaete genus *Osedax* (Amano et al., 2007) weakening areas of the bone, which were subsequently crushed by compaction or addition of sediments prior to final fossilization. *Osedax*-like damage is present in the fossil record (Kiel, 2004), lending support to this interpretation of the evidence.
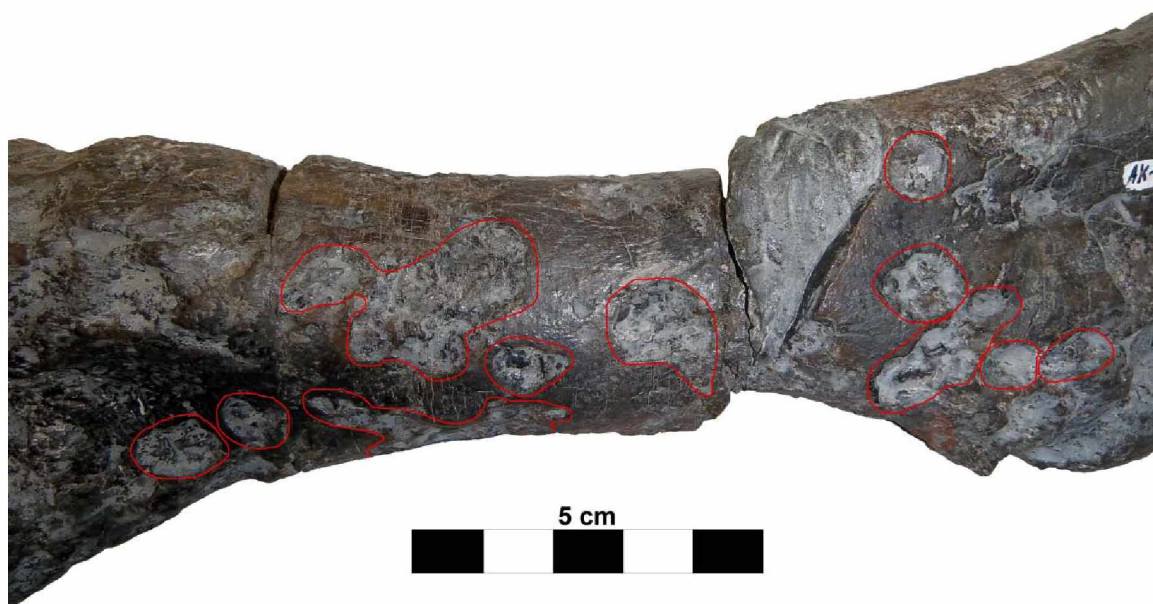
Figure 2.14: Modification of humeral anterolateral surface in close view (left humerus of UAMES 12275). Areas of damage originally interpreted as tooth marks are highlighted in red. Note the variable size and shape of these zones.

Figure 2.15: Modification of the humeral posteromedial surface in close view (left humerus of UAMES 12275). Areas of damage originally interpreted as tooth marks are highlighted in red. Compared to Figure 2.14, this surface is almost pristine.

Based on the original quarry map, the fragmentation of the skeleton during the mobile scavenger phase was not intense. Two sets of caudal vertebrae, two pairs of dorsal vertebrae, and two sets of cervical neural arches were recovered still in articulation. In broad terms, the distribution of limb bones is not inconsistent with what one might expect when a quadruped falls down and lands on its side. The presence of most of both feet indicates that the hind limbs were intact as the dinosaur sank, so the missing left fibula and tibia were removed post-deposition. Whether they were scavenged or accidentally destroyed at the time of discovery cannot be determined. However, the amount of syndepositional/pre-lithification chemical dissolution and/or mechanical destruction of the skeleton (Stages II and III of Smith and Baco, 2003) appear to have been extreme: a large number of unidentifiable fragments of both cancellous and cortical bone were uncovered during preparation of the concretion material. It is quite possible that many of the missing pieces of this animal's postcrania exist as these indeterminate fragments of bone. The lack of evidence for encrusting organisms (absence of shells embedded in bone or borings without collapsed cortical bone in them) seems to suggest that Stage IV of Smith and Baco (2003) either never happened or was short-lived. The lack of evidence for this stage could be interpreted one of two ways:

1. Lack of oxygen prevented encrusting organisms from settling on and exploiting the bones.

2. Rapid sedimentation completely buried the bones before encrusting organisms could establish themselves on the bones.

3. Remains of encrusting organisms were not preserved.

Given the extensive modification most bones have undergone, it seems unlikely that this dinosaur was buried rapidly. Ammonites entombed within the concretion sediments demonstrate that conditions were favorable for the preservation of

calcium carbonate, so any of these "reef-stage" organisms that colonized the skeleton should have been preserved. Therefore, it seems most reasonable to conclude that bottom water oxygen conditions were not favorable for the colonization of the skeleton by encrusting organisms typical of a reef stage.

A. *Comparison to a Maastrichtian New Zealand Plesiosaur*: Barnes and Hiller (2010) reported the discovery of a disarticulated elasmosaurid plesiosaur (catalogue number CM Zfr 145) from the Late Cretaceous Conway Formation of New Zealand's South Island. The Conway Formation is a jarositic, fine silty sandstone with minor glauconite and significant bioturbation (Barnes and Hiller, 2010). Similar to UAMES 12275, the remains of CM Zfr 145 were preserved in a carbonate concretion. The degree of bioturbation present is indicative of a soft-bottom environment below wave-base with low sedimentation rates, and the authors interpreted the environment as analogous to the modern Santa Barbara Basin off southern California (Barnes and Hiller, 2010).

The authors report the presence of pitting and scratches consistent with the action of mobile scavengers. The authors attributed the absence of the skull, cervical vertebrae, and elements of the left pectoral and pelvic girdles to post-mortem processes that occurred before burial: predation, scavenging, or detachment due to decay of soft tissues were cited as possible options. The remaining elements of the skeleton were found scattered and jumbled through the concretion (an approximately 5 m^2 area), and the authors argue this disarticulation was the work of scavengers. Many phalanges are unaccounted for, but similarly-sized caudal vertebra are present, leading the authors to conclude that the missing phalanges were likely removed by scavengers and not moved by currents (Barnes and Hiller 2010).

It is interesting to note the difference in degree of disarticulation between UAMES 12275 and CM Zfr 145. Despite the much greater size of the remains of CM Zfr 145 relative to UAMES 12275, that animal was almost completely disarticulated, with only a series of six partial vertebrae and portions of the pectoral and pelvic girdles remaining closely associated (Figure 2.16, Figure 2.17).
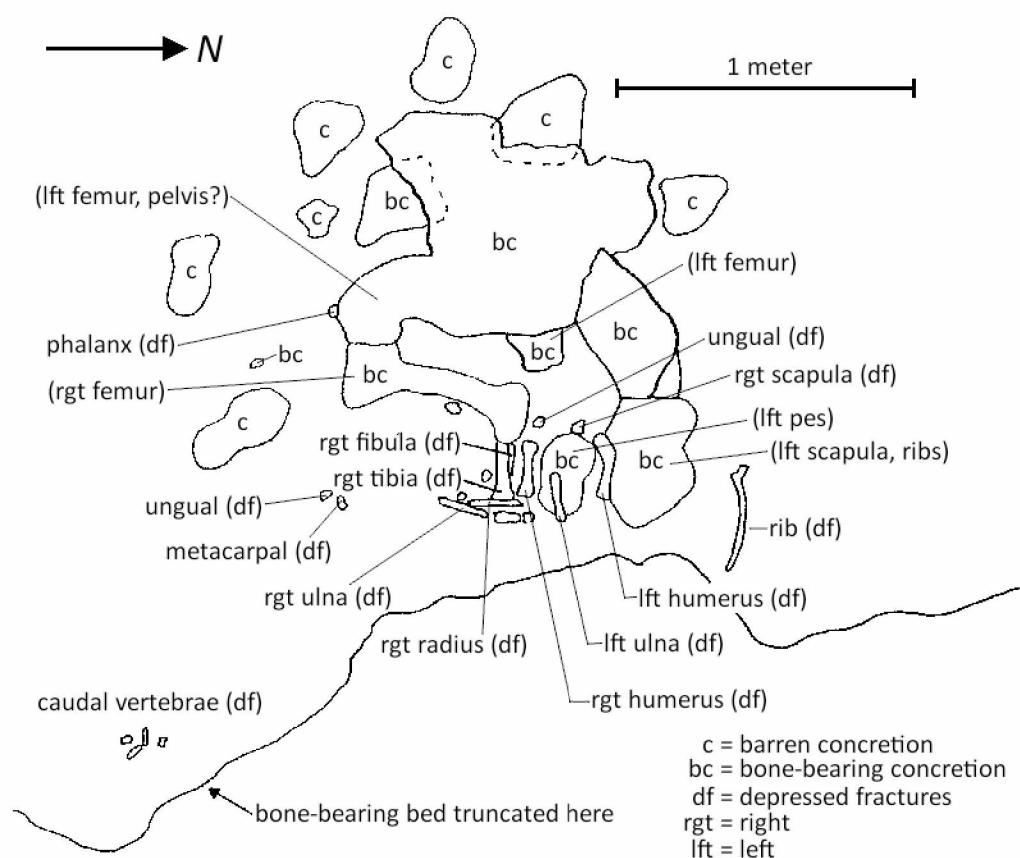
Figure 2.16: *In situ* distribution of UAMES 12275 (reproduction of the quarry map drawn by Pasch and May (Fig. 16.7, 2001)). Note the close association of limb elements in the middle of the image. Bones in parenthesis represent either tentative identifications or bones still encased within the concretion.
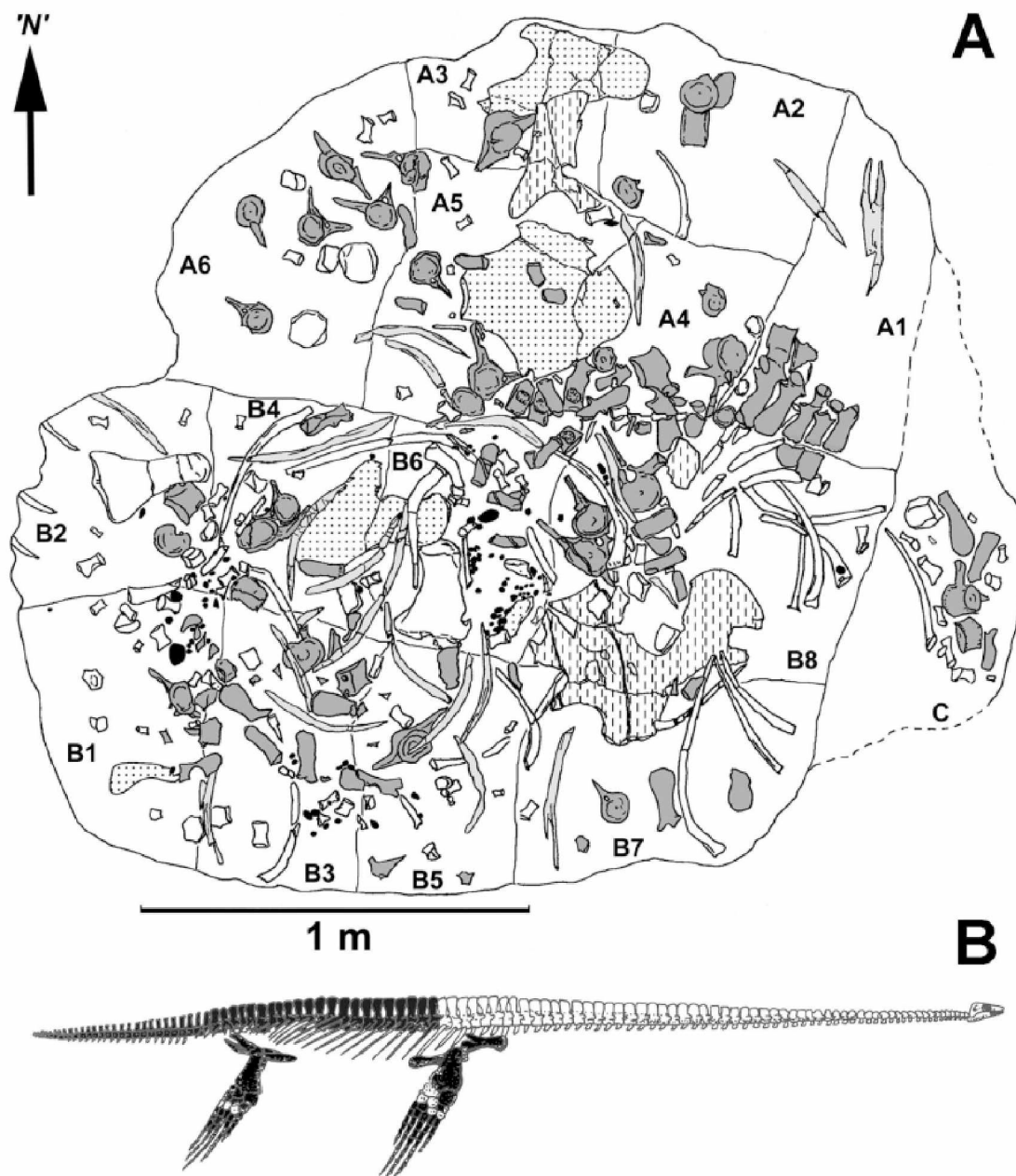
Figure 2.17: *In situ* distribution of CM Zfr 145 (reproduction of the concretion map of Barnes and Hiller (Fig. 2, 2010)). Part A shows the positions of the bones of the skeleton and is coded to represent areas of the skeleton; A1-A6, B1-B8 denote the sub-blocks the two largest pieces of the concretion were divided into; C denotes the smaller third block collected from the field site. Note the extreme amount of disarticulation present, with only a small section of vertebrae (between A4 and A1) in association. Only the fused girdle bones are still articulated. Dark grey: vertebrae and detached neural spines. Pale grey: gastralia. Stipple: pelvic girdle. Dash: pectoral girdle. Un-shaded: limb bones and ribs. Part B shows a reconstruction of the skeleton, with recovered elements colored black. The elasmosaur was recovered from a block of float along the shore of the Waipara River and its original orientation is unknown; the north arrow was arbitrarily assigned to allow the authors to analyze for current modification of remains.

Barnes and Hiller report that in addition to bone modification caused by scavengers, the surfaces of many bones showed signs of exploitation by invertebrates, potentially similar to the modern polychaete genus *Osedax* which exploits whale bones in the Recent (Amano et al., 2007). They note that these signs of invertebrate scavenging are concentrated on the surfaces of elements believed to have been above the sediment-water interface (Barnes and Hiller, 2010) which is consistent with the action of Recent organisms such as *Osedax* sp. Figure 2.18 is a reproduction of Figure 5.B from Barnes and Hiller (2010), showing what invertebrate-modified bone from the elasmosaur looks like. Note the similarities to the anterolateral surface of the humerus of UAMES 12275 in Figure 2.14.

The bone modification in the New Zealand elasmosaur is similar to what is observed in UAMES 12275. Most bones recovered from the shale matrix exhibit extensive signs of postmortem damage, such as crushing, pits, and/or dissolution surfaces. Some caudal vertebrae are missing more than half of the centrum and the entirety of the neural arch, and in many instances, bones have been reduced to unidentifiable fragments of trabecular or cortical bone due to this pitting or dissolution (Figure 2.19-2.21)
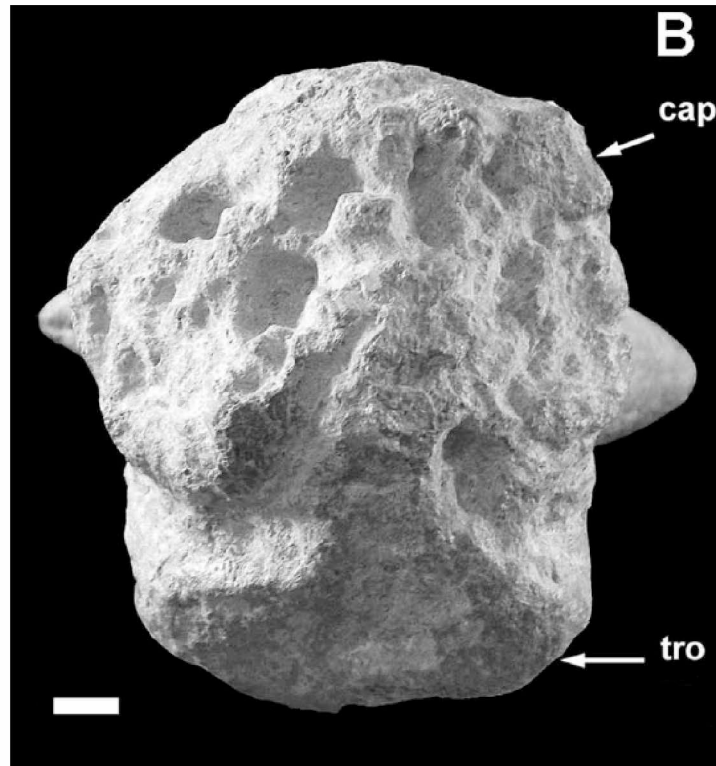
Figure 2.18: Proximal end of the femur of CM Zfr 145 showing bone loss and pitting developed on the capitulum (head) of the element. They note that the trochanter is well-preserved and that stratigraphic up is towards the top of the image. Scale bar: 10mm. Abbreviations: cap = capitulum (head), tro = trochanter

Figure 2.19: Two caudal vertebrae of UAMES 12275 in cranial(?) articular view, illustrating the highly variable nature of preservation. The centrum on the left is missing its neural arch and a small segment of its left dorsolateral surface. The centrum on the right is nearly unrecognizable as a centrum.

Figure 2.20: Two caudal vertebrae of UAMES 12275 in right(?) lateral view (same vertebrae as Figure 2.19), once again illustrating the variable nature of preservation of these elements and severe amount of chemical dissolution and/or bioerosion some elements of this skeleton have experienced.
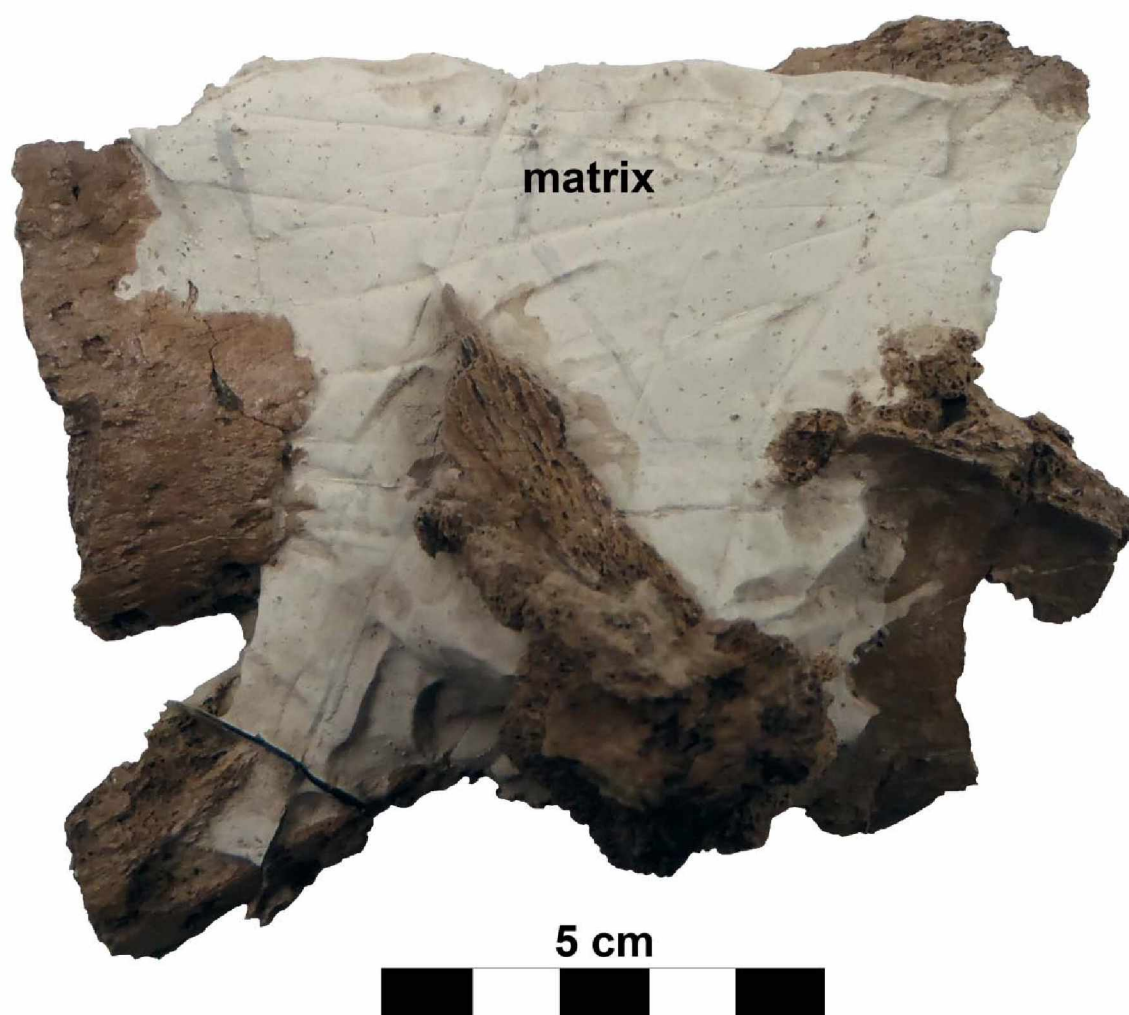
Figure 2.21: A jumble of four(?) postcranial(?) bone fragments in matrix. This agglomeration of bone fragments is typical of the unidentifiable portions of UAMES 12275.

3. Paleoenvironment

Planktonic foraminiferan forms such as *Bathysiphon* sp. are indicative of bathyl to outer neritic paleodepths (Pasch and May, 2001). The finely laminated, fine-grained nature of the shale indicates that the dinosaur sank to a depth below wave base, which Pasch and May (2001) interpreted to be a paleodepth of at least 35 m. The fact that these fine laminae are preserved, combined with the fine-grained nature of the sediment itself, suggests the environment of deposition had to be below storm wave base. Storm wave base can extend to depths exceeding 200 m (Duxbury et al., 2000), so this paleodepth estimate of 35 m is far too shallow.

The presence of a restricted benthic invertebrate community including inoceramid bivalves, an abundance of pyrite on bone surfaces and within the concretion itself, and the relatively small degree of disarticulation all appear to point to a seafloor environment that was suboxic (2.0 ml to 0.2 ml O_2 per L H_2O; Tribovillard et al, 2006). The carcass should be more disarticulated than it appears to be if it had sunk to the sea floor without a substantial amount of soft tissue still holding it together. Likewise, had the environment been more oxygenated, it is likely that it would have been more intensely scavenged by large vertebrates after it settled out and would have been disarticulated to a degree comparable to that of the New Zealand elasmosaur (see Figure 2.15). Invertebrates can tolerate oxygen-deficient waters better than vertebrates (see Breitburg, 1992; Vaquer-Sunyer and Duarte, 2008). However, some vertebrates are willing to risk hypoxic water in their hunt for food (Rahel and Nutzman, 1994). Settling in hypoxic conditions would allow for the development of burrows and other evidence of bioturbation observed in thin section while also discouraging (but not completely precluding) scavenging by large mobile vertebrates. It should be noted that rapid burial of the dinosaur after settling to the seafloor could account for the relative lack of disarticulation. However, the extensive surface modification and outright destruction of many of the bones suggests prolonged

exposure at the sediment-water interface. Lastly, the sediments would exhibit a greater degree of bioturbation (ichnofabric index 3 or higher of Droser and Bottjer, 1986) had the environment been more oxygenated.

4. Biostratigraphic Age of UAMES 12275

The assignment of this fossil to the Turonian is based on invertebrate biostratigraphy. As discussed previously, an attempt at using palynomorphs as a supplement to the existing molluscan biostratigraphy was unsuccessful. The most promising form genera found have stratigraphic ranges too broad to be useful for this purpose. The lack of angiosperm pollen appears problematic at first glance, as angiosperms were well-established and widely distributed by the Turonian. However, there are several possible explanations for the absence of angiosperm pollen.

1. Angiosperm pollen tends to possess thinner walls than either gymnosperm pollen or trilete spores, while the basic conditions which favor preservation of vertebrate bone are unfavorable for the preservation of sporopollenin (Traverse, 2008). It is possible that angiosperm pollen was present in the sediments originally and was either completely destroyed or degraded to the point of being unrecognizable before fossilization. Given the excellent preservation of the spores in the slides, this does not seem likely.

2. Heuser and Balsam (1977) determined that sedimentation of Recent pollen in the marine realm is a process dominated by fluvial input following rain-out of pollen after wind velocities drop below the critical point needed to transport the grains. Such fluvially transported pollen tends to exhibit depositional behavior similar to equivalent-sized siliciclastic particles. However, they also noted that pine pollen and trilete spores are overrepresented in Recent sediments from the abyssal plain, far beyond the influence of most fluvial systems, suggesting preferential transport of certain grain morphologies. Given the presumed depth of water UAMES 12275 was

deposited in and its probable location far from shore, it is possible that angiosperm pollen was not found because it was not as easily transported by water following rain-out from the atmosphere as the spores and bisaccate (gymnosperm) pollen.

3. Modern angiosperms are dominantly insect-pollinated plants. This means that angiosperms produce less pollen than those plants which rely on wind dispersal for fertilization and reproduction, and hence angiosperm pollen forms a smaller proportion of pollen rain-out into rivers than gymnosperm pollen or various spore-producing plants (Traverse, 2008).

4. Angiosperms were not abundant on shore in the region of UAMES 12275 and its final resting place. Peat bogs and boreal forest are just two environments where angiosperms are vastly outnumbered by non-angiosperm fauna in the Recent, and there is no reason to presume other such habitats which were unfavorable for angiosperms did not exist in the Cretaceous. It is possible that UAMES 12275 either lived in such a habitat, or wound up off-shore of one before sinking.

It is likely that the absence of angiosperm pollen is due to a combination of factors, most probably options 2-4 discussed above.

Foraminiferans present include forms corresponding to Faunal Zone A of Bergquist (1961), which he regarded as being of pre-Senonian (Coniacian + Santonian, or ~89.3 Ma to 83.5 Ma). The foraminiferans found in thin sections as a part of this study may belong to genera whose stratigraphic ranges span the Albian to Maastrichtian. While providing less temporal resolution than the molluscan biostratigraphy, the foraminiferan biostratigraphy is consistent with the interpretation that this dinosaur is of Late Cretaceous age.

Pasch and May (1997; 2001) consulted with Will P. Elder of the U.S. Geological Survey to identify the cephalopods, bivalves, and gastropods recovered from the site. Four

species of the bivalve genus *Inoceramus* (*I. cuvieri*, *I hobetsensis*, *I. mamatensis*, and I. *teshioensis*) indicated a late Early Cretaceous to Late Cretaceous age. The presence of the ammonite species *Muramotoceras yezoense* and *Eubostrychoceras japonicum*, both known from the Turonian of Japan, provide the greatest degree of biostratigraphic resolution (Matsumoto, 1977). The inoceramid bivalve *I. hobetensis* was originally reported from the site by Pasch and May (2001) but not listed among the biostratigraphically significant fossils. Takahashi (2005) reported that *I. hobetensis* is known from Turonian sediments of Japan's Yezo Basin, which suggests that *I. hobetensis* from the dinosaur quarry can serve as another indicator of the fossil's Turonian age.

5. Summary

Mineralogically, the quarry shale and quarry carbonate concretions differ markedly from one another. The restriction of apatite to the concretion makes sense if the concretions are interpreted to mark the location of pieces of the dinosaur carcass. Decomposition of the carcass generated conditions favorable for the eventual precipitation of calcium carbonate and pyrite, neither of which are seen to any great degree in the quarry shale. It is highly likely that the localized environments generated by the decomposing carcass are responsible for the other mineralogical differences between the shale and concretions.

Despite the mineralogical differences between the carbonate and the shale, the textural similarities indicate that formation of the concretions is a post-depositional event overprinting the original mineralogy, and that the two lithologies are actually a single lithology. More abundant evidence of bioturbation in the carbonate concretions is neither surprising nor unexpected given the interpretation of their origin, namely that they mark the location of pieces of rotting dinosaur, which would have served as a bonanza for vertebrate, invertebrate, and microbial exploitation.

UAMES 12275 is another example of a "bloat and float" dinosaur that was buried in a marine setting. Paleoenvironmental indicators suggest that it sank in greater than 35 m of water and came to rest in a suboxic/anoxic environment where it experienced relatively little scavenging from marine vertebrates but was extensively exploited by a community of invertebrates and/or microorganisms, potentially similar to that which exploits whale falls in the Recent.

Palynomorphs recovered from sediments around the skeleton cannot be used to precisely date the fossil, but they do provide a broad age bracket that is in agreement with the more precise age determined from mollusan and foraminiferan biostratigraphy. Molluscs and foraminiferans entombed within the same strata as UAMES 12275 point to a Turonian age for this dinosaur, making it one of only three known globally from this part of the Late Cretaceous.

Chapter 3: Description

1. Introduction

Based upon comparison to *Edmontosaurus* sp. material housed in the University of Alaska Museum Earth Science collection and the character descriptions of Prieto-Marquez (2010a), UAMES 12275 is a partial skeleton of a derived hadrosauriform dinosaur (see Table 3.1). UAMES 12275 consists exclusively of postcranial elements from the axial and appendicular skeletons, some in partial articulation, as well as a host of indeterminate fragments. Preserved elements include cervical, dorsal, and caudal vertebrae, dorsal ribs, both scapulae, both humeri, one radius, both ulnae, fragments of the metacarpals, a partial illium, portions of both femora, a partial tibia, a partial fibula, and both pedes.

2. Axial Skeleton

Representative elements from the cervical, dorsal, and caudal series of vertebrae are preserved in UAMES 12275, but sacral vertebrae were not recovered. The ribs mostly consist of fragments, presumably of dorsal ribs due to their size. One nearly complete dorsal rib was recovered. Ossified tendons are also present as scattered fragments found throughout the matrix.

    1. *Cervical vertebrae*: The cervical series is represented by at least five, possibly six, neural arches which broke away from their associated centra along the neurocentral suture. Three or four are contained in one partially prepared block are semi-articulated, and appear to lack transverse processes, suggesting they are from the anterior portion of the cervical series (Fig. 3.1). The remaining cervical neural arches occur individually. One pair of neural arches possesses transverse processes, suggesting that these vertebrae are from the middle or posterior portions of the series (Fig. 3.2, Fig. 3.3). The neural canal as preserved in the articulated posterior

cervicals is oblong and wider than it is tall (Fig. 3.2). The prezygapophyses face posterodorsally and slope medially between 30° and 45° from the horizontal. The transverse processes are abruptly dorsoventrally compressed lateral to the prezygapophyses but widen gradually distally (Fig. 3.4). The postzygapophyseal processes are less than three times the anteroposterior length of the neural arch.
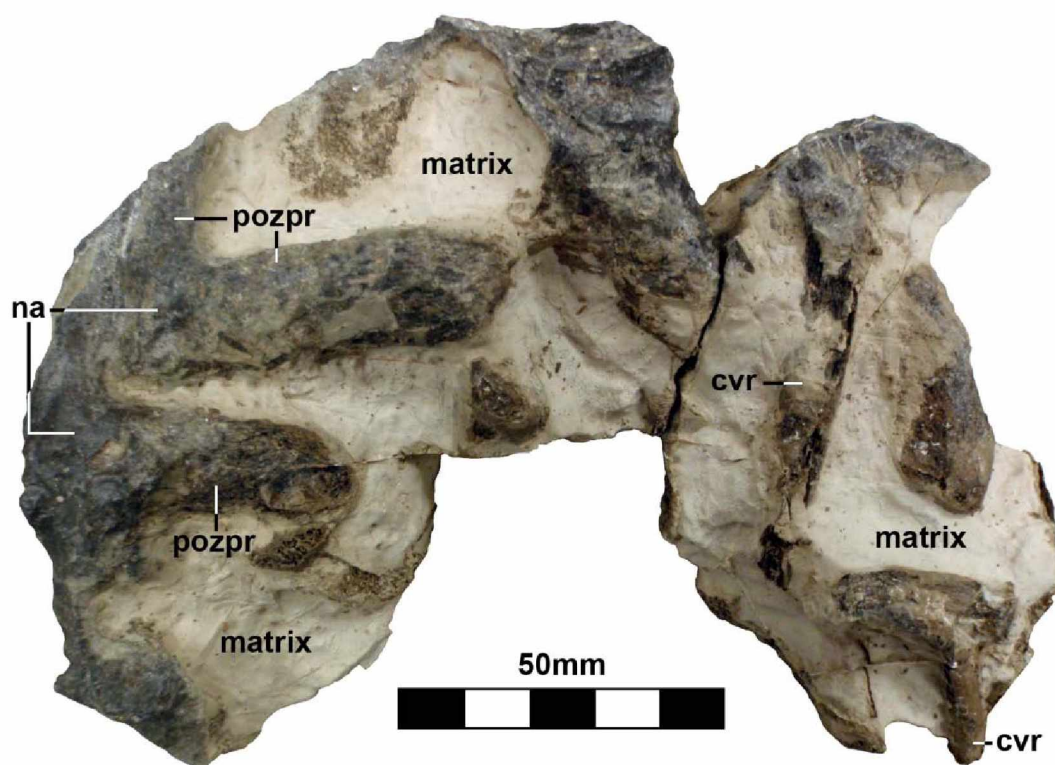
Fig. 3.1: Three partial, articulated cervical vertebrae of UAMES 12275 in dorsal view. Abbrevitiations: na = neural arch, cvr = cervical rib, pozpr = postzygopophyseal process
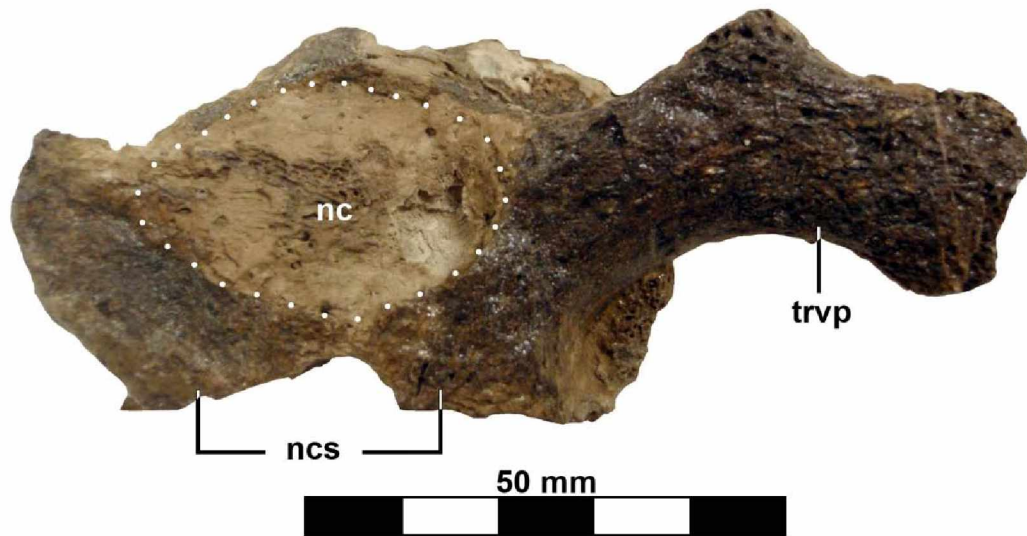
Fig. 3.2: Partial cervical neural arch in cranial articular view; white dots denote margin of neural canal. Abbreviations: ncs = neurocentral suture, nc = neural canal, trvp = transverse process
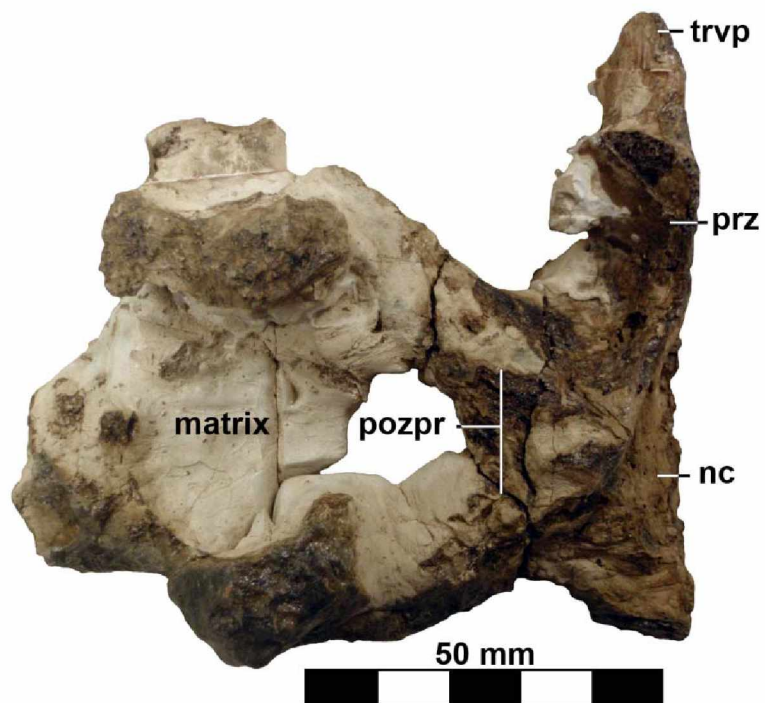
Fig. 3.3: Partial cervical neural arch in dorsal view. Abbreviations: nc = neural canal, pozpr = postzygopophyseal process, prz = prezygapophysis, trvp = transverse process
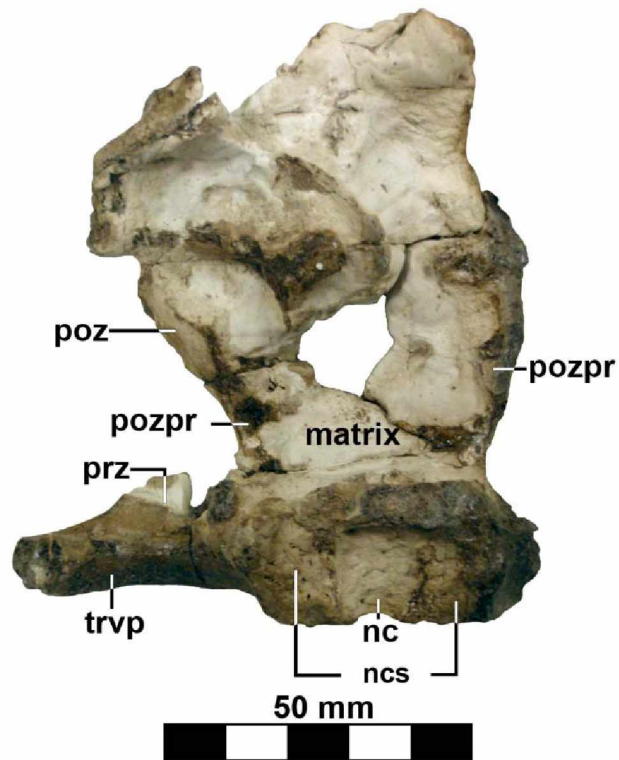
Fig. 3.4: Partial cervical neural arch in ventral view. Abbreviations: nc = neural canal, ncs = neurocentral suture, poz = postzygapophysis, pozpr = postzygopophyseal process, prz = prezygapophysis, trvp = transverse process

2. *Dorsal vertebrae*: The dorsal series is represented by 4 or 5 partially articulated centra. Most of the neural arches are missing, with only the base of the neural arches being preserved. The preserved portion of the vertebrae indicate that the neurocentral suture is fused but the sutural zone is still visible (Fig. 3.5). In anterior view, the neural canal is subcircular and wider than tall in outline, similar to the condition seen in the cervical vertebrae. One prezygapophysis is partially preserved and it appears similar in shape to the prezygapophyses of the cervical vertebrae, though this may be an artifact of damage to the neural arch (Fig. 3.6). The dorsal centra are poorly preserved, making it difficult to discern their morphology. However, one anterior surface is visible and is weakly concave, so the dorsal vertebrae must have been either procoelous or amphicoelous. The ventral surfaces possess a broad midline keel, while the lateral walls of the vertebrae are constricted between the anterior and posterior articular surfaces (Fig. 3.7). Articular facets for the capitula of the dorsal ribs are not visible. In anterior or posterior view, the vertebral centra are heart-shaped, as is typical of hadrosauroid dorsal vertebrae.
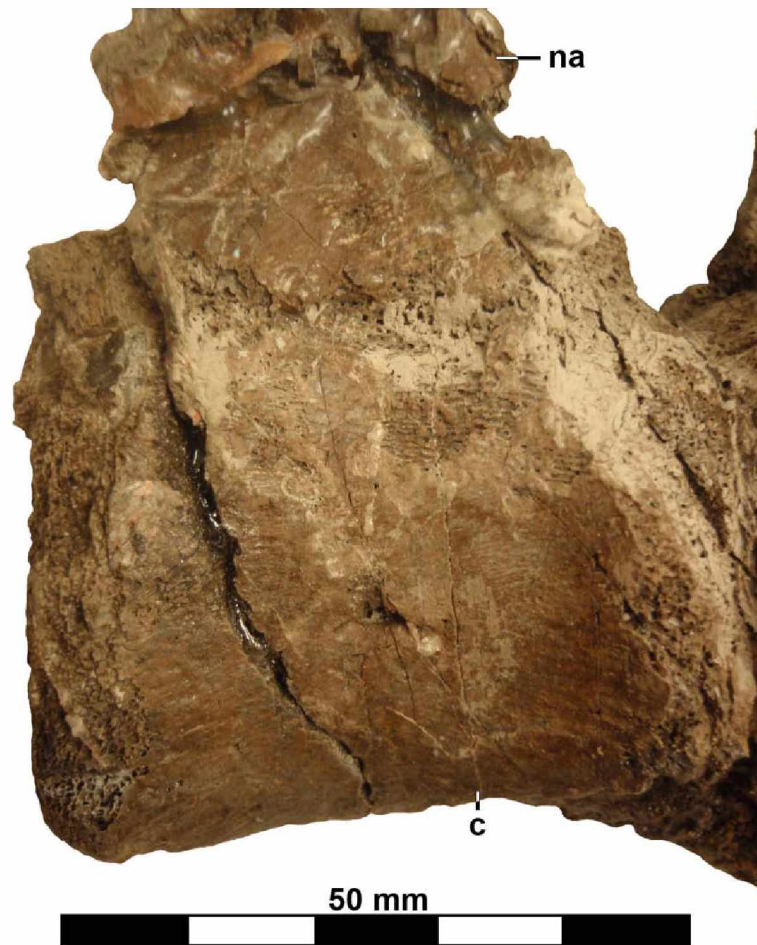
Fig. 3.5: Dorsal vertebrae in left lateral view. The heavily pitted region ventral to the neural arch is interpreted to be the neurocentral suture. Abbreviations: c = centrum, na = neural arch

50 mm

Fig. 3.6: Articulated dorsal vertebrae in dorsal view; anterior is to the right. Abbreviations: nc = neural canal, prz = prezygapophysis

50 mm
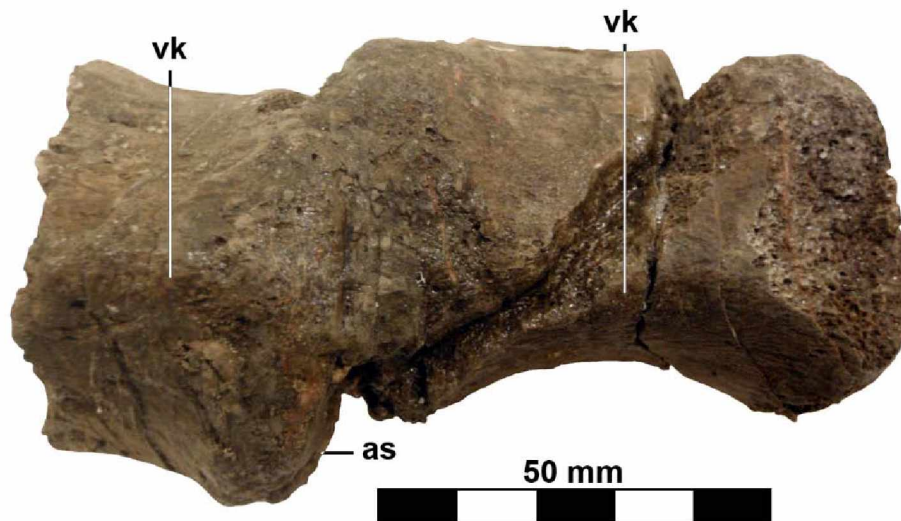
Fig. 3.7: Articulated dorsal vertebrae in ventral view; anterior is to the right. Abbreviations: as = articular surface, vk = ventral keel

3. *Caudal vertebrae*: The caudal series is represented by 28 vertebrae in varying states of preservation. The lateral surfaces of many are heavily pitted, presumably by marine microorganisms mining the bone for nutrients on the seafloor prior to burial, and some are so badly damaged in this fashion that less than one-half of the centrum remains. Several also exhibit signs of crushing that are common to so many other elements of this skeleton. The majority of these vertebral centra occur as discrete series of articulated vertebrae (Fig. 3.8). The caudal centra lack the keels present on the ventral surfaces of the dorsal vertebrae and appear to possess relatively mediolaterally broader articular surfaces than the dorsal centra. The articular surfaces of some of the caudal vertebrae are preserved well enough to show that the centra are weakly amphicoelous. In lateral view, the walls of the caudal centra between the articular surfaces are faceted, giving the centrum a hexagonal view in cross-section (Fig. 3.9). Anterior chevron facets are smaller than posterior facets, following the common iguanodontian pattern for chevron facet size. No complete neural arches are present, but there are some that are partially preserved. As they are all still articulated and inseparable, only the lateral surfaces and exposed cross-sections can be described. In dorsal view, the prezygapophyses are rounded rectangular, tongue-like projections from the anterolateral surfaces of the neural arch that cup the postzygapophyses on the preceding neural spine. The base of the neural spine itself is inclined posteriorly over the vertebra posterior to it at an angle nearly perpendicular to the prezygapophyses and has a nearly symmetrical trapezoidal cross-section, with the posteroventral and anterodorsal surfaces being parallel and significantly shorter than the angled lateral surfaces.

Unlike the dorsal vertebrae, the neurocentral suture in the caudal vertebrae appears completely fused (Fig.3.9). A few chevrons are preserved but they have not been fully prepared and cannot be described (Fig. 3.8).
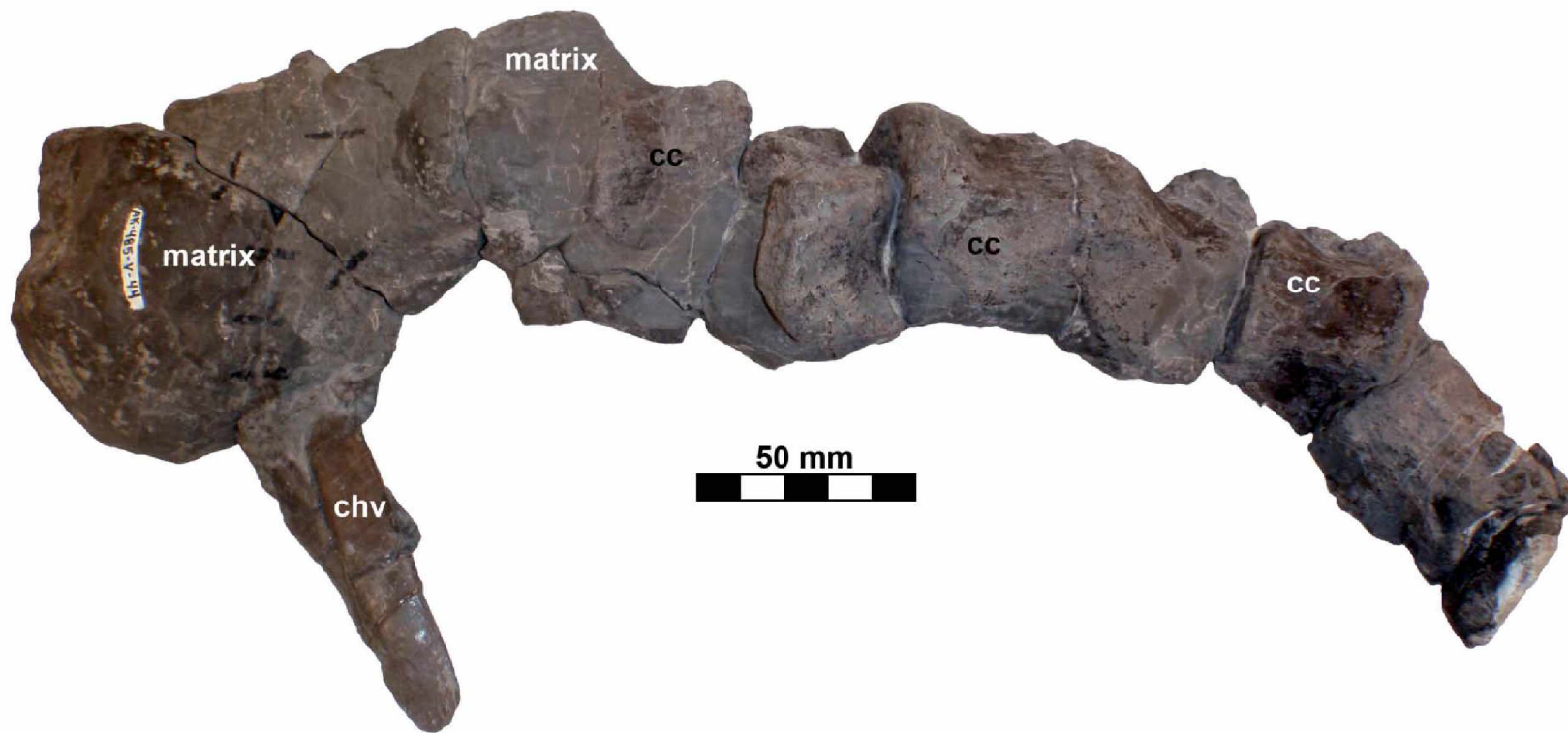
Fig. 3.8: Articulated series of caudal vertebrae of UAMES 12275, lateral view; orientation unknown, but anterior presumably to the left.

Abbreviations: cc = caudal centrum, chv = chevron
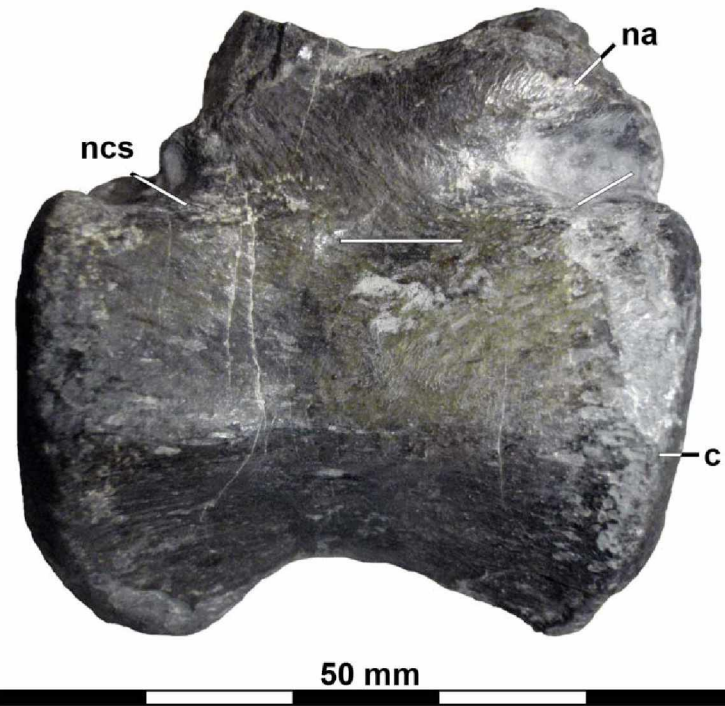
Figure 3.9: Caudal vertebra in right lateral view. Dashed white line approximates location of neurocentral suture. Abbreviations: na = neural arch, c = centrum, ncs = neurocentral suture

4. *Ribs*: No complete cervical ribs are preserved, but one probable left dorsal rib is present (Fig. 3.10). The capitulum is oblong in medial view and slightly broader anteroposteriorly than the shaft of the rib. Between the capitulum and tuberculum, the dorsal margin of the rib is slightly ventrally concave. The tuberculum is oval in dorsal view and has a triangular profile in anterior view. Ventral to the apex of the tuberculum, the rib possesses an approximately square (2x3 mm) tuberosity on the anterior(?) surface, located midway between the dorsolateral and ventromedial surfaces of the rib. Distal to the tuberculum, the rib shaft initially curves gently laterally. Approximately 5 cm from the tuberculum, this gentle lateral curvature changes abruptly into a gentle medial curvature (Fig. 3.10).

Figure 3.10: Left(?) dorsal rib of UAMES 12275, amterior view. Abbreviations: cp = capitulum, tb = tuberculum.

3. Appendicular Skeleton

   1. Pectoral Girdle

   A. *Scapula*: Two elements are preserved whose overall morphology are consistent with that of a hadrosauroid left and right scapula. However, the two elements are not bilaterally symmetrical, which has resulted in uncertainty regarding the identification of these two elements. Each element will be described and the morphological differences will be summarized. Although alternative explanations are discussed in Chapter 4, "Comparative Discussion", for the purposes of this description, they are assumed to be a left and a right scapula.

The *left scapula* (Fig. 3.11, Fig. 3.13, Fig. 3.14) as preserved is approximately 30 cm in length and is missing both its coracoid and glenoid facets (see Table 3.1 for additional measurements). The pseudoacromion process is similarly absent. The deltoid ridge is damaged, making it appear weakly developed, but this is likely a preservation artifact. Consequently, this makes the glenoid fossa appear dorsoventrally broad and shallow. Like most basal hadrosauroid scapulae, the dorsal margin is gently convex dorsally along the proximal half of the element, with the inflection point of the curve situated in the middle of the proximal constriction. Posterior to the proximal constriction, the dorsal margin of the scapula is straight along the anterior two-thirds of the scapular blade. At its distal end, the scapular blade terminates in a straight edge that appears to make approximately right angles to both the dorsal and ventral margins of the scapula. In cross section view, the mediolateral thickness of the scapula decreases markedly from approximately 1.4 cm at the proximal constriction to less than 2 mm near the distal margins of the scapular blade. Cross sections through the scapula show that its lateral surface is convex and its medial surface is flat to very slightly concave, though this concavity may be a preservation artifact.

The *right scapula* (Fig. 3.12 – 3.14) as preserved is approximately 25 cm in length and is missing the coracoid and glenoid facets, as well as the pseudoacromion process (see Table 3.2 for additional measurements). The deltoid ridge appears intact and the glenoid fossa is broad and deep. The proximal half of the dorsal margin is curved dorsally, and the inflection point of the curvature is located in the proximal constriction. Posterior to the proximal constriction, the dorsal margin of the scapular blade is straight along its length, and neither margin appears to possess a convexity. It is unknown how much of the distal margin of the scapular blade is missing, as it is impossible to determine which scapula represents the "normal" morphology for this animal. What is preserved of the right scapular blade tapers to a mediolateral thickness of less than 4 mm on all edges and there is evidence of finished bone on both the dorsal and ventral margins near the damaged distal end of the blade. The lateral surface of the right scapula is convex while the medial surface is flat to very slightly concave.

Table 3.1: Selected dimensions of the left and right scapulae of UAMES 12275. Abbreviations: dist = distal = distal end of scapular blade, ml = mediolateral, pcn = proximal constriction, prox = proximal articular end

	Left scapula	Right scapula
Length	30cm	25cm
height (pcn)	5.5cm	3.8cm
height (distal)	11cm	6.5cm
ml thickness (prox)	1.4cm	2cm
ml thickness (dist)	2mm	< 4mm
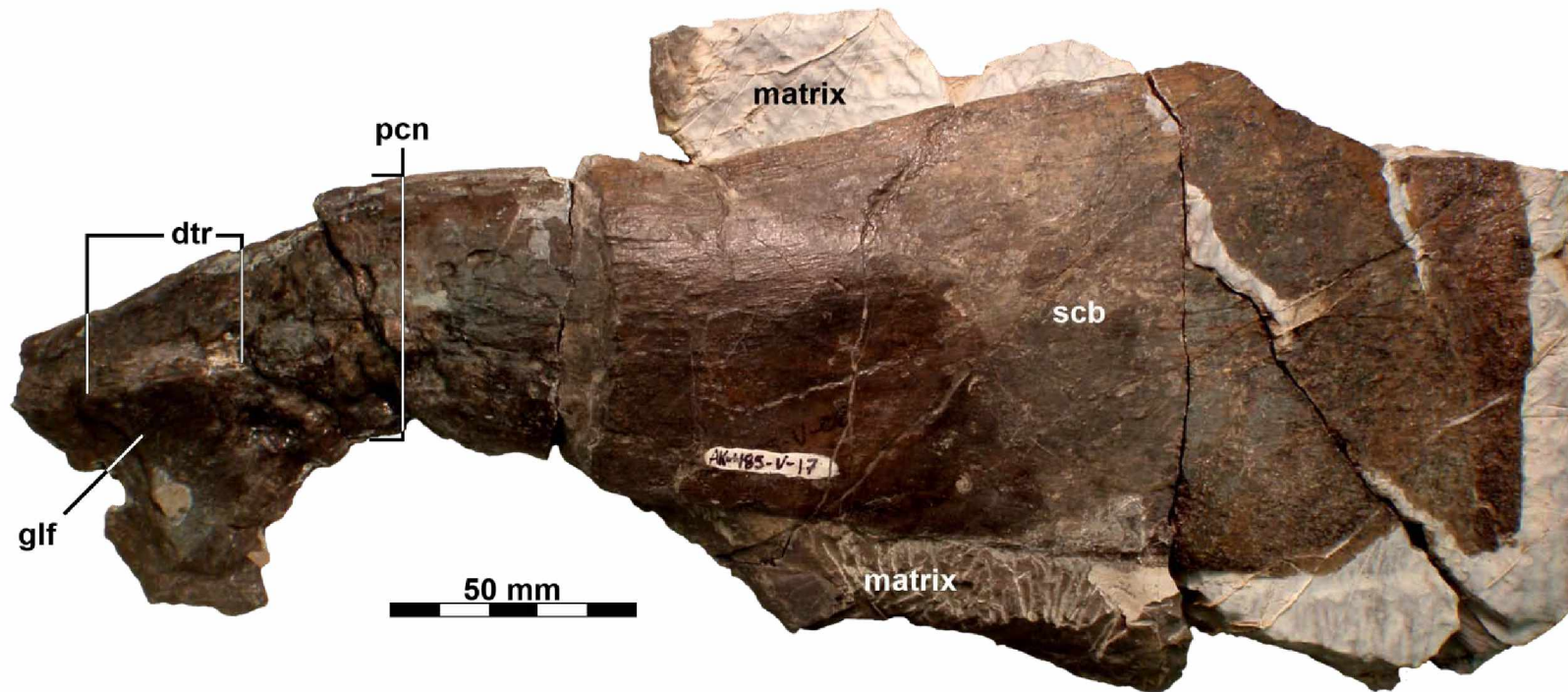
Figure 3.11: Left scapula of UAMES 12275 in lateral view. Abbreviations: dltr = deltoid ridge, glf = glenoid fossa, pcn = proximal constriction, scb = scapular blade
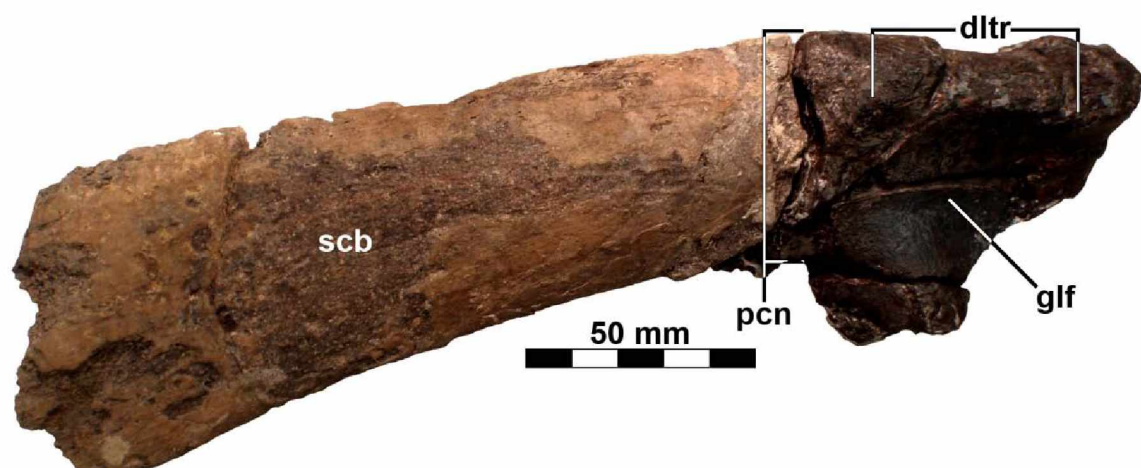
Fig. 3.12: Right scapula of UAMES 12275 in lateral view. Abbreviations: dltr = deltoid ridge, glf = glenoid fossa, pcn = proximal constriction, scb = scapular blade
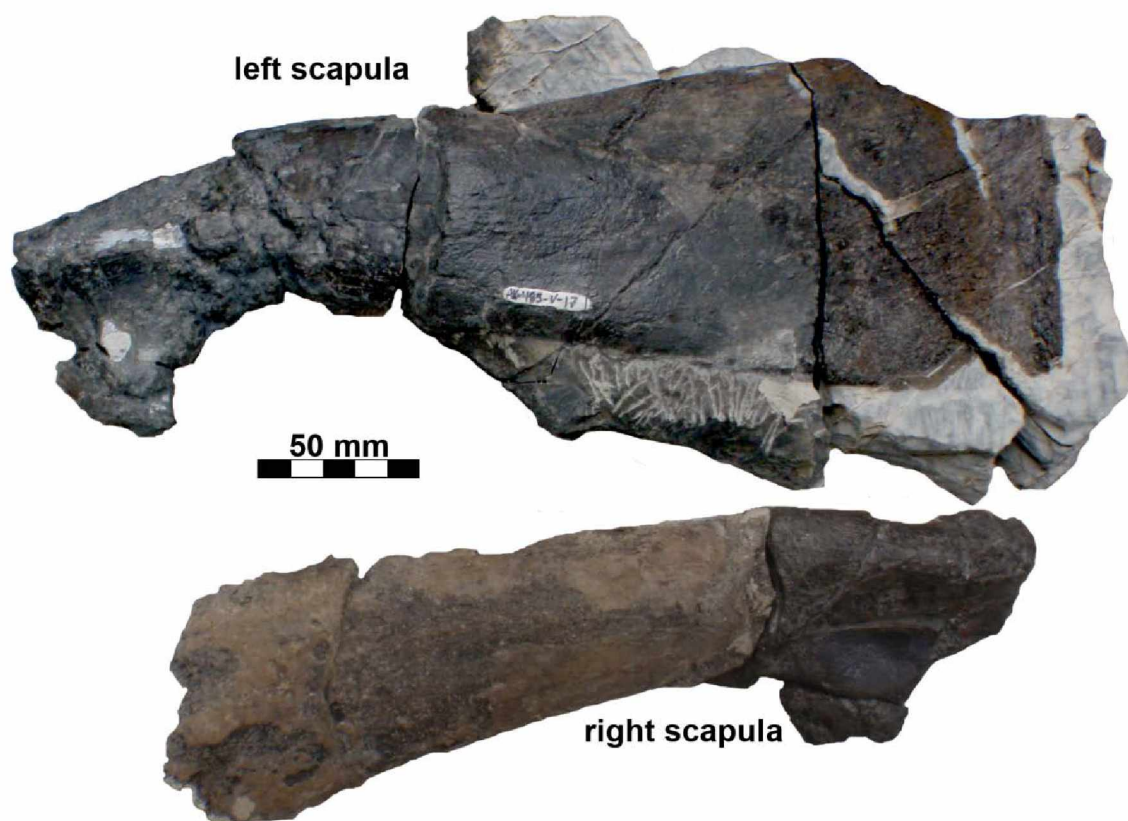
Fig. 3.13: Left and right scapulae of UAMES 12275 in side-by-side comparison.

Fig. 3.14: Left scapula and mirrored right scapulae (white outline) in side-by-side comparison to better illustrate their morphological differences.

B. *Humerus*: The general morphology of the humerus of UAMES 12275 resembles that of derived hadrosauroids and hadrosaurids, rather than more basal hadrosauriforms, in that the deltopectoral crest is nearly half the total length of the humeral shaft (Character 219, state 1 or 2, Prieto-Marquez 2010a). In combination with the medial tuberosity, the deltopectoral crest helps to give the proximal end of the humerus a rectangular outline in anterior or posterior view. The deltopectoral crest of basal hadrosauriforms tends to be shorter (Character 219, state 0, Prieto Marquez 2010) and does not give the proximal end of the humerus a rectangular outline in anterior or posterior view. Neither the left nor the right humerus of UAMES 12275 is complete, but each preserves portions that the other lacks. The description of the proximal half of the humerus and deltopectoral crest is based upon the left humerus, while the description of the distal end is based off of the right humerus.

The proximal end of the left humerus is incomplete, lacking the articular head and proximal terminations of the deltopectoral crest and medial tuberosity. Consult Table 3.2 for selected dimensions of the left humerus of UAMES 12275, and Fig. 3.15 to see how those measurements were obtained.

Table 3.2: Measurements of the left humerus. Explanation: L/D(midshaft) = ratio of length to diameter at midshaft; PL/DL = ratio of length of the proximal end to the distal end; DPC = deltopectoral crest; DPC/length = ratio of deltopectoral crest to humerus length

	Left humerus
Length	24.4 cm
Midshaft diameter	3.5c m
L/D(midshaft)	6.94
Proximal length	11.9 cm
Distal length	12.5 cm
PL/DL	0.95
DPC	11.2 cm
DPC/Length	0.46
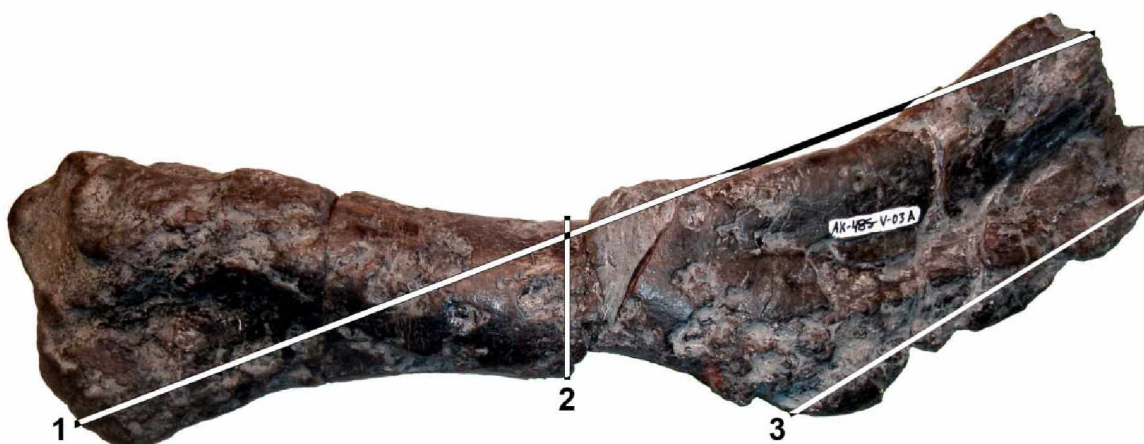
Figure 3.15: Numbers denote measurement vectors for the left humerus. 1 = total humeral length; 2 = midshaft diameter; 3 = length of deltopectoral crest

Comparison with a similar-sized *Edmontosaurus* sp. humerus suggests that less than 3 cm of the proximal end of the humerus, including the articular head, is missing in UAMES 12275. A ridge buttressing the articular condyle emerges from the main shaft at a level approximately in the middle of the deltopectoral crest (Fig. 3.16). This ridge is separated from the medial tuberosity by a broad trough. The deltopectoral crest is separated from the humeral shaft by a deep bicepital sulcus on the anterolateral surface. The deltopectoral crest thickens substantially

mediolaterally at its distal end, where it merges with the shaft of the humerus proximal to the midpoint of the shaft (Fig. 3.17). The humerus is fractured just distal to the end of the deltopectoral crest, providing a view of the egg-shaped cross section of the shaft. The distal articular surface of the lateral radial condyle possesses a triangular outline, with its anterolateral vertex expanded into a short, thickened, laterally directed ridge. This ridge merges with the shaft at the level of the top of the olecranon notch separating the articular condyles. The olecranon notch is of a similar depth and morphology on both the anterior and posterior surfaces and produces a slight saddle on the distal end of the humerus. The medial ulnar condyle is kidney shaped in distal view. The distal end of each humerus is circumscribed by a fine millimeter scale ridge of bone that likely demarcated the extent of the cartilage which capped the articular surface in life. This ridge is best preserved on the right humerus.

Figure 3.16: Left humerus in posterior view. Abbreviations: cbr = condyle buttressing ridge, dpc = deltopectoral crest, mt = medial tuberosity, rc = radial condyle, uc = ulnar condyle

Fig. 3.17: Left humerus in anterior view. Abbreviations: bs = bicpital sulcus, dpc = deltopectoral crest, mt = medial tuberosity, rc = radial condyle, uc = ulnar condyle

C. *Ulna*: Neither ulna is complete; the proximal ends of both ulnae are fairly well preserved, but the distal ends are missing. The proximal end is best preserved on the left ulna, while more of the distal end is preserved on the right ulna. Combining measurements of the two ulnae reveals that they have a minimum length of 20 cm. Comparison with an *Edmontosaurus* sp. ulna of similar proportions suggests that probably less than 4 cm of the distal end is missing, and thus that the ulna of UAMES 12275 was as long as or slightly longer than its humerus, a trait most commonly seen in basal hadrosauroids and basal hadrosauriforms. In proximal view, the olecranon process of the ulna has an outline of a right triangle, with the hypotenuse bowed slightly posterolaterally. In total, it forms a prominent 3 cm-high projection from the proximal end of the ulna. The U-shaped olecranon trough on the anterior surface is deep and very prominent, with steep sides formed by the medial and lateral processes of the ulna. However, some of this morphology may be accentuated by crushing. In anterior view, the lateral process of the ulna forms a triangular flange or fin that thickens proximally. The medial process forms a pronounced ridge of bone that is approximately 1 cm in anteroposterior thickness proximally and extends distally along the anterior surface of the ulna for approximately 10 cm, thinning anteroposteriorly and gradually merging with the shaft of the ulna along its length

(Fig. 3.18). The shaft of the ulna distal to the termination of the medial process has an egg-shaped cross section and is approximately 2 cm wide at its maximum diameter. The distal end of the ulna is incomplete and no further descriptive comments are possible.
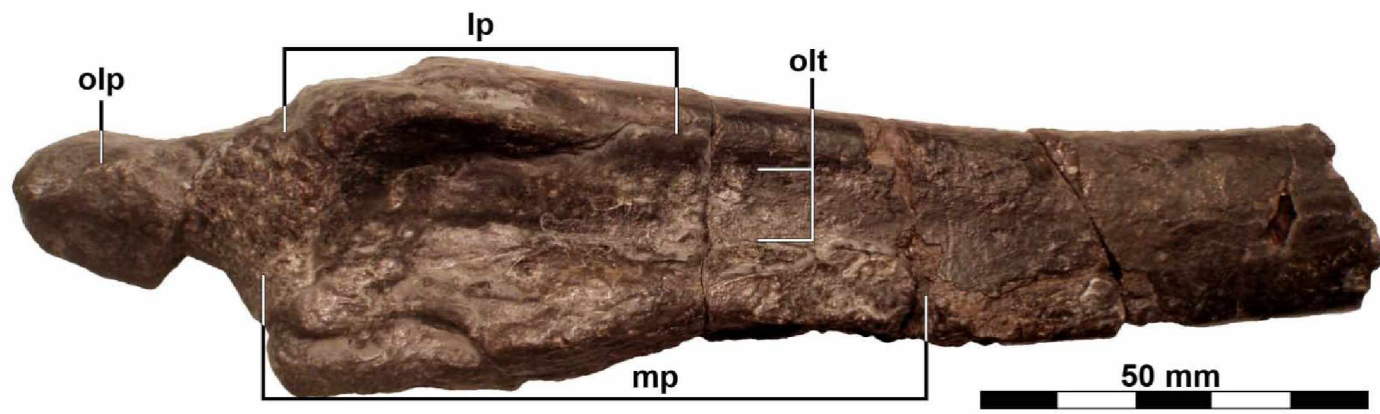
Figure 3.18: Proximal portion of the left ulna of UAMES 12275 in anterior view. Abbreviations: lp = lateral projection, mp = medial projection, olp = olecranon process, olt = olecranon trough

D. *Radius*: Only one poorly preserved radius is present, and it is not possible to tell if it is a right or left. As preserved, the radius is a rod-like element possessing a distinct curvature in both the mediolateral and anteroposterior planes. It is impossible to tell if the apparent curvature is real or an artifact of the damage the fossil has sustained. Only 18 cm of the radius is preserved, and based on comparison with the ulna, it must have been longer than this. One articular condyle is partially preserved, and its general shape suggests that it is the distal condyle. In articular view, the preserved condyle possesses a distinctly U-shaped outline. There is also a millimeter-scale ridge of bone circling the articular condyle, presumably demarcating the extent to which the condyle was capped by cartilage in life.

E. *Carpus and phalanges*: Fragments of metacarpals and possible manual phalanges are preserved but are too incomplete and poorly preserved to warrant description.

2. Pelvic Girdle

A. *Ilium*: A badly preserved left ilium is preserved in UAMES 12275 and was identified based on comparison with the ilia of *Gilmoreosaurus* (AMNH FARB 30736) and *Edmontosaurus* sp. (UAMES 13027). Most of the preserved portion of the ilium consists of the supraacetabular process. A small portion of the anteroventral margin of the iliac plate, just dorsal to the pubic peduncle, and some of the body of the iliac plate ventral to the supraacetabular process are also preserved (Fig. 3.19). The supraacetabular process is D-shaped in dorsal view, with the bow of the D projecting laterally (Fig. 3.20). This D-shape gives the dorsomedial edge of the ilium a nearly straight appearance in dorsal view, though this may be an artifact caused by the very fragmentary nature of the element. Jutting out laterally and nearly perpendicular to the iliac plate, the supraacetabular process overhangs the plate and body of the ilium by nearly 3 cm (Fig. 3.20, Fig. X.21). The supraacetabular process is approximately 2 cm thick at its maximum dorsoventral thickness, and it is not

ventrally deflected to any appreciable degree. The supraacetabular process of UAMES 12275 also lacks a pronounced "saddle" bridging the iliac plate, formed by the ventrolateral surface of the supraacetabular process and the dorsolateral surface of the ischial tuberosity and ischial peduncle, as seen in *Edmontosaurus sp.* (Fig. 3.22). The iliac plate appears very thin, but this is likely due to the extremely damaged nature of the element. An incomplete cross-section of the preacetabular process is present and lacks obvious signs of the laterally projecting dorsal ridge present in other hadrosauroids. The medial surface is badly damaged, if preserved at all, and nothing can be said about the nature of the articulation between the sacral ribs and the ilium.
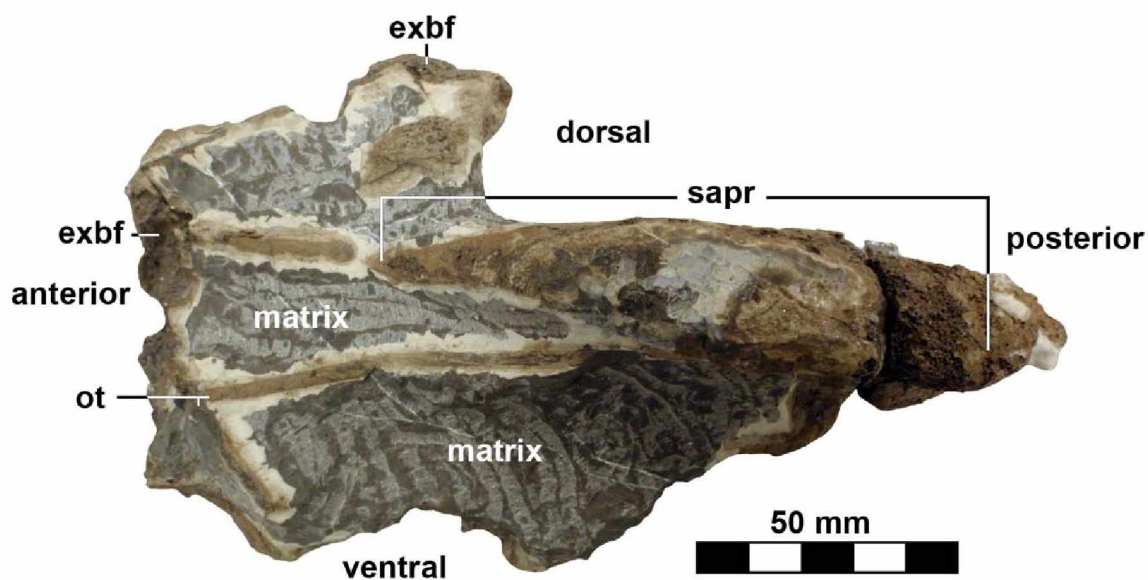
Figure 3.19: Left ilium in lateral view. Abbreviations: exbf = extraneous bone fragment, ot = ossified tendon, sapr = supraacetabular process
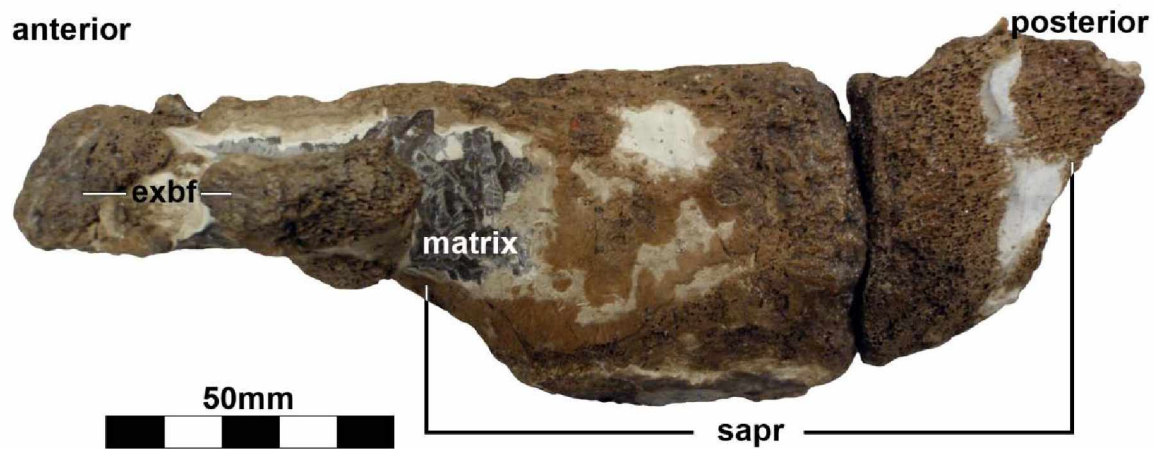
Figure 3.20: Left ilium in dorsal view. Abbreviations: exbf = extraneous bone fragment, sapr = supraacetabular process
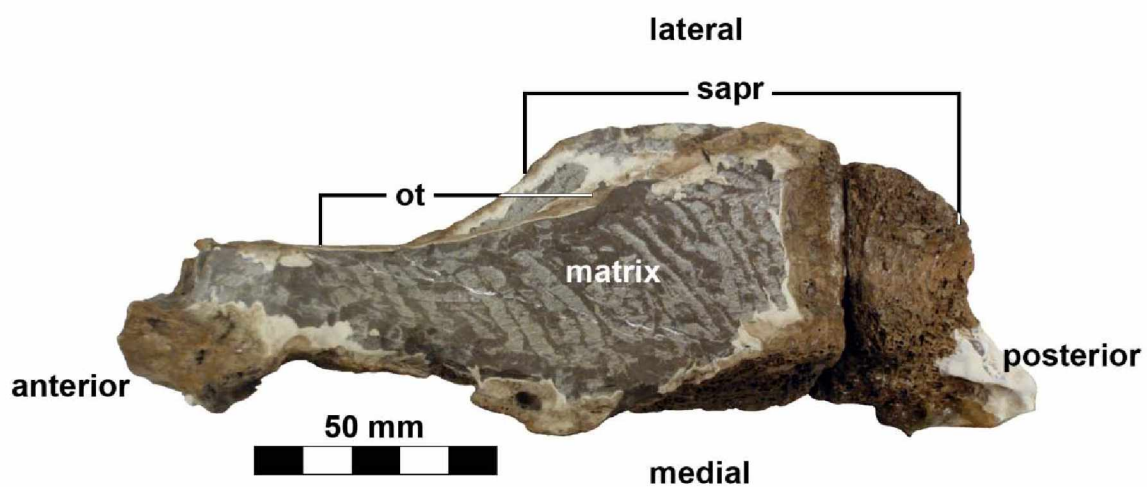
Figure 3.21: Left ilium in ventral view. Abbreviations: ot = ossified tendon, sapr = supraacetabular process

Fig. 3.22: Left ilium of *Edmontosaurus* sp., lateral view. "Saddle" marks the anterior edge of the low area connecting the margins of the supraacetabular process and the ischial peduncle. Compare with Fig. 3.19 and 3.21. Abbreviations: papr = preacetabular process, sapr = supraacetabular process, ischpd = ischial peduncle

B. *Femur*: Partial left and right femora are preserved in UAMES 12275. The left and right femora were differentiated by the position of the fourth trochanter because neither femur preserves either proximal or distal articular condyles (Fig.3.23). The left femur preserves most of the body of the fourth trochanter despite the mediolateral crushing of the shaft. The right femur is missing most of the fourth trochanter, though its location is still apparent.

The shafts of both femora in the area of the fourth trochanter appear to be either straight or very slightly convex anteriorly, and this does not seem to be an artifact of preservation. The left femur preserves the lateral surface of the greater trochanter, as well as the base of a prominent lesser trochanter (Fig. 3.24). The preserved fourth trochanter of the left femur is incomplete but quite well developed and extends approximately 14.5 cm along the length of the shaft. It projects posteriorly from the shaft by a minimum distance of 4.5 cm, but this must be regarded as a minimum dimension because the posteroventral edge of the trochanter is broken and it likely extended further from the shaft. In medial or lateral view, the fourth trochanter has the shape of a scalene triangle and appears to lack a ventrally
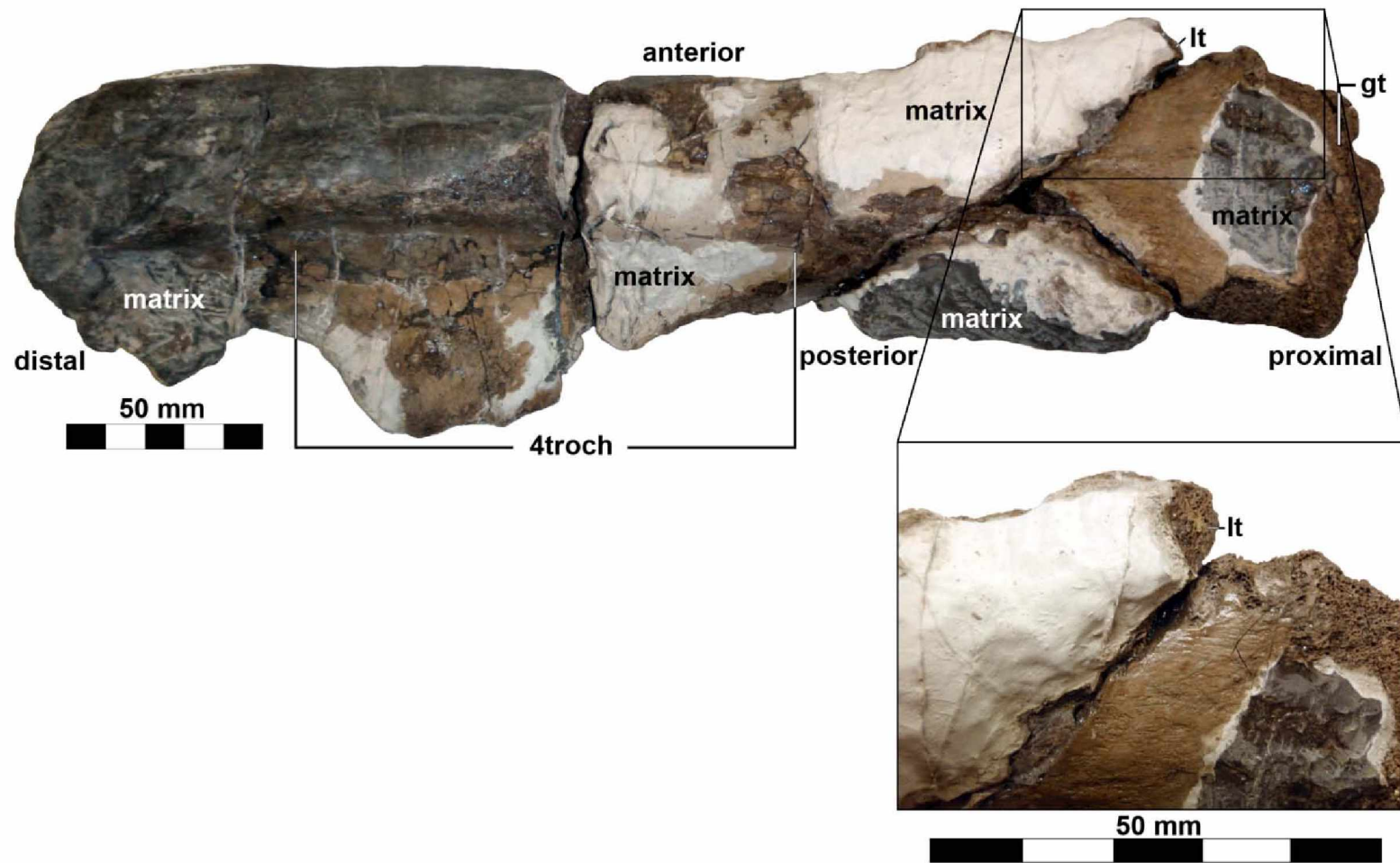
Figure 3.23: Left femur of UAMES 12275 in posterolateral view. Abbreviations: 4troch = fourth trochanter, lt = lesser trochanter, gt = greater trochanter. Blow-up box focuses on region of the lesser trochanter.

directed point, though this area may be damaged. The right femur appears to preserve a similar portion of the shaft as the left and lacks the mediolateral crushing which distorts the shaft of the left femur. The shaft of the right femur in the area of the fourth trochanter is distinctly D-shaped in cross section, with the bow of the D facing anteriorly and the straight edge forming the posterior surface of the shaft (Fig. 3.24). The mediolateral diameter of the shaft is approximately 5.5 cm, while the anteroposterior diameter is approximately 4.5 cm.
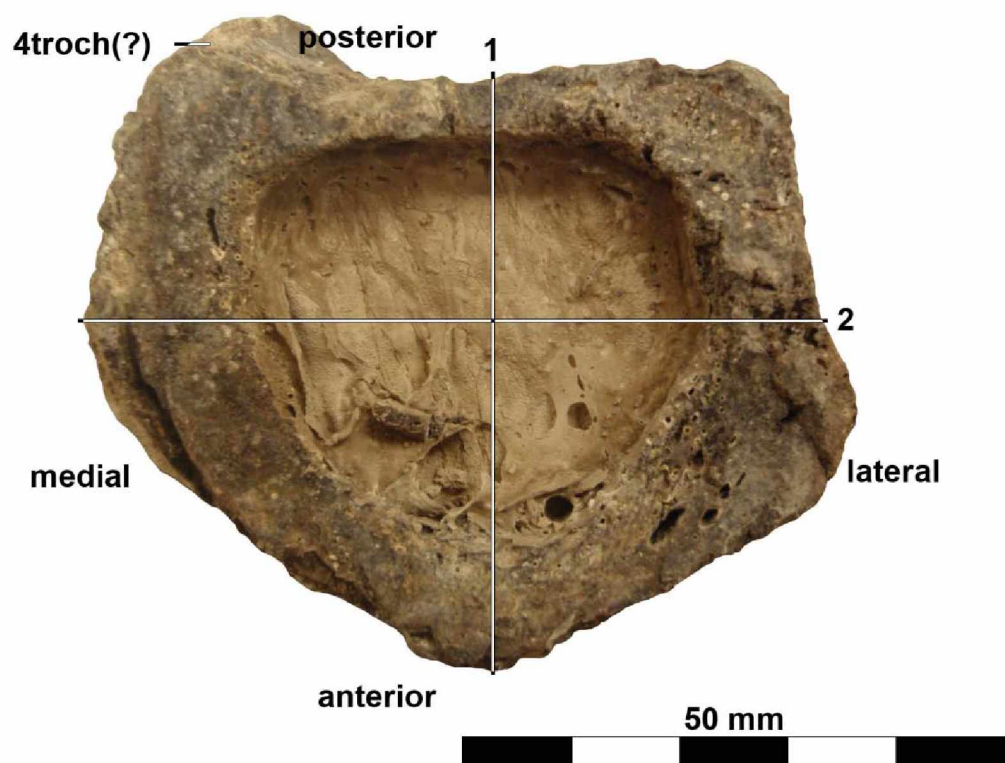
Fig. 3.24: Cross-section of the right femur of UAMES 12275. Numbers denote vectors along which measurements were taken. 1 = anteroposterior, 2 = mediolateral. Abbreviations: 4troch(?) = possibly part of the fourth trochanter

C. *Tibia*: At least one of the tibiae is partially preserved, consisting of the distal end and a portion of the shaft. Damage to the internal malleolus and the intercondylar groove makes it difficult to say whether it is the left or right tibia. What is interpreted to be the proximal end of a tibia is also preserved, but it is incompletely

prepared, so it is difficult to determine whether it is associated with the preserved portion of the distal tibia or is possibly from the other limb. This description will focus on the preserved distal tibia (Fig. 3.25, Fig. 3.26).

In articular view, the distal end of the tibia resembles a parallelogram in profile, though some of this is likely an artifact of the damage to the internal malleolus. In cross section, the shaft of the tibia is egg shaped, being approximately 5.2cm across in the mediolateral dimension and approximately 3.5cm across in the anteroposterior dimension.

Figure 3.25: Distal tibia fragment in posterior? view. Abbreviations: em = external malleolus, im = internal malleolus

Figure 3.26: Distal tibia fragment in anterior? view. Abbreviations: em = external malleolus, im = internal malleolus

D. Tarsals

1. *Astragalus*: This element is represented by a partial *right astragalus* which has varying degrees of damage to all surfaces. The element is mediolaterally broad and trapezoidal in dorsal view. Its anterior margin is slightly posteriorly concave and is mediolaterally longer than its posterior margin. The posterior margin of the astragalus angles slightly caudomedially (Fig. 3.27). Both the lateral and medial margins angle towards the midline of the element.

In dorsal articular view, the proximal articular surface is separated into two distinct bowl-shaped facets by a distinct ridge which forms an angle of approximately 65° to the mediolateral axis of the element. These articular facets are subequal in size, with the lateral facet being larger than the medial, though this may be an artifact of damage to the medial margin of the astragalus. The anterior ascending process is incomplete but is strongly skewed medially. The anterior surface of the anterior ascending process is dominated by an apparently triangular depression

approximately 2 mm deep whose outline parallels that of the process itself (Fig. 3.28). The posterior ascending process is broadly triangular in outline in caudal view with a laterally skewed apex, to a point where its lateral margin is nearly vertically oriented (Fig. 3.29). A shallow saddle oriented perpendicular to the mediolateral axis separates the distal articular surfaces.

Figure 3.27: Right astragalus in dorsal view. Abbreviations: aap = anterior ascending process, pap = posterior ascending process
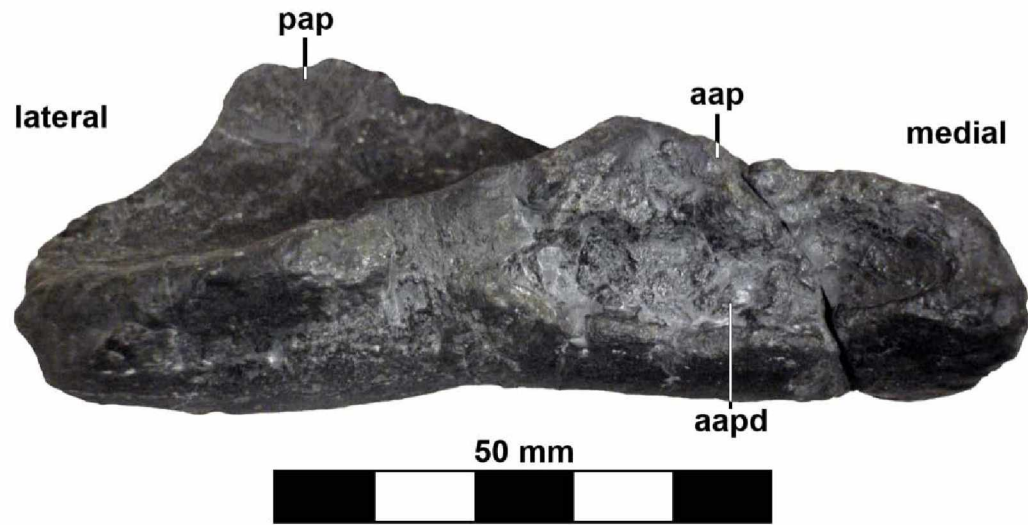
Figure 3.28: Right astragalus in anterior view. Abbreviations: aapd = depression of the anterior ascending process, pap = posterior ascending process
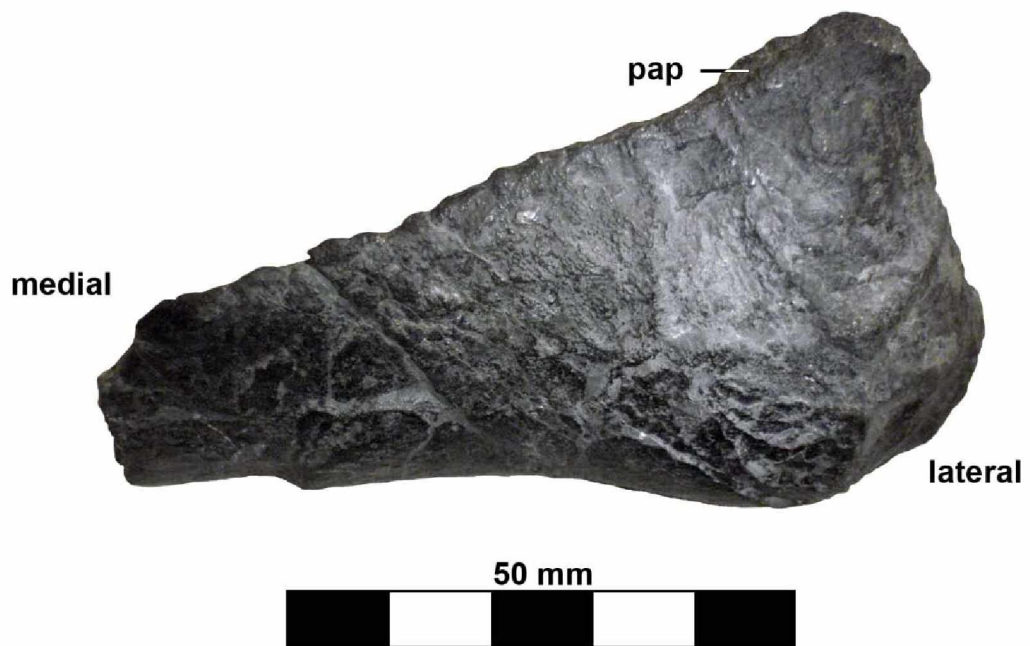
Figure 3.29: Right astragalus in posterior view. Abbreviations: pap = posterior ascending process

2. *Calcaneum*: A partial left(?) calcaneum is preserved, but the damage makes proper identification of structures and orientation of the element difficult. What appears to be the articular facet for the fibula is preserved as an ellipsoidal surface oriented almost perpendicular to the articular facet for the tibia (Fig. 3.30). The articular facet for the tibia is mediolaterally concave and slopes posterolaterally along its long axis (Fig. 3.31). In lateral view, the outline of the calcaneum as preserved approximates a quarter circle.
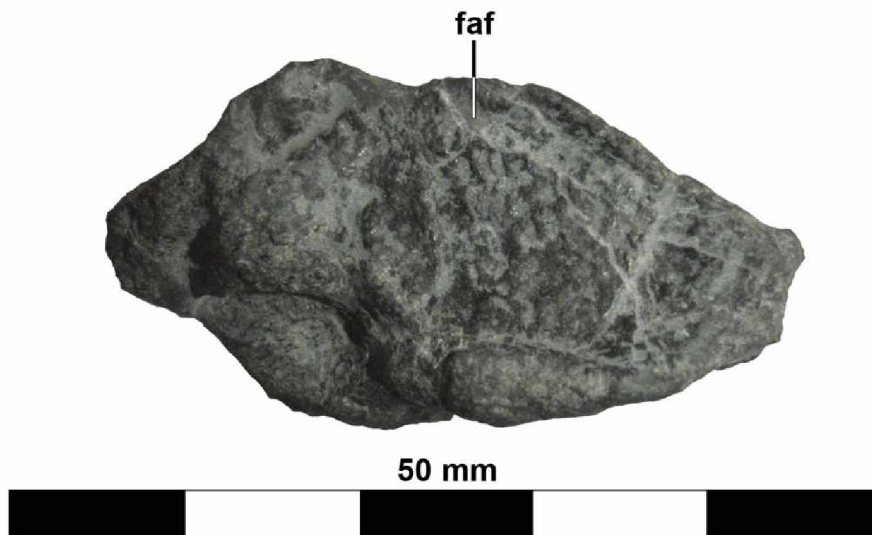
Figure 3.30: Left(?) calcaneum in dorsal(?) view. Abbreviations: faf = fibula articular facet
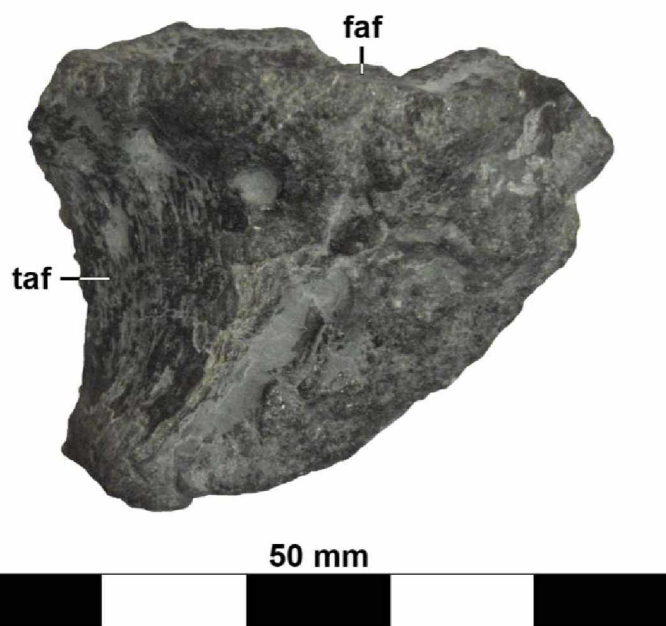
Figure 3.31: Left(?) calcaneum in medial(?) view. Abbreviations: faf = fibula articular facet, taf = tibia articular facet

E. *Pes*: UAMES 12275 preserves two partial pedes, which together preserve nearly all of the elements of the pes. The quality of preservation is highly variable, with those elements encased in a carbonate concretion being better preserved than those recovered from the shale matrix alone.

In general terms, the pes of UAMES 12275 resembles those of other hadrosauroids in being tridactyl, digitigrade, and possessing three closely-appressed metatarsals (metatarsals II, III, and IV; Fig. 3.32). Metatarsals II and IV lack scars or other features indicating that vestigial metatarsal I or metatarsal V were present. Therefore, the phalangeal formula of UAMES 12275 is interpreted to be 0-3-4-5-0, which is typical of hadrosauroids.

1. *Metatarsal II*: The description of the proximal articular end of metatarsal II is based on the right and the description of the distal end is based on the left. In both the left and the right pes, metatarsal II and metatarsal III remain fused together, preventing observation of the lateral surfaces of the metatarsals (Fig.

Fig. 3.32: Articulated partial left pes in dorsal view. Abbreviations: MTII = metatarsal II, MTIII = metatarsal III, MTIV = metatarsal IV

3.32, Fig. 3.33, Fig. 3.35). The proximal articular end is mediolaterally compressed, being almost 2.25 times as plantodorsally tall as it is mediolaterally broad, with a convex medial margin and a lateral margin contoured to appress the medial margin of metatarsal III. The articular surface is irregularly pitted and the proximodorsal, proximolateral, proximomedial, and proximoplantar surfaces are striated for the attachment of soft tissues. In cross section, the shaft has an outline that is nearly a right triangle, with the right angle oriented towards and appressed against the medial surface of metatarsal III. The dorsal margin of the shaft expands into a dorsolaterally projecting ridge or prominence which slightly overlaps metatarsal III. Distally to this expansion, the shaft of metatarsal II diverges slightly medially from metatarsal III, forming an approximately 1 cm wide gap between the metatarsals at its widest point. In distal articular view, the articular condyle of metatarsal II resembles a parallelogram in outline, with deep transverse striations in the middle of its medial and lateral surfaces that extend onto the articular surface as well.
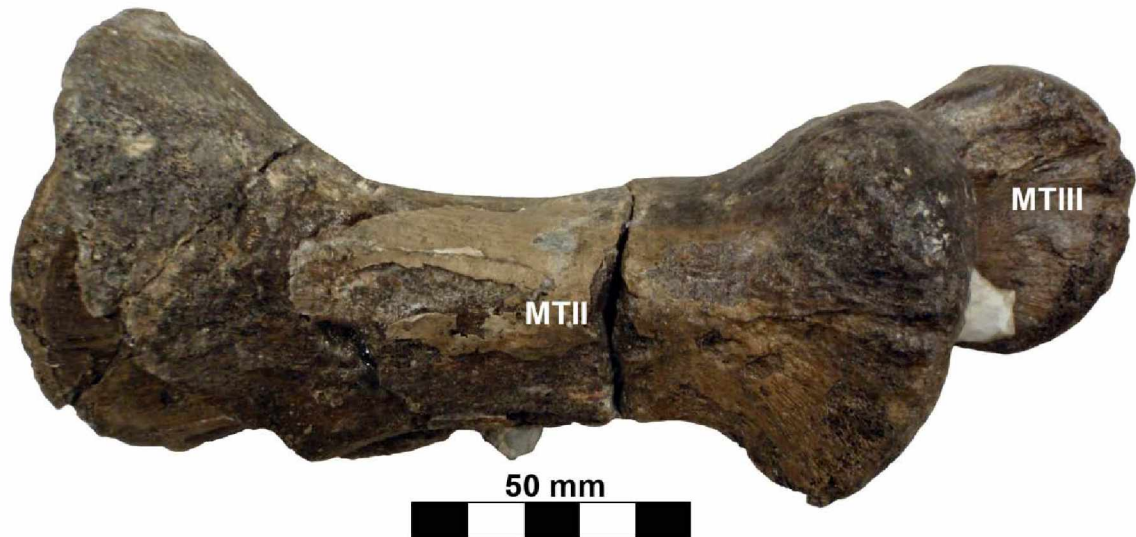
Figure 3.33: Articulated partial left pes in medial view. Abbreviations: MTII = metatarsal II, MTIII = metatarsal III

Figure 3.34: Articulated partial left pes in lateral view. Abbreviations: MTII = metatarsal II, MTIII = metatarsal III

2. *Metatarsal III*: Metatarsal III is best preserved in the left pes. When looking at the proximal articular end, its outline is D-shaped, with the proximomedial surface forming the leg of the D. This surface is concave to accommodate a similarly-shaped expansion of the proximolateral surface metatarsal II. The bulge of the D points laterally and is cupped by the medial margin of metatarsal IV (Fig. 3.35). In cross section, the proximal shaft of metatarsal III strongly resembles an equilateral triangle in profile and is oriented such that its apex is directed dorsally between metatarsal II and metatarsal IV (Fig. 3.36). Metatarsal II and metatarsal IV each articulate with one side of this triangle and are supported by the shaft of metatarsal III. The orientation of this triangle changes distally, so that only metatarsal II remains appressed against the shaft of metatarsal III; metatarsal IV remains in contact but is only supported by a vertex of the triangle. The distal end is trapezoidal in articular view, with a gently convex dorsal margin and an asymmetrically concave plantar margin. The asymmetry of the concavity causes the ventromedial margin to curve further in the plantar direction than the lateromedial margin (Fig. 3.37). As with metatarsal II, the medial and lateral surfaces of the distal articular end are heavily transversely striated in the middle (Fig. 3.32, Fig. 3.33, Fig. 3.35). In dorsal view, the shaft of metatarsal III appears

weakly sigmoidal, curving medially away from metatarsal IV towards metatarsal III. However, some of this apparent curvature may be due to the fracture which offsets the proximal end of metatarsals II and III from the remainder of the shafts in the left pes (Fig. 3.35).
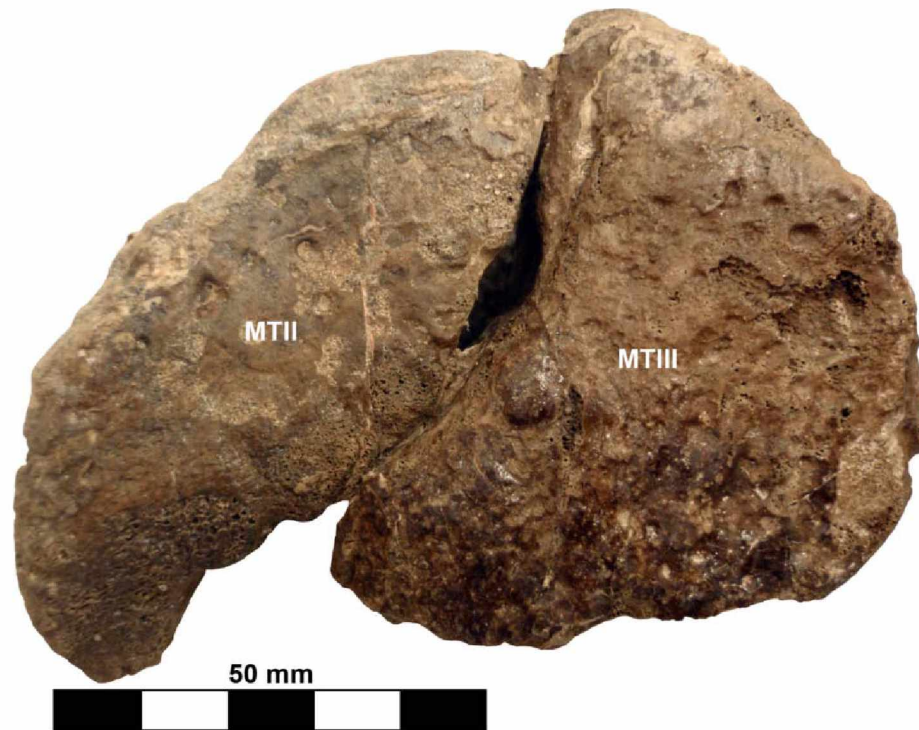
Figure 3.35: Articulated partial right pes in proximal articular view. Abbreviations: MTII = metatarsal II, MTIII = metatarsal III
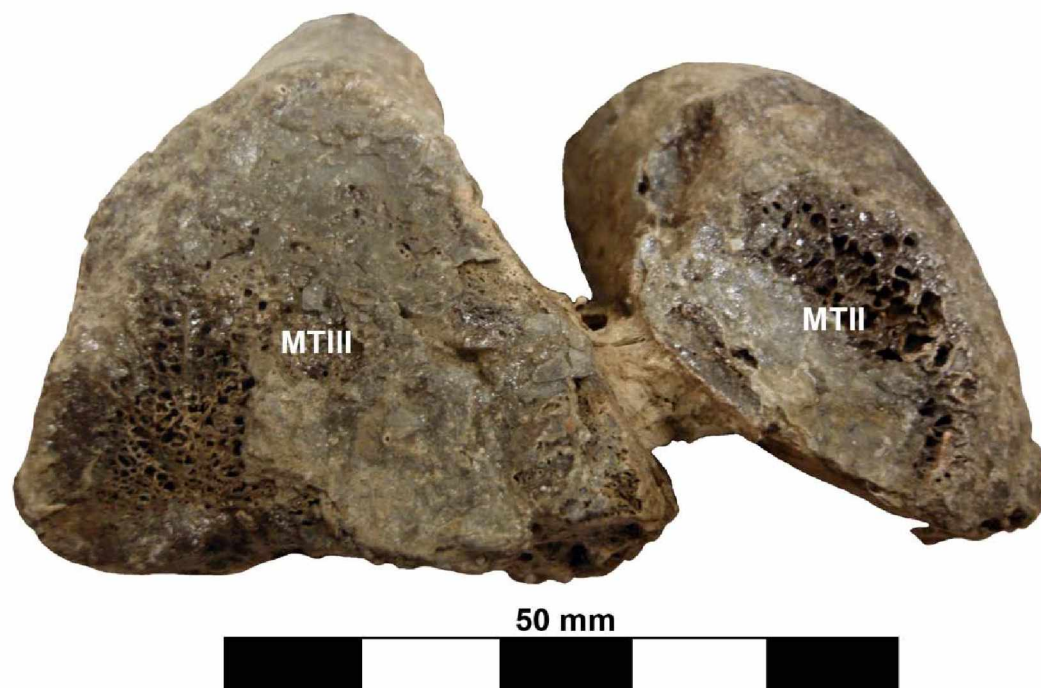
Figure 3.36: Articulated partial right pes in cross-section view, approximately at mid-shaft. Abbreviations: MTII = metatarsal II, MTIII = metatarsal III
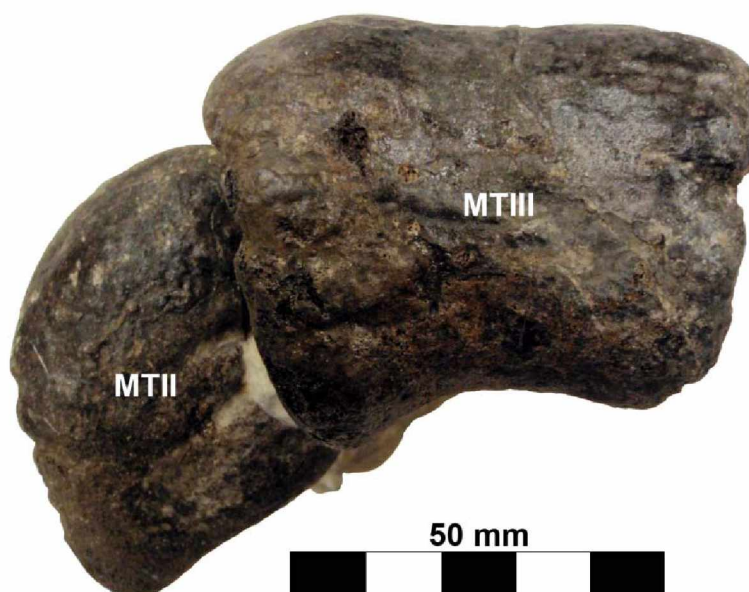
Figure 3.37: Articulated partial left pes in distal articular view. Abbreviations: MTII = metatarsal II, MTIII = metatarsal III

3. *Metatarsal IV*: Left metatarsal IV is incomplete distal to the midshaft, while the proximal end of right metatarsal IV is badly damaged. The proximal articular end is crescent shaped in profile, with a concave medial surface and a convex lateral surface. The concave medial surface of metatarsal IV articulates tightly with the bowed lateral surface of metatarsal III. A rugose, oblong swelling demarcates the final contact point between metatarsals III and IV: distal to this point, metatarsal IV diverges laterally from metatarsal III. The shaft of metatarsal IV is D-shaped in cross section and plantodorsally compressed, with the bow of the D oriented dorsally and the straight edge of the D forming the plantar surface of the metatarsal.

The distal articular surface is damaged but appears to be nearly square in articular view. The mediolateral constriction of the profile of the distal articular end is the most pronounced of all three metatarsals. Like metatarsal II and metatarsal III, the middle of the medial and lateral surfaces of metatarsal IV are transversely striated.

4. *Phalanges and Unguals*: Phalanges and unguals from all three digits of both feet were recovered, generally as isolated elements separate from the metatarsals and each other. Phalanges were identified based on comparison with similar-sized *Edmontosaurus* sp. phalanges and unguals housed at the University of Alaska Museum. The descriptions which follow are based upon phalanges from both pedes. With the exception of the first phalanges of digits II and IV, a distinction between left and right cannot be made.

a. *Right Digit II Phalanx 1 (II-1)*: At 7.3 cm in length along the midline, this is the longest of the three first phalanges (Fig. 3.38 - Fig. 3.41). Its proximal articular surface possesses a triangular outline in articular view, with a convex dorsomedial margin and a laterally skewed proximolateral corner. The dorsal surface of the element slopes gently medially. The long axis of the element

curves slightly laterally in dorsal view. Its distal articular end is an asymmetrical trapezoid in articular view, with a medially-inclined dorsal margin that is shorter than the plantar margin, a nearly vertical lateral margin, and a strongly medially-sloping medial margin. An asymmetric, medially-skewed concavity is present on the plantar surface.

Figure 3.38: First phalanges of the right pes in dorsal view. Abbreviations: DIIP1 = first phalanx of digit II, DIIIP1 = first phalanx of digit III, DIVP1 = first phalanx of digit IV

Figure 3.39: First phalanges of the right pes in plantar view. Abbreviations: DIIP1 = first phalanx of digit II, DIIIP1 = first phalanx of digit III, DIVP1 = first phalanx of digit IV

Figure 3.40: First phalanges of the right pes in proximal articular view. Abbreviations: DIIP1 = first phalanx of digit II, DIIIP1 = first phalanx of digit III, DIVP1 = first phalanx of digit IV.

Figure 3.41: First phalanges of the right pes in distal articular view. Abbreviations: DIIP1 = first phalanx of digit II, DIIIP1 = first phalanx of digit III, DIVP1 = first phalanx of digit IV.

b. *Digit III Phalanx 1 (III-1)*: This is the second longest of the first three phalanges, being subequal in length with II-1 (Fig. 3.38 - Fig. 3.41). Its proximal articular end is ovoid in articular view. The dorsal surface of the element possesses a slight convexity absent from the plantar surface and it lacks any significant mediolateral slope. The element is almost perfectly symmetrical about the midline and exhibits the greatest constriction between proximal and distal trochlea of all the first phalanges. The lateral and medial margins of the element form nearly right angles to the dorsal and plantar surfaces, giving the element a somewhat blocky appearance. Distally, the dorsomedial and dorsolateral margins of III-1 expand into prominent, symmetric protrusions. The distal trochlea of the element is trapezoidal in articular view and its plantar margin is plantodorsally concave.

c. *Right Digit IV Phalanx 1 (IV-1)*: This is the shortest of the three first phalanges (Fig. 3.38). Its proximal articular surface mirrors that of II-1 almost exactly in articular view (Fig. 3.38). The dorsal surface of the element slopes laterally, rather than medially as in II-1 (Fig. 3.38 - Fig. 3.41). Unlike II-1, the long axis of this element lacks mediolateral curvature. Its distal articular trochlea is

trapezoidal in articular view and has a concave plantar margin, the concavity of which is slightly skewed laterally.

d. *Digit II Phalanx 2 (II-2)*: II-2 is approximately 50% of the length of II-1. It lacks the curvature of the long axis seen in II-1 (Fig. 3.40, Fig. 3.41). Its articular surfaces possess trapezoidal outlines of similar shape to the distal articular surface of II-1 in articular view (Fig. 3.42, Fig. 3.43). Its dorsal surface slopes medially, but not as steeply as II-1 (Fig. 3.43). The plantar surface of the distal articular end is more concave than the plantar surface of the proximal articular end.

Figure 3.42: Second phalanges in dorsal view. Abbreviations: II-2 = second phalanx of digit II, III-2/III-3 = second or third phalanx of digit III
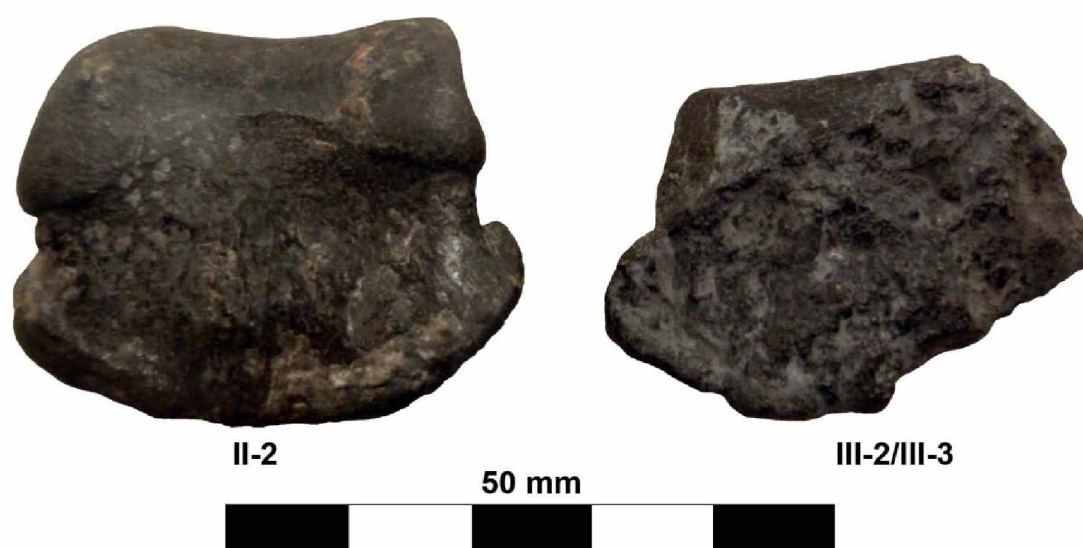
Figure 3.43: Second phalanges in plantar view. Abbreviations: II-2 = second phalanx of digit II, III-2/III-3 = second or third phalanx of digit III

e. *Digit III Phalanx 2 or 3 (III-2 or III-3)*: This phalanx is partially preserved, making its identification uncertain; judging from its size it appears to be either phalanx 2 or 3 (Fig. 3.42 – Fig. 3.45). Its proximal articular trochlea possesses a highly convex dorsal margin and a slightly convex plantar margin, giving it a D-shaped appearance in articular view. The medial and lateral corners of the plantar surface flare out from the main body of the phalanx. In distal view, the dorsal edge of the distal articular trochlea possesses a rectangular aspect.

f. *Digit IV Phalanx 2 (IV-2)*: This is the shortest of the second phalanges and can best be described as a shortened, blockier, version of IV-1.

g. *Unguals*: Two of the preserved unguals are nearly complete and the remainder are only partially complete (Fig. 3.46, Fig. 3.47). They are elongate, arrowhead-like elements unlike the short, blunt, hoof-like unguals of hadrosaurids. The longest of the preserved unguals is nearly the same length as phalanx 1 of digit III. All of the unguals are at least twice as proximodistally long as they are mediolaterally wide. Regardless of size, all taper from the proximal

articular trochlea to the tip, rather than flaring out abruptly into a spade-shape as in hadrosaurids. It is possible that this appearance is due to damage and does not accurately reflect the true shape of these unguals. The extreme length of the ungual of digit III seems to preclude the possibility that these unguals were originally hoof-like. However, hoof-like unguals are typically of similar length and width to pedal phalanx 1 of digit IV.

Figure 3.44: Second phalanges in proximal articular view. Abbreviations: II-2 = second phalanx of digit II, III-2/III-3 = second or third phalanx of digit III

Figure 3.45: Second phalanges in distal articular view. Abbreviations: II-2 = second phalanx of digit II, III-2/III-3 = second or third phalanx of digit III

Figure 3.46: Unguals in dorsal view. The left is interpreted to be phalanx III-4; the right is either II-3 or IV-5.

Figure 3.47: Unguals in plantar view. The left is interpreted to be phalanx III-4; the right is either II-3 or IV-5.

Chapter 4: Comparative Discussion

1. Introduction

The taxa compared to UAMES 12275 were selected on the basis of stratigraphic age and/or phylogenetic position within Hadrosauriformes (using the phylogeny of Prieto-Marquez, 2010a), in an effort to assemble a temporally and phylogenetically broad sample for comparison. This had the additional effect of providing a set of geographically widely dispersed comparators.

The fossil record of Hadrosauriformes from the late Cenomanian to late Santonian (approximately 95 Ma to 84 Ma) represents a major gap in our understanding of the clade's evolution. The remains of UAMES 12275 were recovered from Turonian-aged sediments of the Matanuska Formation in southern Alaska. The only other positively known Turonian-aged hadrosauroids include *Jeyawati rugoculous* (New Mexico) and the Asian taxon *Levnesovia transoxiana* (Uzbekistan). The ages of *Bactrosaurus johnsoni* (Mongolia) and *Gilmoreosaurus mongoliensis* (Mongolia) are problematic, being either Turonian-Coniacian in age (Nessov 1995, 1997; Averianov, 2002; Sues and Averianov, 2009) or Campanian-Maastrichtian in age (Van Itterbeek et al., 2005; Prieto-Marquez, 2010b). The ages and geographic distribution of these taxa show that hadrosauroids were established and geographically widespread some time before the Turonian.

Preliminary comparisons of UAMES 12275 with material currently attributed to *Edmontosaurus* sp. demonstrated that UAMES 12275 is certainly a derived iguanodontian, likely of hadrosauriform grade at least, and possibly more derived. For these reasons, comparative taxa were selected from a broad morphological range of members of Hadrosauriformes (*sensu* Prieto-Marquez 2010a) whose postcrania are well-known. Selected taxa include the basal hadrosauriforms *Iguanodon bernissartensis* (Barremian-Albian, Belgium; Norman, 1980), *Mantellisaurus*

atherfieldensis (Hauterivian-Aptian, United Kingdom; Norman, 1986), and
Ouranosaurus nigeriensis (Albian, Nigeria; Taquet, 1976); the basal hadrosauroids
Altirhinus kurzanovi (Aptian-Albian, Mongolia; Norman, 1998), *Bactrosaurus johnsoni*
(Turonian-Coniacian/Campanian-Maastrichtian, Mongolia; Godefroit et al., 1998),
Eolambia caroljonesa (Cenomanian, Utah; Kirkland, 1998), *Gilmoreosaurus*
mongoliensis (Turonian-Coniacian/Campanian-Maastrichtian, Mongolia; Prieto-
Marquez and Norell, 2010; personal observations), *Levnesovia transoxiana* (Turonian,
Uzbekistan; Sues and Averianov, 2009), *Nanyangosaurus zhugeii* (Albian, China; Xu et
al., 2000), *Probactrosaurus gobiensis* (Albian, China; Norman, 2002) and
Telmatosaurus transsylvanicus (Maastrichtian, Romania; Weishampel et al., 1993);
and one hadrosaurid, *Edmontosaurus* sp. (Campanian-Maastrichtian, North America;
personal observations). *Protohadros byrdi* (Cenomanian, Texas; Head, 1998) and
Jeyawati rugoculus (Turonian, New Mexico; McDonald et al. 2010) were not included
because their postcrania are very poorly known.

2. Axial Skeleton

The poor preservation of the cervical neural arches, dorsal vertebrae, and dorsal ribs
prevents any taxonomically informative discussion of these elements.

The caudal vertebrae in UAMES 12275 are elongated, cylindrical, and weakly
amphicoelous, conditions which are typical of non-hadrosauroid hadrosauriform and
non-hadrosaurid hadrosauroid dinosaurs. Hadrosaurids such as *Edmontosaurus sp.*
possess anteroposteriorly short, disc-like, weakly amphicoelous caudal vertebrae
whose articular surfaces possess a rounded, hexagonal outline in articular view.

3. Appendicular Skeleton

1. Pectoral Girdle

A. *Scapula*: The hadrosauriform scapula is an element which exhibits significant taxonomically informative morphologic variation (Table 4.1).

Of the taxa considered for this study, *Iguanodon bernissartensis* possesses a scapula most similar to the basal iguanodontian morphology. The proximal head of the scapula is approximately twice the dorsoventral height of the distal end of the blade,

Table 4.1: Comparative character matrix of taxonomically significant morphologic traits of the scapula. Abbreviations: dvh = dorsoventral height, l = left scapula, r = right scapula

Taxon	dvh head > dvh end	dvh head dvh e ≤	straight dorsal margin	convex dorsal margin	deltoid ridge weakly developed / absent	strongly developed deltoid ridge	proximal constriction weakly developed or absent	proximal constriction strongly developed	straight distal termination of scapular blade
Iganodon bernissartensis	X		X		X		X		
Mantellisaurus atherfieldensis		X	X		X				X
Ouranosaurus nigeriensis	X			X	X				X
Altirhinus kurzanovi	X			X	?	?		X	
Probactrosaurus gobiensis	X		X		X	X			
Bactrosaurus johnsoni		X	X		X			X	
Glmoreosaurus mongoliensis		X		X	X			X	
Telmatosaurus transsylvanicus		X		X		X		X	
Edmontosaurus sp.		X		X		X		X	
UAMES 12275		*X (l)*		*X (l,r)*	*X (l,r)*			*X (l,r)*	*X (l)*

its dorsal and ventral margins are sub-parallel, it lacks a proximal constriction between the head and distal blade, the deltoid ridge is absent, and the distal termination of the scapular blade forms a straight edge.

The scapula of *Gilmoreosaurus mongoliensis* possesses a gently dorsally convex dorsal margin, a moderately well-developed deltoid ridge, a moderately well-developed proximal constriction, a ventral margin that flares away from the dorsal margin posterior to the proximal constriction, and a distal termination of the scapular blade which is subequal in dorsoventral height to the scapular head. *Telmatosaurus transsylvanicus* possesses a scapula with the most well-developed deltoid ridge of the non-hadrosaurid hadrosauroid taxa considered for this study. It possesses a dorsally convex dorsal margin, pronounced proximal constriction, ventrally flaring ventral margin, and a distal termination of the scapular blade that is dorsoventrally taller than the proximal end of the scapula.

In *Edmontosaurus sp.* the deltoid ridge is prominent and anteroposteriorly long, the dorsal margin is strongly dorsally convex, the dorsal and ventral margins of the scapular blade flare away from each other, and the distal termination of the scapular blade is subequal in dorsoventral height to the scapular head.

The dorsal margin of the left scapula in UAMES 12275 is strongly dorsally convex, similar to the condition seen in *Edmontosaurus* sp., while its deltoid ridge is weakly developed, as in non-hadrosaurid hadrosauroids such as *Gilmoreosaurus mongoliensis*. The straight edge of its distal termination is similar to that seen in non-hadrosauroid hadrosauriforms, while the greater dorsoventral height of the distal termination than the articular head is similar to that observed in *Telmatosaurus transsylvanicus*. Despite the dissimilarities between the left and right scapulae, both possess a dorsally convex dorsal margin, weakly developed deltoid ridges, and well-developed proximal constrictions. These character states are seen

in the scapulae of non-hadrosaurid hadrosauroids such as *Gilmoreosaurus* and *Telmatosaurus*. In summary, the scapulae of UAMES 12275 are similar to those of basal hadrosauroids but also possess a suite of characters which demonstrate that they may be morphologically distinct from the scapulae of other taxa examined in this study.

1. The Scapula Problem

As discussed above, the scapulae of UAMES 12275 are not bilaterally symmetrical and the differences between the two are profound enough to question their identity. In fact, this level of variation is typically associated with generic-level differences. Initially, it was assumed that the left scapula, being the larger of the two elements, had been misidentified and was possibly a partial pubis, but this notion was dispelled by research and communication with several hadrosaur experts who insisted that both elements were scapulae. Accepting this general consensus of the experts queried, an attempt was made to come up with alternative explanations for the great morphological differences between the two elements. The differences between the left and right scapula are summarized below (Fig. 4.1):

1) The dorsoventral height at the proximal constriction differs by approximately 2 cm.

2) The blade of left scapula expands to nearly twice the dorsoventral height of the blade of the right scapula distally.

3) The dorsal margin of the left scapula possesses greater curvature in the region of the proximal constriction than the dorsal margin of the right scapula.

Despite the obvious morphological differences between the two bones, it is also obvious that both bones very strongly resemble hadrosauroid scapulae—hence

Figure 4.1: Comparison of left and mirrored right scapula (white outline) at the same scale to illustrate their substantial morphological differences.

the confusion surrounding their identification. Three hypotheses are advanced in an effort to explain these morphological differences. They are presented in order of increasing probability, along with a summary of the evidence refuting each hypothesis.

1) Plastic deformation of bone from increased stress loads.

Both elements in question, along with most every other element from this animal and many portions of the concretion it was encased in, clearly show brittle failure of bone and rock in response to compression or loading stresses (i.e. compaction of sediments, tectonic forces, or some combination thereof), rather than plastic deformation. The crushing experienced by the left scapula cannot account for the differences in dorsoventral height between it and the right scapula. All fractures which have broken completely through the element are oriented perpendicular to the proximodistal axis (Fig. 4.1). These fractures could account for some small amount of expansion along the proximodistal axis, but would not allow for dorsoventral expansion. Similarly, there is no sign of crushing damage to the right scapula oriented parallel to the proximodistal axis that could have compacted the right scapula down to its present dimensions from an original shape that resembled the left scapula.

2) Only one element is a scapula, and the other has been misidentified.

Only the skull, pectoral girdle, and pelvic girdle contain elements with parts that can be described as blade-like. The sheer size of the problematic bones, let alone their shapes, precludes the possibility of either of them having come from the skull. The coracoids and sternal plates of the pectoral girdle are significantly smaller than and bear little resemblance to the scapulae. The misidentified element would therefore be from the pelvic girdle if it is neither from the skull nor the pectoral girdle. Of the bones of the pelvic girdle, the element which most resembles the scapula in a broad sense is the pubis, and particularly the prepubic process. Neither the ilium nor the ischium possess blade-like structures. However, the prepubic process of the pubis is separated from the acetabular margin by a proximal constriction that is defined by a ventrally concave dorsal margin and a dorsally concave ventral margin, which is plesiomorphic for Hadrosauriformes (Prieto-Marquez 2010a). As shown in Fig. 4.1, both bones have one convex and one concave margin, consistent with a scapula but not a prepubic process. It is possible that one of the concavities is not apparent simply because of the damage and/or loss, but this seems doubtful given the remarkable similarities between the proximal ends of the bones in articular view and the fact that neither seem to be missing a significant portion of their proximal ends. Additionally, neither element resembles the pubes of any of the taxa considered as part of this study, or any of the pubes figured in Prieto-Marquez (2010a).

3) Both are scapulae, but one belongs to a different animal.

The section of the Matanuska Formation this animal was recovered from represents a deep-shelf marine setting, meaning that the carcass was washed out to sea and floated for an indeterminate amount of time before eventually sinking to the seafloor. Even if the animal had been caught up in a mass-

mortality event such as a flood, it is likely that it would have been widely dispersed from the others, especially considering the offshore setting in which it was found. In addition, the fossil was partially articulated when it was collected from a horizon approximately 10-15 cm in thickness and of less than 3 m^2 in areal extent. I made trips to the quarry site in 2009 and 2010 to search for invertebrates and take samples for palynological analysis which failed to turn up any other vertebrate remains. A lone, millimeter-sized teleost tooth is the only other sign of vertebrate life found thus far at this site. Given that the remains were discovered via heavy machinery, other elements, either from this animal or others, may have been destroyed in excavation; however, the original collectors sieved the debris piles several times over multiple seasons and failed to recover additional bone fragments. Finally, no other overlapping portions of the hadrosauroid skeleton were found (i.e., three humeri or femora of similar size), precluding the possibility that there are two or more individuals preserved in the quarry.

Thus, three of the most plausible explanations for the morphological differences between the elements are rejected, and it is concluded that both elements are the scapulae of a single individual. In the words of Sherlock Holmes, "...when you have eliminated the impossible, whatever remains, however improbable, must be the truth" (Doyle, 1890). Until such time as this working hypothesis is falsified, both elements are interpreted to be scapulae.

B. *Humerus*: The proximal end of the humerus is the most taxonomically informative region of the element. This discussion focuses on comparisons of the structures present on both the anterior and posterior surfaces of the proximal end of the humerus, as well as on the morphology of the medial tuberosity and deltopectoral crest (Table 4.2).

Table 4.2: Comparative character matrix of taxonomically significant morphologic traits of the humerus. Abbreviations: dpc = deltopectoral crest

Taxon	curved lateral margin of dpc	straight lateral margin of dpc	dpc < 1/3 humerus length	1/3 humerus length < dpc < 1/2 humerus length	dpc > 1/2 humerus length	proximal end of humerus rectangular in outline	proximal end of humerus not rectangular in outline	presence of anterior bicipital sulcus	presence of distinct ridge on posterior surface of humerus
Iguanodon bernissartensis	X		X				X		
Mantellisaurus atherfieldensis	X		X				X		
Ouranosaurus nigeriensis		X		X			X	X	
Altirhinus kurzanovi		X		X			X	?	
Nanyangosaurus zhugeii	X			X			X	X	?
Probactrosaurus gobiensis		X		X	X				
Eolambia caroljonesa		X		X			X	X	
Levnesovia Transoxiana	?	?	?	?	?		X	X	X
Gilmoreosaurus mongoliensis		X		X			X	X	
Bactrosaurus johnsoni		X		X			X	X	
Edmontosaurus sp.		X			X	X		X	
UAMES 12275		*X*		*X*		*X*		*X*	*X*

Among basal hadrosauriforms, *Iguanodon bernissartensis* possesses a humerus with the shortest deltopectoral crest relative to overall humeral length, and the only humerus out of those examined with a medially concave lateral margin of the deltopectoral crest. The deltopectoral crest extends distally approximately one-third the overall length of the humeral shaft. Distal to the bend in the humeral shaft, the diameter of the humerus does not constrict appreciably before expanding into the distal articular condyles, which are subequal in total mediolateral width to the proximal end of the humerus. The medial tuberosity of the humerus does not expand significantly medially.

The humerus of *Probactrosaurus gobiensis* is much simpler in comparison, with an egg-shaped proximal articular condyle positioned closer to the medial tuberosity than the deltopectoral crest and a medial tuberosity that does not expand significantly medially. Slight depressions on the posterior surface of the humerus offset the deltopectoral crest and the medial tuberosity from the humeral shaft. The humerus of *Levnesovia transoxiana* as preserved is incomplete. It possesses an egg-shaped proximal articular condyle that is located in the middle of the proximal end and buttressed on the posterior surface by a distinct ridge offset from the medial and lateral tuberosities by broad, shallow troughs. The proximal articular condyle is prominent in anterior view, giving the proximal margin of the humerus a rounded outline. The medial tuberosity is weakly expanded relative to the medial margin of the humeral shaft. A bicipital sulcus is present on the anterior surface but appears weakly developed, though this may be an artifact of its partial preservation.

In *Edmontosaurus sp.*, the proximomedial corner of the medial tuberosity is not greatly expanded medially, so that the outline of the proximal end of the humerus in anterior view is rectangular. The deltopectoral crest extends distally for more than half the length of the humerus and is separated from the humeral shaft on the anterior surface by a triangular bicipital sulcus. The articular head is well defined on

the posterior surface as a lozenge-shaped protuberance that appears to be supported by a weakly defined ridge which is separate from the medial tuberosity and the deltopectoral crest by broad, shallow troughs.

The humerus of UAMES 12275 possesses a combination of characters observed individually in *Probactrosaurus, Levnesovia*, and *Edmontosaurus*. Similar to *Probactrosaurus, Levnesovia*, and *Edmontosaurus*, the medial tuberosity of the humerus of UAMES 12275 is weakly expanded relative to the medial margin of the humeral shaft. Dissimilar to *Levnesovia* but similar to *Probactrosaurus* and *Edmontosaurus*, the humerus of UAMES 12275 possesses a straight lateral margin of the deltopectoral crest, giving the proximal end of the humerus a semi-rectangular outline in anterior view. Similar to *Levnesovia*, the humeral head of UAMES 12275 is buttressed by a distinct ridge on the posterior surface of the proximal end that was offset from the medial and lateral tuberosities by broad, deep troughs. The humerus of UAMES 12275 differs from that of *Probactrosaurus* and *Levnesovia* in possessing a broad, deep bicipital sulcus on the anterior surface which separates the deltopectoral crest from the humeral shaft. It differs from that of *Edmontosaurus* in possessing a shorter deltopectoral crest, and in being more gracile than similarly sized *Edmontosaurus* humeri. In summary, the humerus of UAMES 12275 resembles those of non-hadrosaurid hadrosauroids such as *Probactrosaurus* and *Levnesovia*, while also possessing a suite of characters which demonstrate that it is morphologically distinct from the humeri of other taxa examined in this study.

C. *Radius and Ulna*: The poor preservation of both of these bones in UAMES 12275, as well as their conservative morphologies, prevents any meaningful discussion or comparison with those of other hadrosauriformes.

D. *Carpus, Metacarpus, and Phalanges*: As manual elements of UAMES 12275 consist chiefly of indeterminate fragments of bone, no meaningful discussion can be made.

2. Pelvic Girdle

A. *Ilium*: Given the fragmentary nature of the ilium in UAMES 12275, comparisons of this element focus on the size and morphology of the supraacetabular process (Table 4.3).

In basal hadrosauriforms such as *Iguanodon* and *Mantellisaurus*, the supraacetabular process is an undifferentiated part of a more or less continuous, laterally directed ridge along the dorsolateral margin of the iliac plate (here used to refer to the region of the ilium between the pre- and postacetabular processes), which can extend cranially onto the preacetabular process and caudally onto the postacetabular process. This is similar to the condition seen in *Ouranosaurus*, *Eolambia*, *Gilmoreosaurus*, and *Probactrosaurus*. However, in these taxa the supraacetabular process forms a distinct swelling or process of bone that stands out from the rest of the ridge. *Bactrosaurus* and *Levnesovia* both appear to possess a supraacetabular process that is separate and distinct from the laterally directed ridge running along the dorsal margin of the ilium. In hadrosaurids such as *Edmontosaurus*, the supraacetabular process forms a discrete lateroventrally projecting flange of bone that is separate from any laterally-directed, dorsally located ridge running along the iliac plate and/or the preacetabular process.

The extent to which the dorsal margin of the iliac plate is formed by the supraacetabular process is another taxonomically informative characteristic of hadrosauriforms. In taxa where the supraacetabular process is incorporated into the laterally directed dorsal ridge of the ilium, it is difficult to assess this character. In contrast, the supraacetabular process of most derived hadrosaurids, such as

Table 4.3: Comparative character matrix of taxonomically significant morphologic traits of the ilum. Abbreviations: supraacetabular process = supraacetabular process

Taxon	sapr forms part of uniform, continuous dorsal ridge	sapr forms part of non-uniform, continuous dorsal ridge	sapr forms discrete flange of bone	sapr ventrally deflected	sapr not ventrally deflected	sapr linked by saddle to ischial peduncle
Iguanodon bernissartensis	X			X		
Mantellisaurus atherfieldensis	X			X		
Ouranosaurus nigeriensis		X		X		
Altirhinus kurzanovi		X		X		
Probactrosaurus gobiensis		X		X		
Eolambia caroljonesa		X			X	X(?)
Levnesovia transoxiana			X	X		
Gilmoreosaurus mongoliensis		X		X		
Bactrosaurus johnsoni			X(?)	X		
Edmontosaurus sp.			X	X		X
UAMES 12275			**X**		**X**	

Edmontosaurus, forms between one quarter and one half of the dorsal margin of the iliac plate. *Bactrosaurus* possesses a supraacetabular process which forms approximately two-thirds of the dorsal margin of the iliac plate.

An additional difference between the ilia of various grades of hadrosauriforms can be seen in the presence or absence of a "saddle" connecting the ventrolateral margin of the supraacetabular process with the dorsolateral margin of the ischial peduncle (Fig. 4.2A, B).
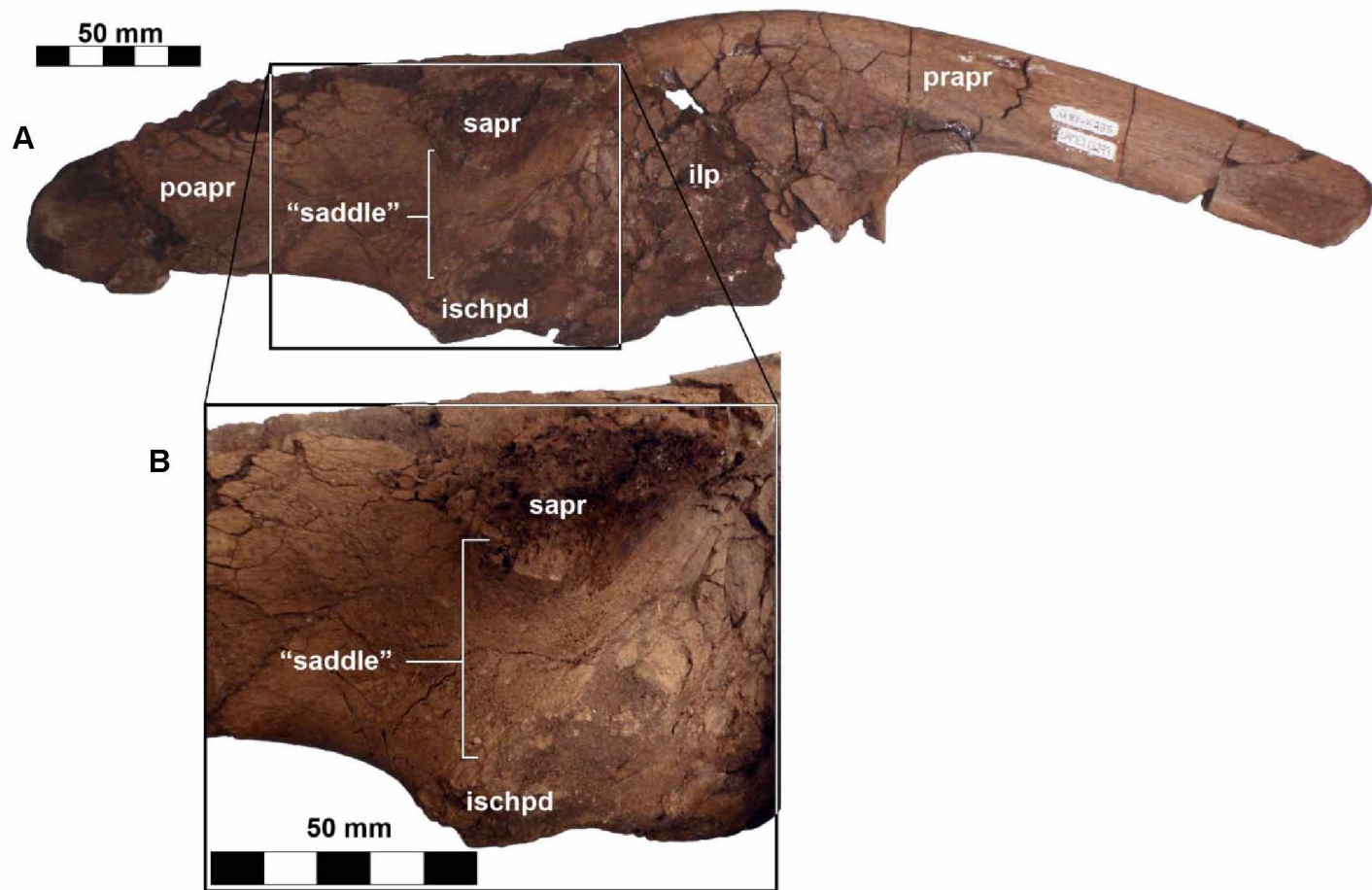
Fig. 4.2: A— Right ilium of *Edmontosaurus* sp. in right lateral view; specimen UAMES 13291 from the University of Alaska Museum Earth Science collection. B—Right ilium of *Edmontosaurus* sp. zoomed in on the region of the supraacetabular process and ischial peduncle. Abbreviations: ilp = iliac plate, ischpd = ischial peduncle, poapr = postacetabular process, prapr = preacetabular process, sapr = supraacetabular process, "saddle" = anteroposteriorly convex surface formed by the lateroventral surface of the supraacetabular process and the dorsolateral surface of the ischial peduncle.

Hadrosaurids such as *Edmontosaurus* possess such a saddle, and one appears to be weakly developed in the basal hadrosauroid *Eolambia*, whereas this is absent in basal hadrosauriforms and other basal hadrosauroids.

The ilium of UAMES 12275 is unique among the ilia considered as part of this study for several reasons. First, the supraacetabular process of UAMES 12275 is discrete and separate from any laterally-directed ridge that ran along the dorsolateral surface of the ilium. This is unlike the morphology of the supraacetabular process from every other non-hadrosaurid hadrosauriform examined except *Levnesovia transoxiana* and possibly *Bactrosaurus johnsoni*. Second, the anteroposterior length of the supraacetabular process of UAMES 12275 is significantly greater than that of most other taxa considered as part of this study. It appears to have formed approximately three-quarters of the dorsal margin of the iliac plate. It may have formed less, as the iliac plate is incomplete. The only taxon examined which has a long supraacetabular process is *Bactrosaurus johnsoni*, but the supraacetabular process of this taxon only forms approximately two-thirds of the dorsal margin of the iliac plate. Third and most importantly, unlike the supraacetabular process of every other taxon examined as part of this study, the supraacetabular process of the ilium in UAMES 12275 is not deflected ventrally to any appreciable degree. Instead, it extends laterally from the iliac plate at an almost right angle.

B. *Femur*: As previously discussed, the femora of UAMES 12275 are incomplete and consist of the fourth trochanter and portions of the shaft proximal to this structure. Fortunately, the fourth trochanter and the femoral shaft in the vicinity of it are taxonomically informative regions (Table 4.4).

Of the basal hadrosauriforms examined, *Mantellisaurus atherfieldensis* possesses a femur which exhibits many traits similar to iguanodontian femora: a well-developed lesser trochanter, strong anteroposterior curvature of the shaft in medial view, and

Table 4.4: Comparative matrix of taxonomically informative morphologic traits of the femur and fourth trochanter. Abbreviations: ap = anteroposteriorly, 4th troch = fourth trochanter, int = intermediate, Y = yes, N = no

Taxon	Femur shaft ap curved	Femur shaft ap straight	4th troch laterally deflected	4th troch not deflected	4th troch scalene	4th troch int	4th troch isosceles	height of 4th troch < shaft diameter	height of 4th troch ≥ shaft diameter	lesser trochanter?
Iguanodon bernissartensis		X		X	X			X		Y
Mantellisaurus atherfieldensis	X		X		X			X		Y
Ouranosaurus nigeriensis	X			X	X			X		Y
Altirhinus kurzanovi	X		?	?	?	?	?	?	?	Y
Nanyangosaurus zhugeii	X		?	?	X			X		?
Eolambia caroljonesa	X			X	X			X		Y
Probactrosaurus gobiensis	X		X				X	X		Y
Bactrosaurus johnsoni	X			X			X	X		Y
Gilmoreosaurus mongoliensis	X			X		X		X		Y
Telmatosaurus transsylvanicus		X		X	X			X		N
Edmontosaurus sp.		X		X			X	X		N
UAMES 12275	**X**			**X**	**X**				**X**	**Y**

a fourth trochanter with a laterally deflected apex in posterior view and the outline of a scalene right triangle in medial view. In addition, the fourth trochanter projects posteriorly to a maximum height approximately one-half the diameter of the shaft and its proximodistal length is approximately one-quarter the length of the femur as a whole.

Eolambia caroljonesa possesses a femur with a prominent lesser trochanter, anteroposterior curvature of the femoral shaft in medial view, and a fourth trochanter that is not laterally deflected and possesses the outline of a scalene right triangle. The fourth trochanter projects posteriorly to a maximum height between one-third and one-half the diameter of the shaft and its proximodistal length is approximately one-third that of the femur. In *Gilmoreosaurus mongoliensis*, the lesser trochanter is very well developed. The femur possesses strong mediolateral curvature of the shaft but lacks appreciable anteroposterior curvature. The fourth trochanter possesses an outline intermediate between an isosceles and a scalene right triangle and is subparallel to the curvature of the shaft, so that it does not appear laterally deflected. The fourth trochanter projects posteriorly to a maximum height between one-half and three-quarters the diameter of the shaft and its proximodistal length is approximately one-third that of the shaft.

The femur of *Edmontosaurus sp.* lacks a lesser trochanter and possesses a straight shaft with an isosceles fourth trochanter that is not laterally deflected. The fourth trochanter projects posteriorly to a maximum height between two-thirds and three-quarters the diameter of the femur and its proximodistal length is approximately one-quarter to one-third the length of the femur.

Similar to *Eolambia* and *Gilmoreosaurus*, the lesser trochanter of UAMES 12275 appears well developed and the shaft of the femur possesses a very weak anteroposterior curvature. The fourth trochanter of UAMES 12275 has an outline

intermediate between an isosceles and a scalene triangle, similar to *Gilmoreosaurus*. Unlike all other taxa examined for this study, the fourth trochanter of UAMES 12275 projects posteriorly to a height equal to the diameter of the shaft and possibly further, given that part of the posterior margin of the fourth trochanter is missing. In summary, the femora of UAMES 12275 resemble those of non-hadrosaurid hadrosauroids such as *Eolambia* and *Gilmoreosaurus*, while also possessing a suite of characters which demonstrate that they are morphologically distinct from the femora of other taxa examined in this study.

C. *Tibia*: The distal end of the hadrosauriform tibia is fairly morphologically consistent between taxa, with the chief observable difference being whether the articular surface of the medial malleolus is approximately even with that of the lateral malleolus or offset dorsally. Unfortunately, the medial malleolus of the tibia in UAMES 12275 is incomplete, so no meaningful comparison or discussion is possible.

D. *Astragalus*: The astragalus is a fairly morphologically conservative element in Hadrosauriformes. It varies dominantly in its mediolateral breadth, and does so inconsistently among different subgroups of Hadrosauriformes. In UAMES 12275, the astragalus is mediolaterally broad enough that it appears to cap the entire medial malleolus of the tibia, a state seen in morphologically disparate taxa such as *Iguanodon bernissartensis* and *Edmontosaurus* sp..

E. *Calcaneum*: The calcaneum of UAMES 12275 is so poorly preserved that it is difficult to determine which ankle it belongs to and no meaningful morphologic comparisons can be made.

F. *Metatarsals*: These elements are fairly morphologically consistent between taxa, differing mainly in their relative robustness or gracility. The metatarsals in UAMES 12275 are more gracile than similarly-sized metatarsals of *Edmontosaurus sp.*.

G. *Pedal Phalanges and Unguals*: At first glance, the pedal phalanges of hadrosauriform dinosaurs do not appear to vary much except in the morphology of the unguals. However, meaningful variation exists among the first phalanges (Table 4.5).

Phalanges II-1 through IV-1 of *Mantellisaurus atherfieldensis* are fairly symmetrical about their own midlines, lacking significant curvature or other distortion, and differ chiefly in mediolateral width, with phalanx III-1 being the mediolaterally broadest of the first phalanges. The distal articular ends of all three first phalanges possess a dorsal margin which curves posterodorsally at the midline of the phalanx, forming a crescent-shaped extension of the articular surface onto the dorsal surface of the phalanx. The unguals of *Mantellisaurus* are shaped like blunted arrowheads and possess well-developed claw grooves. In *Gilmoreosaurus mongoliensis*, phalanx II-1 is the longest of the first phalanges, while phalanges III-1 and IV-1 are subequal in proximodistal length. Phalanx III-1 is nearly as mediolaterally broad as it is proximodistally long, and phalanx IV-1 shares this blocky appearance. The unguals appear to be mediolaterally broad, blunted arrowheads lacking claw grooves. In *Edmontosaurus sp.*, phalanges II-1 and III-1 are subequal in size and proximodistally longer than phalanx IV-1. The plantar margin of the mediodistal surface of phalanx II-1 is expanded medially, while the plantar margin of the laterodistal surface of phalanx IV-1 is expanded laterally. Like other hadrosaurids, the unguals of *Edmontosaurus* are broad, spade-shaped, and hoof-like.

The pedal phalanges of UAMES 12275 are fairly gracile elements. Phalanx II-1 is the longest and exhibits a distinct mediolateral curvature along its long axis, and the plantar margin of its mediodistal surface is expanded medially, as in *Edmontosaurus*. Phalanx III-1 exhibits strong mediolateral constriction approximately at the midpoint of the element. In addition, distal to the point of greatest constriction, the mediolateral and dorsolateral margins of phalanx III-1 expand into prominent

Table 4.5: Comparative matrix of taxonomically significant morphologic traits of the pedal phalanges and unguals. Abbreviations: ml = mediolaterally, w/ = with, w/o = without

Taxon	II1-IV1 blocky, subequal	II1-IV1 variable length / width	II1, IV1 ml straight	II1, IV1 ml curved	III1 w/distal expansions of dorsal surface	unguals blunted, claw-like, w/claw grooves	unguals blunted, claw-like, w/o claw grooves	unguals hoof-like
Iguanodon bernissartensis	X		X			X		
Mantellisaurus atherfieldensis	X		X			X		
Nanyangosaurus zhugeii	?	?	?	?	?			X
Probactrosaurus gobiensis		X	X			X		
Bactrosaurus johnsoni	?	?	?	?	?		X	
Levnesovia transoxiana	?	?	?	?	?			X
Gilmoreosaurus mongoliensis		X	X					X
Edmontosaurus sp.		X		X				X
UAMES 12275		*X*		*X*	*X*		*X*	

semicircular flanges of bone, a condition not noted in any of the other taxa considered for this study. Phalanx IV-1 is the shortest of the three first phalanges and possesses a plantar distal margin that is laterally expanded, similar to *Edmontosaurus*. The unguals are long and claw-like, with phalanx III-4 being the longest and nearly the same length as phalanx III-1. The better-preserved unguals of digit three and digit two or four show that when complete, the unguals possess a stout arrowhead-like morphology lacking claw grooves, similar to *Gilmoreosaurus*.

4. Summary

Of the basal hadrosauriforms *Iguanodon bernissartensis*, *Mantellisaurus atherfieldensis*, and *Ouranosaurus nigeriensis*, only *Mantellisaurus* possesses a scapular head with a dorsoventral height less than or equal to the dorsoventral height of the distal termination of the scapular blade, while only *Ouranosaurus* possesses a dorsally convex dorsal margin of the scapula. Both traits are observed in UAMES 12275. None of the humeri of these basal hadrosauriforms possesses a distinct ridge on the posterior surface of the proximal end of the humerus which supports the humeral head, as in UAMES 12275. In addition, all possess ventrally deflected supraacetabular processes of the ilium and lack fourth trochanters which project posteriorly to a height subequal to the anteroposterior diameter of the femur, in stark contrast to that seen in UAMES 12275. Therefore, there are no grounds for attributing UAMES 12275 to any of these basal hadrosauriforms.

The basal hadrosauroids examined share more characteristics of the postcrania in common with UAMES 12275 than basal hadrosauriforms, but no single basal hadrosauroid taxon possesses the same combination of characters as those seen in UAMES 12275, including: a straight distal termination of the scapular blade, a distinct ridge on the posterior surface of the proximal end of the humerus which supports the humeral head, a supraacetabular process which is not ventrally deflected and which

forms a discrete flange of bone on the dorsolateral margin of the ilium, and a fourth trochanter which projects posteriorly to a height greater than or equal to the anteroposterior diameter of the shaft of the femur. For these reasons, UAMES 12275 cannot be confidently referred to any of the non-hadrosaurid hadrosauroids considered in this study (*Altirhinus kurzanovi*, *Bactrosaurus johnsoni*, *Eolambia caroljonesa*, *Gilmoreosaurus mongoliensis*, *Levnesovia transoxiana*, *Nanyangosaurus zhugeii*, *Probactrosaurus gobiensis*, *Telmatosaurus transsylvanicus*).

While stratigraphy is not something that can be considered in the context of establishing a new taxon, it is nevertheless a helpful aspect of a fossil to examine, especially when the taxon in question may exist in a temporal gap in the fossil record of a group.

As discussed in "Chapter 2: Geology and Taphonomy", UAMES 12275 was recovered from Turonian sediments of the Matanuska Formation in south-central Alaska. Only two unambiguously Turonian basal hadrosauroids are known: *Jeyawati rugoculus* of New Mexico and *Levnesovia transoxiana* of Uzbekistan. Two other taxa might be Turonian in age: *Bactrosaurus johnsoni* and *Gilmoreosaurus mongoliensis*, both of the Mongolian Iren Dabasu Formation, may be considered Turonian-Coniacian (Nessov 1995 and 1997; Averianov 2002; both cited in Sues and Averianov 2009) or Campanian-Maastrichtian (Van Itterbeek et al., 2005; Prieto-Marquez 2010b) in age. The New Mexican taxon *Jeyawati rugoculus* lacks diagnostic postcranial material. Unfortunately, the skull of UAMES 12275 is unknown. With no overlapping elements and paleogeographic reconstructions that place several mountain ranges and a shallow seaway between what are now the Talkeetna Mountains and New Mexico, there are no grounds for referring UAMES 12275 to *Jeyawati*. Though *Levnesovia transoxiana* possesses a humerus and ilium which are very similar to those of UAMES 12275, the midshaft region of the femur is unknown, its pedal unguals are hoof-like, and its pedal phalanx III-1 lacks the expansions of the dorsal surface seen in UAMES

12275. Therefore, UAMES 12275 cannot be attributed to *Levnesovia*, either. Regardless of the exact stratigraphic range of *Bactrosaurus* and *Gilmoreosaurus*, the comparative discussion indicates there is no basis for referring UAMES 12275 to either taxon.

This study included every described non-hadrosaurid hadrosauroid from the Albian to the Santonian (~112-83.5 Ma) with known postcranial material. While the comparative taxa may possess one or more morphological similarities with UAMES 12275, none share the unique suite of character combinations observed in UAMES 12275. Therefore, given the morphologic, stratigraphic, and geographic data discussed in this chapter, UAMES 12275 is interpreted to be a new hadrosauroid taxon and the third unambiguously Turonian hadrosauroid thus far described.

Chapter 5: The Phylogenetic Relationships of UAMES 12275

1. Introduction

The results of the comparative analysis (Chapter 4) indicated that UAMES 12275 was most similar to known non-hadrosaurid hadrosauroid taxa such as *Levnesovia transoxiana*, *Bactrosaurus johnsoni*, and *Gilmoreosaurus mongoliensis*. To further test the systematic position of this specimen within Hadrosauriformes, I performed a maximum parsimony analysis using PAUP* v. 4.0b10 (Swofford, 2002).

A suitable pre-existing data matrix required numerous non-hadrosaurid hadrosauriform taxa and a large number of postcranial characters, and so the matrix of Prieto-Marquez (2010a) was selected. Prieto-Marquez (2010a) analyzed the phylogenetic relationships of all known non-hadrosaurid and hadrosaurid hadrosauroids and the data matrix includes a large number of postcranial characters. Other available phylogenies, such as that of Head (1998), McDonald et al. (2010) or Sues and Averianov (2009) examine even more basal relationships or use exclusively cranial characters. Lacking a skull and morphologic evidence to suggest that UAMES 12275 falls outside of the Hadrosauriformes, the data matrices used by McDonald et al. (2010) and Sues and Averianov (2009) were eliminated as options.

2. Methods

UAMES 12275 was scored into the data matrix of Prieto-Marquez (2010a). Although Prieto-Marquez (2010a) constructed his dataset to determine ingroup relationships within Hadrosauridae specifically, his matrix included 196 cranial and 90 postcranial characters and 12 non-hadrosaurid hadrosauriform dinosaurs (ten basal hadrosauroids and two basal hadrosauriforms).

Although Prieto-Marquez (2010a) did include many postcranial characters in his analysis of Hadrosauridae, the majority of his characters (196 out of 286, or 68.5% of

all characters) were derived from the cranium. For UAMES 12275, only 20 characters (or ~7% of the total data matrix), could be scored for this specimen, and only if one is willing to make certain (seemingly reasonable) assumptions. Otherwise, only 16 characters could be scored (or ~5.5% of the data matrix). This led to UAMES 12275 being analyzed twice, once operating under a few reasonable assumptions (the relaxed scoring) and second time where only characters whose identification required no assumptions were included in the matrix (the conservative scoring).

The relaxed scoring included Characters 212-214 and 279. Characters 212-214 all examine aspects of the scapula. As discussed previously, the scapulae of UAMES 12275 are incomplete and of distinctly different morphologies. Thus, scoring these characters required that one scapula be deemed "normal" relative to the other. The left scapula was used because it is the more complete of the two elements.

Character 212: Scapular length, ratio between the craniocaudal length of the scapula (from the cranial end of the pseudoacromion process to the distal margin of the blade) and the dorsoventral depth of the cranial end (from the cranial end of the pseudoacromion process to the ventral apex of the glenoidal facet) (SCP2, http://www.morphbank.net/show/?id=46714): relatively short scapula, ratio of up to 4 (sample mean ratio of 3.54) (0); relatively long scapula, ratio of greater than 4 (sample mean ratio of 4.64) (1) (Prieto-Marquez, 2010a). The caudal margin of the left scapula is complete, but the pseudoacromion process and glenoid facet are not preserved. Despite the missing landmarks, the scapula as preserved possesses a length/height ratio of 4.16. In order for the scapula of UAMES 12275 to possess a length/height ratio less than 4.00, the cranial end would have to expand dorsoventrally by at least .5 cm without expanding any further craniocaudally. Given the missing landmarks, expansion in one dimension without expansion in the other seems unlikely and so this character was scored as state 1 (see Table 5.1).

Character 213: Dorsoventral expansion of the distal region of the scapular blade (measured as a ratio between the depth of the distal end of the blade and the depth of the proximal region) (SCP4, http://www.morphbank.net/Show/?id=461716): ratio less than 1 (sample mean ratio of 0.80) (0); ratio of 1 or greater (sample mean ratio of 1.15) (1) (Prieto-Marquez, 2010a). The dorsoventral height of the distal blade was estimated by extrapolating the dorsal margin of the blade as a straight line perpendicular to the distal margin of the blade to complete the missing caudodorsal corner. Despite the incompleteness of the scapula, the measurements of what is preserved yield a ratio of 1.32. In order for this ratio to be less than 1.00 for UAMES 12275, the cranial end of the scapula would have to expand at least 2.5 cm dorsoventrally while the caudal end remained the same height. Such a pronounced expansion of the cranial end of the scapula (to at least 133% of its size as preserved) seems unlikely and so this character was scored as state 1 (see Table 5.1).

Character 214: Scapula. Proximal constriction (scapular 'neck'), ratio between the dorsoventral width of the proximal constriction and the dorsoventral depth of the cranial end of the scapula (SCP5, http://www.morphbank.net/Show/?id=461717): narrow 'neck', ratio of up to 0.60 (sample mean ratio of 0.53) (0); relatively broad 'neck', ratio of greater than 0.60 (sample mean ratio of 0.68) (1) (Prieto-Marquez, 2010a). As preserved, this ratio is 0.63 for UAMES 12275. This character was scored as state 0 because a change of 0.45 cm in the dorsoventral height of the cranial end of the scapula is all that is required to push the ratio below the cut-off value, and the cranial end of the scapula is likely dorsoventrally taller than what is preserved (see Table 5.1).

Character 279: Astragalus. Development of the medial platform of the astragalus (AS, http://www.morphbank.net/Show/?id=461790): it extends medially to completely underlie the medial malleolus of the tibia (0); short, wedges laterally, underlying only part of the medial malleolus of the tibia (1). The distal end of the tibia of UAMES

	Character 212	Character 213	Character 214	Character 279
Table 5.1: A simplified data matrix summarizing the differences between conservative and relaxed analyses of UAMES 12275.				
UAMES 12275 relaxed scoring	1	1	0	0
UAMES 12275 conservative scoring	?	?	?	?

12275 is incomplete, but comparison of the astragalus with the tibia reveals that the astragalus is mediolaterally broad enough to underlie the breadth of the tibia as preserved and also extend past the preserved margin of the tibia. Those hadrosauriforms scored as state 1 in the data matrix of Prieto-Marquez (2010a) possess an astragalus that is less than or equal to half the mediolateral width of the distal end of the tibia. Despite the incompleteness of the distal end of the tibia, this character was scored as state 0 due to the mediolateral width of the astragalus (see Table 5.1).

The matrix of Prieto-Marquez (2010a) was used as-is, with no additions or deletions of characters. The conservative scoring was added to the data matrix first in Mesquite v. 2.74 (build 550, Maddison and Maddison., 2010) for Windows Vista and saved as a NEXUS file there. Once the conservative scoring had been analyzed, it was replaced with the relaxed scoring and the matrix was analyzed again.

Initial attempts to use a traditional heuristic search for most parsimonious trees (MPTs) in PAUP* v. 4.0b10 (Swofford, 2002) proceeded at a glacial pace: after approximately 1 week of computing time, fewer than 100 replicates of the search had been performed and the memory allotted for storage of MPTs during the search had been filled and purged by PAUP* four times. Due to time and computing constraints, the effort to implement a traditional heuristic search in PAUP for MPTs of this dataset was abandoned. The Parsimony Ratchet as implemented by Sikes and Lewis (2001)

was utilized instead, after first testing to see whether or not the Ratchet could recover a tree topology congruent with that of Prieto-Marquez (2010a).

PAUPRat is an application that implements the Parsimony Ratchet method of Kevin Nixon (1999) utilizing any version of PAUP* (in this case, v. 4.0b10). Sikes and Lewis (2001) summarized the logical approach behind the Ratchet as an effort to search as much of tree-space as possible in the shortest amount of time. Two searches of a specified length are run per iteration of the Ratchet, one in which none of the characters are weighted and a second in which a specified number of characters or a percentage of characters are given different weights than the other. Trees are generated utilizing tree-bisection-reconnection (TBR) and random stepwise addition. PAUPRat saves one arbitrarily chosen tree from a given iteration of a search and uses it as the starting point for the next search iteration, thereby helping to avoid starting on or visiting "bad" tree islands (Sikes and Lewis, 2001).

A 1,000 replicate bootstrap analysis of the data matrix was attempted. However, after a week of computing time, fewer than 24 replicates had been completed. Time and computational constraints rendered this amount of progress unacceptable and the bootstrap analysis was abandoned. An attempt at computing Bremer support statistics also failed due to time and computing constraints, undermining the potential validity of these results.

3. Results

Prieto-Marquez (2010a) utilized TNT 1.0 (Goloboff et al., 2001) to conduct a heuristic search of 10,000 replicates with random addition sequences and subsequent tree-bisection-reconnection. This yielded 160 most parsimonious trees with lengths of 906 steps. The strict consensus tree had an ensemble consistency index of 0.51 and an ensemble retention index of 0.81 (Prieto-Marquez 2010a). The consensus tree of Prieto-Marquez (2010a) is simplified and redrawn as Figure 5.1.
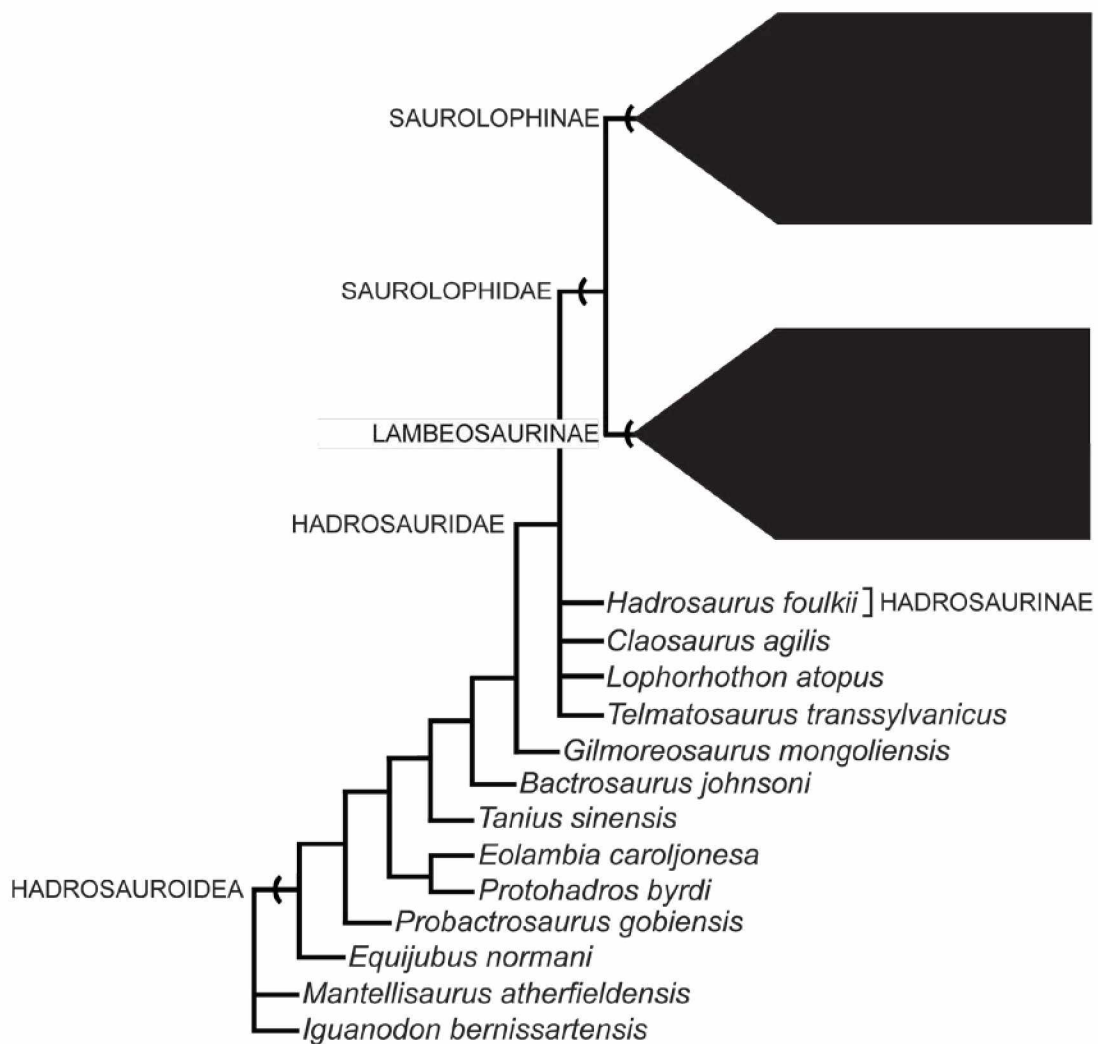
Figure 5.1: Strict consensus tree redrawn from Prieto-Marquez (2010). CI: 0.51. RI: 0.81. Tree length: 906 steps. *Telmatosaurus transsylvanicus*, *Lophorhothon atopus*, *Claosaurus agilis*, and *Hadrosaurus foulkii* have not been condensed like the members of the Saurolophinae and Lambeosaurinae because they represent a polytomous sister group to the monophyletic Saurolophidae. This construction of the Hadrosauridae will be used in all subsequent phylogenies.

As an independent test of the ability of the Ratchet method to recover a tree topology similar to that of Prieto-Marquez (2010a), that data matrix was analyzed without the addition of UAMES 12275.

According to Sikes and Lewis (2001), PAUPRat works best when multiple smaller searches are run instead of a single long search. 10 searches of 1,000 replicates each were conducted for a total of 10,000 replicates, in an effort to mimic as closely as possible the methods of Prieto-Marquez (2010a). All command strings were set to their default values in PAUPRat, and in each replicate of the search 5% of characters were perturbed.

These methods yielded a total of 10,010 trees total because PAUPRat saves all trees found in a given search. The trees found by PAUPRat in each individual search must be compiled into a single file and then the most parsimonious trees can be extracted from the composite tree file using tree filters in PAUP. In this case, the filter used was "Best Tree(s) based on current optimality criterion." Parsing the best of the resultant trees from the analysis yielded 2,279 MPTs of 907 steps each, 1 step (or 0.11%) longer than the tree of Prieto-Marquez (2010a). The ensemble consistency index is 0.46 and the ensemble retention index is 0.78. The strict consensus tree of those 2,279 MPTs is drawn in Figure 5.2.

In general, the results of the PAUPRat iterations were largely congruent with those of Prieto-Marquez (2010a). In particular, the relationships recovered among non-hadrosaurid taxa were identical (Figure 5.2). All instances where the strict consensus tree generated using the PAUPRat method was incongruent with that of Prieto-Marquez (2010a) occurred within the Hadrosauridae, which is outside the scope of this study.

Satisfied that PAUPRat could closely approximate the original strict consensus tree in length, topology, and consensus statistics, the conservative and relaxed scorings of

Figure 5.2: Replicated strict consensus tree of 2,279 MPTs recovered using PAUP* v. 4.0b10 and PAUPRat as a test to verify the validity of the method for use with the dataset of Prieto-Marquez (2010). Compare to Figure 5.1. CI = 0.46. RI = 0.78. Tree length: 907 steps.

UAMES 12275 were added to different copies of Prieto-Marquez's (2010a) original matrix. Each new matrix was analyzed using the same parameters described above.

1. UAMES 12275 Conservative Scoring Iteration

Excluding the worst of the resultant trees from this analysis yielded 1,623 MPTs of 910 steps each, 4 steps longer than the tree of Prieto-Marquez (2010a). Similar to the PAUPRat test consensus tree, the ensemble consistency index is 0.46 and the ensemble retention index is 0.78. Figure 5.3 is the strict consensus tree of the MPTs from this analysis.

UAMES 12275 was recovered as a non-hadrosaurid hadrosauroid, more derived than *Eolambia* + *Protohadros* but more basal than *Tanius sinensis*. The relationships among other basal hadrosauroids were otherwise identical to those recovered in Prieto-Marquez (2010a). As with the PAUPRat test tree, all topological differences between this tree and the original tree of Prieto-Marquez (2010a) are confined to the Hadrosauridae.

Figure 5.3: Strict consensus tree using the conservative scoring of UAMES 12275 added to the data matrix of Prieto-Marquez. CI: 0.46. RI: 0.78. Tree length: 910 steps.

2. UAMES 12275 Relaxed Scoring Iteration

Excluding the worst of the resultant trees from this analysis yielded 2,181 MPTs of length 912 steps, 6 steps longer than the tree of Prieto-Marquez (2010a). The ensemble consistency index was 0.46 and the ensemble retention index was 0.78. As with the consensus tree using the conservative scoring, UAMES 12275 was recovered as a non-hadrosaurid hadrosauroid more derived than *Eolambia + Protohadros* but less derived than *Tanius sinensis* (Figure 5.4). This seems to suggest that either the four additional characters added to this matrix are phylogenetically unimportant this basal in the Hadrosauriformes, or that the assumptions made to score these characters were reasonable. The topology of this strict consensus tree was otherwise identical to that of the tree obtained by attempting to replicate the original tree of Prieto-Marquez (2010a).
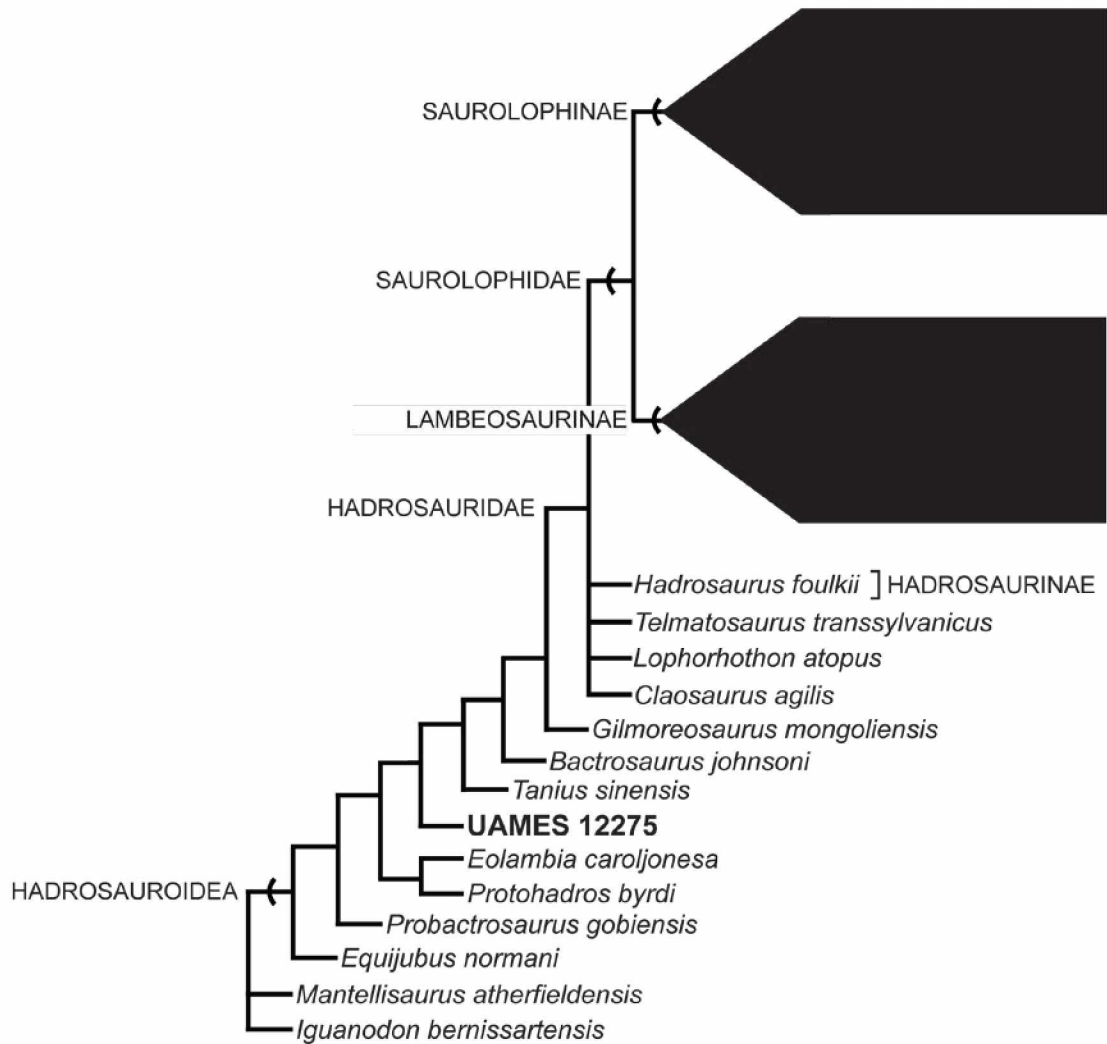
Figure 5.4: Strict consensus tree using the relaxed scoring of UAMES 12275 added to the data matrix of Prieto-Marquez (2010). CI: 0.46. RI: 0.78. Tree length: 912 steps.

4. Discussion

Despite the lack of Bremer support statistics, the phylogenies obtained using both the conservative and relaxed scorings of UAMES 12275 are perfectly congruent with the tree of Prieto-Marquez (2010a) in the basal hadrosauroid taxa and vary only slightly within the Hadrosauridae, a clade outside the scope of this study. In addition, the constructed phylogenies are in general agreement with the conclusions of the comparative analysis (Chapter 4) in that UAMES 12275 is most similar to non-hadrosaurid hadrosauroids.

Finally, the phylogenies also fit well within the biostratigraphic framework of the derived Hadrosauriformes. The earliest hadrosaurid is the Asian lambeosaurine *Jaxartosaurus aralensis* from the late Santonian of Kazakhstan (Prieto-Marquez 2010b), and the vast majority of hadrosaurids have been found in Campanian-Maastrichtian strata. The existence of a derived non-hadrosaurid hadrosauroid in the Turonian is consistent with available data (see McDonald et al., 2010; Prieto-Marquez, 2010b; Sues and Averianov, 2009; Xu et al., 2000).

5. Summary

Phylogenetically, UAMES 12275 is a non-hadrosaurid hadrosauroid, being more derived than the clade *Eolambia jonesi* + *Protohadros byrdi* (North America) and less derived than *Tanius sinensis* (Asia). Support statistics for the phylogenetic position of UAMES 12275 are nonexistent due to the size of the data matrix and limitations of available computing power, but the phylogeny is consistent with the stratigraphic age of the fossil and the known biogeography of derived members of the Hadrosauriformes.

Chapter 6: Summary

1. Taphonomy and Depositional Environment of UAMES 12275

UAMES 12275 represents another "bloat and float": a terrestrial vertebrate that was swept out to sea due to buoyancy caused by decomposition gases. Subsequent burial on the sea floor followed decomposition (or scavenging) sufficient to breach the body cavity and allow the accumulated gases to escape (Pasch and May 1997; 2001).

Pasch and May (1997; 2001) concluded that the carcass came to rest in water at least 35 m deep, citing the invertebrate fossil assemblage as evidence that deposition must have been in an upper bathyal or neritic setting. Several lines of evidence lead me to conclude that 35 m is too shallow an estimate and that we cannot adequately estimate the depth of deposition. First, minimal signs of bioturbation of quarry shale (ichnofabric index 2 or 3, *sensu* Droser and Bottjer, 1986) and the presence of pyrite as coatings on the bones and framboids in the concretion sediment suggest that the carcass sank into oxygen-deficient waters. Second, comparison of this fossil to that of a Late Cretaceous elasmosaurid plesiosaur of significantly greater size reveals that UAMES 12275 was not scavenged intensely after settling to the sea floor. Evidence for extensive post-depositional modification of bone surfaces indicates the carcass was exposed on the sea floor for an extended period of time. The marks originally interpreted as evidence for mosasaur scavenging likely represent traces of bone-mining organisms, likely similar to *Osedax* sp. and other animals that exploit Recent whale falls. Both the minimal disruption of the skeleton and the lack of obvious tooth marks seem to support the idea that the carcass sank into waters that, if not necessarily oxygen-deficient, were in some way hostile to vertebrate scavengers. Third, the preservation of fine sediment laminae in the quarry shale indicate a low-energy depositional environment. 35 m is well within the possible depth range of storm wave base. Storms would periodically oxygenate bottom waters, thus enabling

vertebrate scavengers, and disrupt fine laminae. Unfortunately, storm wave base is not a fixed depth and there is no evidence in the fossil or the rocks to suggest what that depth might have been. As discussed previously (p. 49), storm wave base can exceed 200 m water depth. This must be used as a minimum depth of deposition for UAMES 12275 until more conclusive paleobathymetric evidence becomes available.

2. Taxonomy and Phylogeny of UAMES 12275

Comparative analysis of UAMES 12275 demonstrates that this Alaskan animal is a non-hadrosaurid hadrosauroid and is distinct from other described non-hadrosaurid hadrosauroid dinosaurs. UAMES 12275 possesses the following suite of post-cranial characters that distinguish it from all other known non-hadrosaurid hadrosauroids:

1. The humerus possesses a bicepital sulcus on the anterolateral surface and a pronounced ridge on the posteromedial surface which supports the humeral head.

2. The supraacetabular process of the ilium is separated from a laterally directed dorsal ridge, extends from the iliac plate at an almost right angle, is not ventrally deflected, and the dorsoventral thickness of the process is less than 25% of the dorsoventral height of the iliac plate.

3. The fourth trochanter of the femur projects posteriorly to a height greater than or equal to the diameter of the femoral shaft.

In the phylogenetic analysis, UAMES 12275 is recovered as a non-hadrosaurid hadrosauroid more derived than *Protohadros* + *Eolambia* and less derived than *Tanius*, supporting the conclusion reached through visual inspection of the remains. This, in turn, is congruent with what is currently known about hadrosauroid biogeography and diversification in the early Late Cretaceous. Hadrosauroids were geographically widespread by the Late Cretaceous, and several exchanges of fauna between North America and Eurasia are believed to have occurred in the time preceding the

appearance and diversification of the Hadrosauridae (Lund and Gates, 2006; Sues and Averianov, 2009; McDonald et al., 2010; Prieto-Marquez, 2010b). Figure 6.1 is a composite area cladogram showing the geographic locations of taxa considered as a part of this study. The spatial clustering (in a broad sense) of taxa is apparent in the basal hadrosauriforms and non-hadrosaurid hadrosauroids.
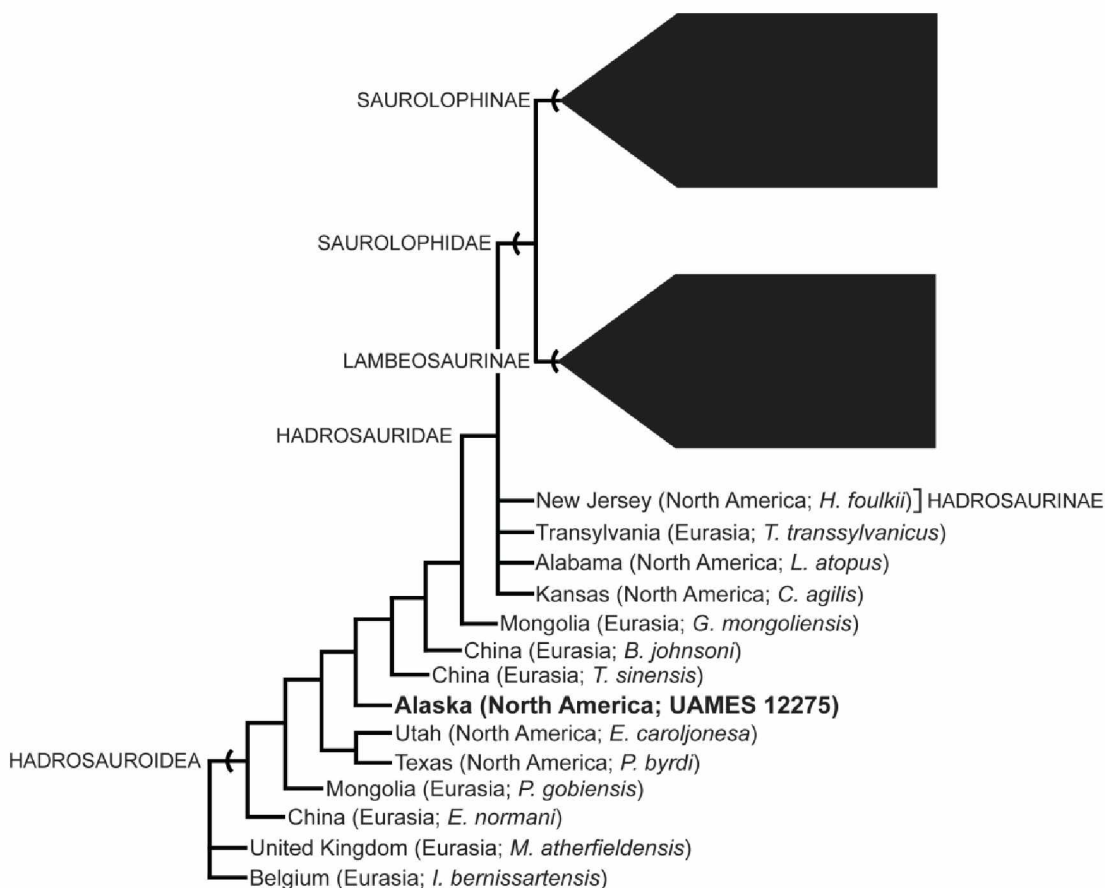

Figure 6.1: Area cladogram of non-saurolophid hadrosauriforms, showing the geographic distribution of known taxa.

3. Significance of UAMES 12275

At the regional scale, UAMES 12275 represents the oldest and most complete hadrosauroid found in Alaska to date. It is also the first uniquely Alaskan hadrosauroid dinosaur of any sort currently known.

Given the seemingly sudden appearance and diversification of the Hadrosauridae in the fossil record of the Late Cretaceous, it is astonishing how poorly known and understood their early evolutionary history is. As a non-hadrosaurid hadrosauroid, UAMES 12275 represents a significant addition to the dataset of hadrosaurid evolution due to its age (Turonian), its geographic location (North America), and its status as a potentially new taxon. Turonian taxa from any continent are a rarity (Lund and Gates, 2006; Sues and Averianov, 2009). Furthermore, paleogeographic reconstructions of the Hadrosauriformes suggest multiple exchanges of basal hadrosauroid taxa between Eurasia and North America prior to the appearance of the Hadrosauridae in the Santonian (Prieto-Marquez, 2010b; Sues and Averianov, 2009). As illustrated previously by Figure 7.1, UAMES 12275 is apparently part of a North American radiation of hadrosauroids which was preceded and succeeded by Eurasian (particularly Chinese/Mongolian) radiations of hadrosauroids.

4. Shortcomings

Understanding the paleobiogeography of the derived hadrosauriforms (Hadrosauroidea + Hadrosauridae) is vital to understanding their evolutionary history, as it provides context for the patterns and interrelationships observed in the fossil record. I included a brief and oversimplified discussion of the paleogeography of UAMES 12275, but a more detailed analysis of the paleogeographic position of the Wrangellia Composite Terrane falls far outside the scope and purpose of this thesis.

Although the phylogenetic analysis of UAMES 12275 has ensemble consistency and retention indices similar to those of the original dataset (Prieto-Marquez, 2010a; C.I. = 0.54 and R.I. = 0.81 versus C.I. = 0.46 and R.I. = 0.78 in this study), the lack of Bremer or bootstrap values for this dataset is problematic. This is mitigated somewhat by the fact that I inserted a taxon into a pre-existing dataset, as the addition of a single taxon to an existing data matrix should not significantly alter support statistics for the rest of the tree. On a lesser scale, only a handful of characters from this data matrix could be scored for UAMES 12275. Despite this, the fossil was recovered as a non-hadrosaurid hadrosauroid, a position consistent with its biostratigraphic age and the comparative analysis.

5. Future Work

With regard to taphonomy of UAMES 12275, it may be possible to more accurately quantify oxygen content of the water column. Tribovillard et al. (2006) describe using concentrations of trace metals in marine sediments as proxies for paleo redox conditions. Time and monetary constraints prevented such analyses from being conducted, but they would be useful for coming to a better understanding of the taphonomy of UAMES 12275.

A topic of particular interest would be the comparison of UAMES 12275 to better-preserved postcranial remains of *Jeyawati rugoculous* McDonald (2010) to determine whether or not these two Turonian North American non-hadrosaurid hadrosauroids are distinct taxa, should such postcrania ever be found. As it is currently known, the postcrania of *Jeyawati rugoculous* consist of a handful of very poorly preserved, nondiagnostic vertebrae. Paleogeography and the current lack of equivalent skeletal elements suggest that UAMES 12275 and *Jeyawati* are distinct taxa, but paleogeography alone is not enough to allow for such a conclusion and the lack of overlapping skeletal elements constitutes an absence of evidence, not proof.

A closer comparison of this taxon with either *Levnesovia transoxiana* or *Jeyawati rugoculous* (assuming more complete and better-preserved postcranial remains of *Jeyawati* are found) would be most enlightening in a paleobiogeographic context. All three are Turonian non-hadrosaurid hadrosauroids and all three presumably share a common ancestor, despite being widely separated geographically. Determining their interrelationships would allow a date assignment for one of the proposed hadrosauroid faunal interchanges that are believed to have occurred, and it may have more far-reaching implications than that depending upon how these taxa fall out with respect to one another (for example, the directionality of the faunal interchange).

The phylogenetic trees generated by Prieto-Marquez (2010a) and this thesis present some interesting implications for the existence of faunal exchanges between North America during the evolution of non-hadrosaurid hadrosauroids and also the timing of those events (see Figure 6.1, above). Other papers examined for this work (McDonald et al., 2010; Sues and Averianov, 2009) show similar relationships between clusters of North American and Eurasian taxa. Pulling these disparate trees together into a single phylogenetic analysis and distilling a time-calibrated phylogeny would likely prove very useful to elucidating paleobiogeographical relationships between various groups of non-hadrosaurid hadrosauroids.

Works Cited

Averianov, A.O. 2002. An ankylosaurid (Ornithischia: Ankylosauria) braincase from the Upper Cretaceous Bissekty Formation of Uzbe-kistan. Bulletin de l'Institut Royal des Sciences Naturelles de Bel-gique, Sciences de la Terre 72:97-110.

Barnes, K.M., and N. Hiller. 2010. The taphonomic attributes of a Late Cretaceous plesiosaur skeleton from New Zealand. Alcheringa 29:333-344.

Bergquist, H.R. 1961. Foraminiferal zoning in Matanuska Formation, Squaw Creek-Nelchina River area, south-central Alaska. Bulletin of the American Association of Petroleum Geologists 45:1994-2011.

Berner, R.A. 1968. Calcium carbonate concretions formed by the decomposition of organic matter. Science 159:195-197.

Berner, R.A. 1970. Sedimentary pyrite formation. American Journal of Science 268:1-23.

Breitburg, D.L. 1992. Episodic hypoxia in Chesapeake Bay: interacting effects of recruitment, behavior, and physical disturbance. Ecological Monographs 62:525-546.

Butler, I.B., and D. Rickard. 2000. Sedimentary pyrite formation via the oxidation of iron (II) monosulphide by hydrogen sulphide. Geochimica et Cosmochimica Acta 64:2665-2672.

Coney, P.J., D.L. Jones, and J.W.H. Monger. 1980. Cordilleran suspect terranes. Nature 288:329-333.

Deer, W.A., R.A. Howie, and J. Zussman. 1996. An Introduction to the Rock Forming Minerals (2nd Edition). Pearson Education Limited.

Doyle, Sir A.C. 1890. The Sign of the Four, Chapter 6 pp. 111. Spencer Blackett.

Droser, M.L., and D.J. Bottjer. 1986. A semiquantitative field classification of ichnofabric. Journal of Sedimentary Petrology 56:558-559.

Duxbury, A.C., A.B. Duxbury, and K.A. Sverdrup. 2000. Chapter 9: The Waves. in Duxbury, A.C., A.B. Duxbury, and K.A. Sverdrup (eds) An Introduction to the World's Oceans (6th Edition). McGraw-Hill Publishers.

Fiorillo, T. 2006. Review of the dinosaur record of Alaska with comments regarding Korean dinosaurs as comparable high-latitude fossil faunas. Journal of the Paleontological Society of Korea 22:15-27.

Folk, R.L. 2005. Nannobacteria and the formation of framboidal pyrite: Textural evidence. Journal of Earth System Science 114:369-374.

Gangloff, R.A. 1998. Arctic dinosaurs with emphasis on the Cretaceous record of Alaska and the Eurasian-North American connection. in Lucas, S.G. et al. (eds.) Lower and Middle Cretaceous Terrestrial Ecosystems. New Mexico Museum of Natural History and Science Bulletin 14:211-220.

Gangloff, R.A., A.R. Fiorillo, and D.W. Norton. 2005. The first pachycephalosaurine (Dinosauria) from the paleo-arctic of Alaska and its paleogeographic implications. Journal of Vertebrate Paleontology 79:997-1001.

Garver, J.I. 1992. Provenance of Albian-Cenomanian rocks of the Methow and Tyaughton basins, southern British Columbia: a mid-Cretaceous link between North America and the Insular terrane. Canadian Journal of Earth Science 29:1274-1295.

Godefroit, P., Z-M Dong, P. Bultynck, Li, H., and L. Feng. 1998. Sino-Belgian Cooperative Program. Cretaceous dinosaurus and mammals from Inner Mongolia: 1) new Bactrosaurus (Dinosauria: Hadrosauroidea) material from Iren Dabasu (Inner

Mongolia, P.R. China). Bulletin de l'Institute Royal des Sciences Naturelles du Belgique 68:1-70.

Godefroit, P., H. Li, and C.Y. Shang. 2005. A new primitive hadrosauroid dinosaur from the Early Cretaceous of Inner Mongolia (P.R. China). C. R. Paleovol 4:697-705.

Goloboff, P., S. Farris, K. Nixon. 2002. TNT: Tree Analysis Using New Technology http://www.cladistics.com/webtnt.html

Grantz, A. 1964. Stratigraphic reconnaissance of the Matanuska Formation in the Matanuska Valley, Alaska. Contributions to General Geology. Geological Survey Bulletin 1181-I: I1-I33.

Hampton, B.A., K.D. Ridgway, J.M. O'Neill, G.E. Gehrels, J. Schmidt, and R.B. Blodgett. 2007. Pre-, syn-, and postcollisional stratigraphic framework and provenance of Upper Triassic-Upper Cretaceous strata in the northwestern Talkeetna Mountains, Alaska. in K.D. Ridgway et al. (eds.), Tectonic Growth of a Collisional Continental Margin: Crustal Evolution of Southern Alaska. Geological Society of America Special Paper 431:401-438.

Head, J.J. 1998. A new species of basal hadrosaurid (Dinosauria, Ornithischia) from the Cenomanian of Texas. Journal of Vertebrate Paleontology 18:718-738.

Heusser, L. and W.L. Balsam. 1977. Pollen distribution in the Northeast Pacific Ocean. Quaternary Research 7:45-62.

Hogler, J.A. 1994. Speculations on the roll of marine reptile deadfalls in Mesozoic deep-sea paleoecology. Palaios 9:42-47.

Horner, J.R. 1979. Upper Cretaceous dinosaurs from the Bearpaw Shale (marine) of south-central Montana with a checklist of Upper Cretaceous dinosaur remains from marine sediments in North America. Journal of Paleontology 53:566-577.

Horner, J.R., D.B. Weishampel, and C.A. Forster. 2004. Chapter Twenty: Hadrosauridae. in Weishampel, D.B. et al (eds.) The Dinosauria (2nd Edition). University of California Press.

Johnston, S.T. 2001. The Great Alaskan Terrane Wreck: reconciliation of paleomagnetic and geological data in the northern Cordillera. Earth and Planetary Science Letters 193:259-272.

Kiel, S., J.L. Goedert, W.A. Kahl, and G.W. Rouse. 2010. Fossil traces of the bone-eating worm *Osedax* in early Oligocene whale bones. PNAS 107:8656-8659.

Kirkland, J.I. 1998. A new hadrosaurid from the upper Cedar Mountain Formation (Albian-Cenomanian: Cretaceous) of eastern Utah—the oldest known hadrosaurid (lambeosaurine?). in Lucas, S.G. et al. (eds.) Lower and Middle Cretaceous Terrestrial Ecosystems. New Mexico Museum of Natural History and Science Bulletin 14:283-295.

Lund, E.K., and T.A. Gates. 2006. A historical and biogeographical examination of hadrosaurian dinosaurs. in Lucas, S.G. and R.M. Sullivan (eds.) Late Cretaceous vertebrates from the Western Interior. New Mexico Museum of Natural History and Science Bulletin 35:263-276.

McDonald, A.T., D.G. Wolfe, and J.I. Kirkland. 2010. A new basal hadrosauroid (Dinosauria: Ornithopoda) from the Turonian of New Mexico. Journal of Vertebrate Paleontology 30:799-812.

Maddison, W.P. and D.R. Maddison. 2010. Mesquite: a modular system for evolutionary analysis. Version 2.74. http://mesquiteproject.org.

Mahoney, J.B., P.S. Mustard, J.W. Haggart, R.M. Friedman, C.M. Fanning, and V.J. McNicoll. Archean zircons in Cretaceous strata of the western Canadian Cordillera: the "Baja B.C." hypothesis fails a "crucial test." Geology 27:195-198.

Matsumoto, T. 1977. Some heteromorph ammonites from the Cretaceous of Hokkaido. Kyushu University Memoirs of the Faculty of Science, series D, Geology 23:303-366.

Mozer, A. 2010. Authigenic pyrite framboids in sedimentary facies of the Mount Wawel Formation (Eocene), King George Island, West Antarctica. Polish Polar Research 31:255-272.

Nessov, L.A. 1995. Dinozavri severnoi Yevrazii: Novye dannye o sostave kompleksov, ekologii i paleobiogeografii [Dinosaurs of northern Eurasia: new data about assemblages, ecology, and paleobiogeography]. Institute for Scientific Research on the Earth's Crust, St. Petersburg State University 165 pp. [Russian with English summary].

Nessov, L.A. 1997. Nyemorskiye pozvonochnyye myelovogo pyerioda Syev-yernoi Yevrazii [Cretaceous nonmarine vertebrates of northern Eur-asia]. Sankt-Pyetyerburgskii Gosudarstvyennyi univyerityet Nauch-ko-isslyedovatyelskii institut zyemnoi koryi 218 pp. [Russian with English summary].

Nixon, K.C. 1999. The parsimony ratchet, a new method for rapid parsimony analysis. Cladistics 15:407-414.

Norman, D.B. 1980. On the ornithischian dinosaur *Iguanodon bernissartensis* from the Lower Cretaceous of Bernissart (Belgium). Mémoires de L'Institut Royal des Sciences Naturelles de Belgique, 178: 1–104.

Norman, D.B. 1986. On the anatomy of *Iguanodon atherfieldensis* (Ornithischia: Ornithopoda). Mémoires de L'Institut Royal des Sciences Naturelles de Belgique 56:281-372.

Norman, D.B. 1998. On Asian ornithopods (Dinosauria: Ornithischia). A new species of iguanodontid dinosaur. in Norman, D.B. et al. (eds.) A study of fossil vertebrates. Zoological Journal of the Linnean Society 122:291-348.

Norman, D.B. 2002. On Asian ornithopods (Dinosauria: Ornithischia). 4. *Probactrosaurus* Rozhdestvensky, 1966. Zoological Journal of the Linnean Society 136:113-144.

Norman, D.B. 2010. A taxonomy of iguanodontians (Dinosauria: Ornithopoda) from the lower Wealden Group (Cretaceous: Valanginian) of southern England. Zootaxa 2489:47-66.

Ohfuji, H. and D. Rickard. 2005. Experimental syntheses of framboids—a review. Earth-Science Reviews 71:147-170.

Pasch, A. D. and K. C. May. 1997. First occurrence of a hadrosaur (Dinosauria) from the Matanuska Formation (Turonian) in the Talkeetna Mountains of south-central Alaska; pp. 99-109 in Clough, J. G. and Larson, F. (eds.), Short Notes on Alaska Geology. Alaska Department of Natural Resources, Professional Report 118.

Pasch, A.D. and K.C. May. 2001. Taphonomy and paleoenvironment of a hadrosaur (Dinosauria) from the Matanuska Formation (Turonian) in south-central Alaska; pp. 219-236 in Tanke, D.H. and K. Carpenter (eds.), Mesozoic Vertebrate Life. Indiana University Press, Bloomington.

Plafker, G. and H.G. Berg. 1994. Overview of the geology and tectonic evolution of Alaska; pp. 989-1021 in Plafker, G. and H.G. Berg (eds.), The geology of Alaska. Geological Society of America.

Plotinskaya, O.Yu., E.O. Groznova, V.A. Kovalenker, K.A. Novoselav, and R. Seltmann. 2009. Mineralogy and formation conditions of ores in the Bereznyakovskoe Ore Field, the southern Urals, Russia. Geology of Ore Deposits 51:371-397.

Prieto-Marquez, A. 2010a. Global phylogeny of Hadrosauridae (Dinosauria: Ornithopoda) using parsimony and Bayesian methods. Zoological Journal of the Linnean Society 159:435-502.

Prieto-Marquez, A. 2010b. Global historical biogeography of hadrosaurid dinosaurs. Zoological Journal of the Linnean Society 159:503-525.

Prieto-Marquez, A. and M. Norell. 2010. Anatomy and relationships of Gilmoreosaurus mongoliensis (Dinosauria: Hadrosauroidea) from the Late Cretaceous of Central Asia. American Museum Novitiates 3694:1-52.

Rahel, F.J. and J.W. Nutzman. 1994. Foraging in a lethal environment: fish predation in hypoxic waters of a stratified lake. Ecology 75:1246-1253.

Reid, S.L. and A.D. Pasch. 1999. The significance of Turonian spore and pollen flora from the Matanuska Formation, Talkeetna Mountains, Alaska. Palynology 24:264

Schaff, R.G. and W.G. Gilbert (eds.). 1987. Alaska South COSUNA (SAL). American Association of Petroleum Geologists, Tulsa, Oklahoma.

Sikes, D.S. and P.O. Lewis. 2001. Software manual for PAUPrat: A tool to implement Parsimony Ratchet searches in PAUP*. Department of Ecology and Evolutionary Biology, University of Connecticut, Storrs, CT, USA.

Smith, C.R. and A.R. Baco. 2003. Ecology of whale at the deep-sea floor; pp. 311-354 in Gibson, R.N. and R.J.A. Atkinson (eds.), Oceanography and Marine Biology: An Annual Review. Taylor and Francis.

Stamatakos, J.A., J.M. Trop, and K.D. Ridgway. 2001. Late Cretaceous paleogeography of Wrangellia: Paleomagnetism of the MacColl Ridge Formation, southern Alaska, revisited. Geology 29:947-950.

Sues, H.D. and A. Averianov. 2009. A new basal hadrosauroid dinosaur from the Late Cretaceous of Uzbekistan and the early radiation of duck-billed dinosaurs. Proceedings of the Royal Society B 276:2549-2555.

Sullivan, R.M. 2006. A taxonomic review of the Pachycephalosauridae (Dinosauria, Ornithischia). in Lucas, S.G. and R.M. Sullivan (eds.), Late Cretaceous vertebrates from the Western Interior. New Mexico Museum of Natural History and Science Bulletin 35:347-365.

Swofford, D.L. 2002. PAUP*: Phylogenetic analysis using parsimony (and other methods), 4.0b10. Sinauer Associates, Sunderland, Massachusetts.

Takahashi, A. 2005. Responses of inoceramid bivalves to environmental disturbances across the Cenomanian/Turonian boundary in the Yezo forearc basin, Hokkaido, Japan. Cretaceous Research 26:567-580.

Taquet, P. 1976. Geologie et paleontologie du gisement de Gadoufaoua (Aptien du Niger), Cahier Paleont., C.N.R.S. Paris. 191 pp. [French]

Traverse, A. 2008. Appendix 3: Fossil Palynomorphs. pp. 632-648 in Landman, N.H. and D.S. Jones (eds) Paleopalynology – 2nd Edition. Springer.

Tribovillard, N., T.J. Algeo, T. Lyons, and A. Riboulleau. 2006. Trace metals as paleoredox and paleoproductivity proxies: An update. Chemical Geology 232:12-32.

Trop, J.M. and K.D. Ridgway. 2007. Mesozoic and Cenozoic tectonic growth of southern Alaska: A sedimentary basin perspective. pp. 55-94 in Ridgway, K.D., J.M. Trop, J.M.G. Glen, and J.M. O'Neill (eds.), Tectonic growth of a collisional continental margin: crustal evolution of southern Alaska. Geological Society of America Special Paper 431, Boulder, Colorado, USA.

Trop, J.M. 2008. Latest Cretaceous forearc basin development along an accretionary convergent margin: south-central Alaska. GSA Bulletin 120:207-224.

Trop, J.M., K.D. Ridgway, J.D. Manuszak, and P. Layer. 2002. Mesozoic sedimentary-basin development on the allochthonous Wrangellia composite terrane, Wrangell

Mountains basin, Alaska: A long-term record of terrane migration and arc construction. GSA Bulletin 114:693-717.

Umhoefer, P.J. 2003. A model for the North America Cordillera in the Early Cretaceous: Tectonic escape related to arc collision of the Guerrero Terrane and a change in North America plate motion; pp. 117-134 in Johnson, S.E. et al. (eds.), Tectonic evolution of northwestern Mexico and the southwestern USA. Geological Society of America Special Paper 374, Boulder, Colorado, USA.

Umhoefer, P.J. and R.C. Blakey. 2006. Moderate (1600km) northward translation of Baja British Columbia: An attempt at reconciliation of paleomagnetism and geology; pp. 305-327 in Haggart, J.W. et al. (eds.), Paleogeography of the North American Cordillera: Evidence for and against large-scale displacements. Geological Association of Canada Special Paper 46.

Van Itterbeek, J., D.J. Horne, P. Bultynck, and N. Vandenberghe. 2005. Stratigraphy and palaeoenvironment of the dinosaur-bearing Upper Cretaceous Iren Dabasu Formation, Inner Mongolia, People's Republic of China. Cretaceous Research 26:699-725.

Vaquer-Sunyer, R. and C.M. Duarte. 2008. Thresholds of hypoxia for marine biodiversity. PNAS 105:15452-15457.

Vecchia, F.M.D. 2009. *Tethyshadros insularis*, a new hadrosauroid dinosaur (Ornithischia) from the Upper Cretaceous of Italy. Journal of Vertebrate Paleontology 29:1100-1116.

Weishampel, D.B., D.B. Norman, and D. Grigorescu. 1993. *Telmatosaurus transsylvanicus* from the Late Cretaceous of Romania: the most basal hadrosaurid dinosaur. Palaeontology 36:361-385.

Wignall, P.B. and R. Newton. 1998. Pyrite framboid diameter as a measure of oxygen deficiency in ancient mudrocks. American Journal of Science 298:537-552.

Wilkin, R.T., H.L. Barnes, and S.L. Brantley. 1996. The size distribution of framboidal pyrite in modern sediments: An indicator of redox conditions. Geochimica et Cosmochimica Acta 60:3897-3912.

Wilkin, R.T. and H.L. Barnes. 1997. Formation processes of framboidal pyrite. Geochimica et Cosmochimica Acta 61:323-339.

Wyld, S.J. and P.J. Umhoefer. 2006. Reconstructing northern Cordilleran terranes along known Cretaceous and Cenozoic strike-slip faults: Implications for the Baja British Columbia Hypothesis and other models; pp. 277-298 in Haggart, J.W. et al. (eds.), Paleogeography of the North American Cordillera: Evidence for and against large-scale displacements. Geological Association of Canada Special Paper 46.

Xu, X., X.J. Zhao, J.C. Lü, W.B. Huang, Z.Y. Li, Z.M. Dong. 2000. A new iguanodontian from Sanping Formation of Neixiang, Henan and its stratigraphical implication. Vertebrata PalAsiatica 38:176-191.

You, H.L. and D.Q. Li. 2009. A new basal hadrosauriform dinosaur (Ornithischia: Iguanodontia) from the Early Cretaceous of northwestern China. Canadian Journal of Earth Science 46:949-957.